

10-39
MANEUVER LOADS BRANCH COPY

SECTION COPY

NATIONAL ADVISORY COMMITTEE FOR AERONAUTICS

TECHNICAL NOTE

No. 1239

WIND-TUNNEL INVESTIGATION OF THE EFFECT OF POWER AND FLAPS
ON THE STATIC LONGITUDINAL STABILITY CHARACTERISTICS
OF A SINGLE-ENGINE LOW-WING AIRPLANE MODEL

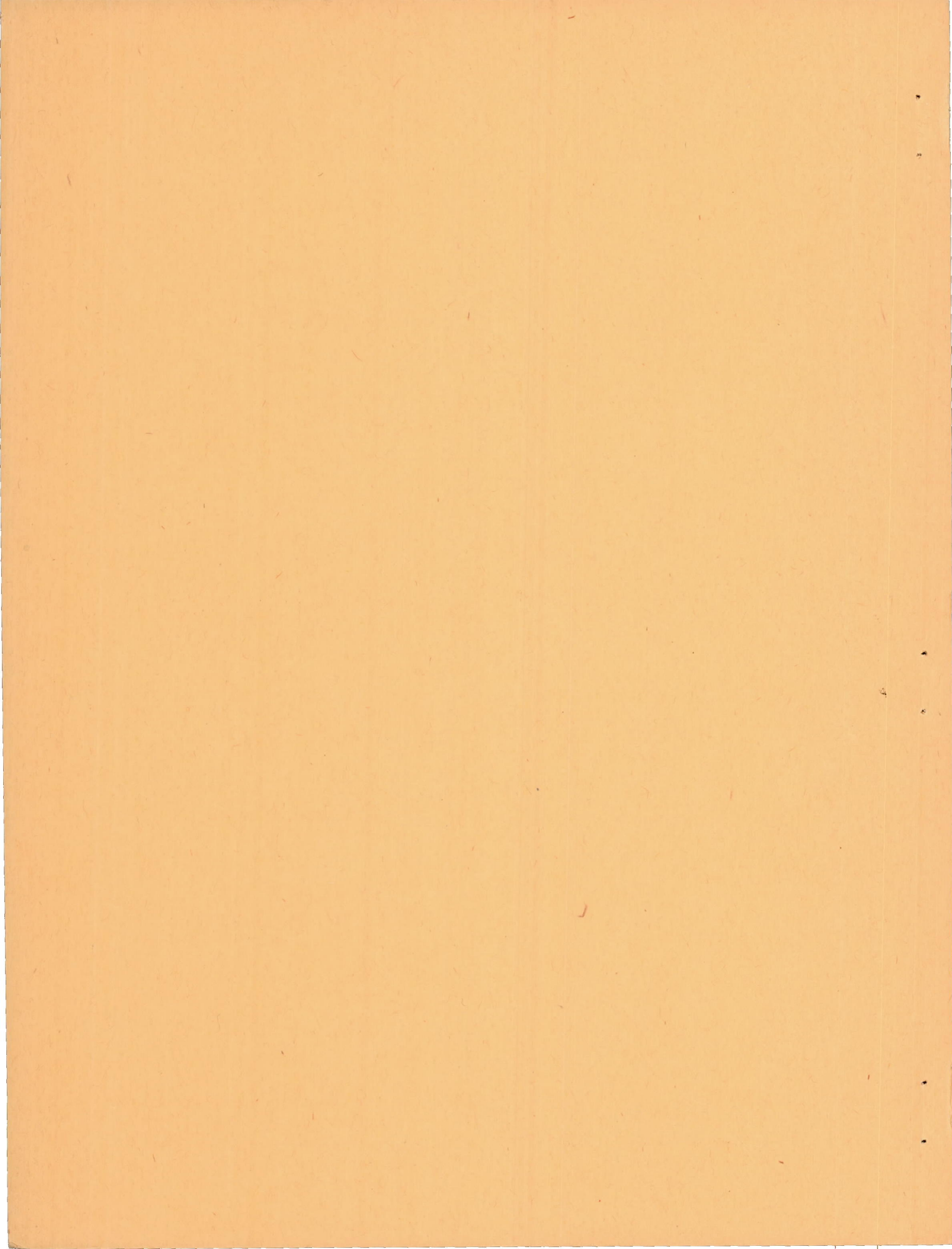
By Arthur R. Wallace, Peter F. Rossi,
and Evalyn G. Wells

Langley Memorial Aeronautical Laboratory
Langley Field, Va.



Washington

April 1947



NATIONAL ADVISORY COMMITTEE FOR AERONAUTICS

TECHNICAL NOTE NO. 1239

WIND-TUNNEL INVESTIGATION OF THE EFFECT OF POWER AND FLAPS
ON THE STATIC LONGITUDINAL STABILITY CHARACTERISTICS
OF A SINGLE-ENGINE LOW-WING AIRPLANE MODEL

By Arthur R. Wallace, Peter F. Rossi,
and Evalyn G. Wells

SUMMARY

As part of a comprehensive investigation of the effect of power, flaps, and wing position on static stability, tests were made in the Langley 7- by 10-foot tunnel to determine the longitudinal stability characteristics with and without power of a typical low-wing, single-engine airplane model with flaps neutral, with a full-span single slotted flap, and with a full-span double slotted flap. The horizontal tail incorporated a leading-edge slot for the flap-deflected conditions and was placed high to avoid the slipstream. Some data are presented for the isolated horizontal tail. With the double slotted flap deflected some air-flow surveys were made in the region of the tail and the wing stall was studied by means of tufts.

With flaps deflected, lift increments were increased by 0.16 for the single slotted flap and 0.42 for the double slotted flap when power was applied. Power also increases the slope of the untrimmed lift curves (increase of 0.034 for the double-slotted-flap condition).

Deflecting the flaps increased longitudinal stability slightly. The windmilling propeller shifted the neutral point forward from 1 to 5 percent mean aerodynamic chord. The effect of power on longitudinal stability was small except for an erratic effect with the single slotted flap and at very high lift coefficients with the double slotted flap. The success in obtaining power-on stability with the double slotted flap was attributed to the fact that the tail was out of the slipstream. The stabilizer nose slot improved the stability and delayed the tail stall but reduced the elevator effectiveness. Sufficient control was provided by the tail as tested. In order to avoid possible tail stall, however, the flaps should be deflected slowly. A larger tail volume would be desirable to provide the necessary tail loads encountered at more forward center-of-gravity locations.

INTRODUCTION

With the development of higher-powered airplane engines, the effects of power on airplane stability have become of considerable importance. The propeller itself has an appreciable effect on airplane stability even when it is in the windmilling condition. When power is applied, the effect of the propeller is much greater. The effect of power on airplane stability may be divided into two parts: first, the direct effects of the propeller - that is, thrust, torque, normal force, and so forth - that act on the airplane through the propeller shaft; and second, the effects of the slip-stream on the other parts of the airplane. Some of the effects of power are shown in references 1 and 2.

Another trend in aeronautical progress is the development of better high-lift devices to improve performance. Recent work has shown that satisfactory lateral-control devices can be developed for full-span flaps, which make the widespread use of such flaps probable. Flaps are known to increase the difficulty of obtaining longitudinal trim and stability for all flight conditions and to increase the adverse effects of power in many cases. The use of higher-lift flaps can be expected to increase the foregoing difficulties until they become very important.

The location of the wing on the fuselage has pronounced effects on airplane stability. High-wing airplanes tend to have more longitudinal stability at medium and high lift coefficients. The vertical location of the wing also influences the effective dihedral and vertical tail effectiveness appreciably (references 3 and 4).

The present paper is the first of a series on an investigation of the effects of power, flap deflection, and vertical position of the wing on longitudinal and lateral stability and control. The results presented herein include only the longitudinal stability and control of the model as a low-wing airplane.

COEFFICIENTS AND SYMBOLS

The results of the tests are presented as standard NACA coefficients of forces and moments. Pitching-moment coefficients are given about the center-of-gravity location shown in figure 1 (26.7 percent M.A.C.). The data are referred to the stability axes, which are a system of axes having their origin at the center of

gravity and in which the Z-axis is in the plane of symmetry and perpendicular to the relative wind, the X-axis is in the plane of symmetry and perpendicular to the Z-axis, and the Y-axis is perpendicular to the plane of symmetry. The positive directions of the stability axes, of angular displacements of the airplane and control surfaces, and of hinge moments are shown in figure 2.

The coefficients and symbols are defined as follows:

| | |
|----------------|--|
| C_L | lift coefficient (Lift/qS) |
| $C_{L_{\max}}$ | maximum lift coefficient |
| ΔC_L | increment in lift coefficient due to flap deflection |
| C_{L_a} | slope of lift curve $\left(\frac{dC_L}{da}\right)$ |
| C_{L_t} | horizontal-tail lift coefficient ($L_t/q_t S_t$) |
| C_X | longitudinal-force coefficient (X/qS) |
| C_m | pitching-moment coefficient (M/qSc') |
| C_{m_0} | tail-off pitching-moment coefficient |
| C_{m_e} | pitching-moment coefficient about the effective tail-off aerodynamic center |
| C_{m_t} | pitching-moment coefficient provided by the tail ($C_{m_{tail\ on}} - C_{m_{tail\ off}}$) |
| C_{h_e} | elevator hinge-moment coefficient ($H_e/qb_e c_e^2$) |
| T_c' | effective thrust coefficient based on wing area (T_{eff}/qS) |
| Q_c | torque coefficient ($Q/\rho V^2 D^3$) |
| V/nD | propeller advance-diameter ratio |
| η | propulsive efficiency ($T_{\text{eff}}V/2\pi n Q$) |
| v_t | horizontal-tail volume coefficient ($S_t l_t / Sc'$) |
| Lift = -Z | |

| | |
|----------------------------|---|
| X} | forces along axes, pounds |
| Z} | |
| M | moment about Y-axis, pound-feet |
| L _t | horizontal-tail lift, positive upward, pounds |
| H _e | elevator hinge moment, pound-feet |
| T _{eff} | propeller effective thrust, pounds |
| Q | propeller torque, pound-feet |
| W | airplane weight, pounds |
| R _e | effective Reynolds number |
| q | free-stream dynamic pressure, pounds per square foot $\left(\frac{\rho V^2}{2}\right)$ |
| q _t | effective dynamic pressure at tail, pounds per square foot |
| S | wing area (9.44 sq ft on model) |
| S _t | horizontal-tail area (1.92 sq ft on model) |
| c | airfoil section chord, feet |
| c* | wing mean aerodynamic chord (1.36 ft on model) |
| \bar{c}_e | elevator root-mean-square chord back of hinge line (0.264 ft on model) |
| b | wing span (7.458 ft on model) unless otherwise designated |
| b _e | elevator span along hinge line (2.546 ft on model) |
| l _t | tail length measured from center of gravity to quarter-chord point of horizontal tail mean aerodynamic chord (3.29 ft on model) |
| V | air velocity, feet per second |
| V _i | indicated airspeed, miles per hour $\left(\frac{\sqrt{\sigma} V}{1.467}\right)$ |
| V _s | rate of descent, feet per second |
| V _{s_i} | indicated rate of descent, feet per second $(\sqrt{\sigma} V_e)$ |

D propeller diameter (2.00 ft on model)

n propeller speed, rps

σ ratio of air density at altitude to air density at sea level

ρ mass density of air, slugs per cubic foot

α angle of attack of fuselage center line, degrees

α_t angle of attack of tail chord line, degrees

ϵ angle of downwash, degrees

i_t angle of stabilizer with respect to fuselage center line,
positive when trailing edge is down, degrees

δ_e elevator deflection, degrees

δ_{f1} deflection of forward part of double slotted flap with
respect to airfoil chord, degrees

δ_{f2} deflection of rearward part of double slotted flap with
respect to forward part, degrees

β propeller blade angle at 0.75 radius (25° on model)

n_o tail-off aerodynamic-center location, percent wing mean
aerodynamic chord

n_p neutral-point location, percent wing mean aerodynamic chord
(center-of-gravity location for neutral stability in
trimmed flight)

Subscript:

b trimmed conditions with center of gravity at the neutral point

MODEL AND APPARATUS

The tests were made in the Langley 7- by 10-foot tunnel described in references 5 and 6. No landing gear was used for the tests. Figure 1 is a three-view drawing of the model. The wing was fitted with a 40-percent-chord double slotted flap covering 93 percent of the span and was designed from the data of reference 7. For the flap-neutral tests the flap was retracted and the gaps were faired to the airfoil contour with modeling clay. For the single-slotted-flap tests, the rear part of the flap was deflected 30° ,

and for tests with the double slotted flap both parts of the flap were deflected 30° (see detail of flap in fig. 1). For the flap-deflected conditions, the gap between the inboard ends of the flap (directly below the fuselage) was sealed with Scotch cellulose tape.

A more detailed drawing of the tail assembly is shown in figure 3. The horizontal tail had an inverted Clark Y section and was equipped with a fixed leading-edge slot. The slat had a constant chord but was located to approximate the best slot shape given in reference 8. The reason for the unusually high tail location (figs. 1 and 3) is given in the section entitled "Discussion." The isolated tail was mounted in the tunnel as shown in figure 4.

Power for the 2-foot-diameter, three-blade, right-hand, metal propeller was obtained from a 56-horsepower water-cooled induction motor mounted in the fuselage. Motor speed was measured by means of an electric tachometer. The dimensional characteristics of the propeller are given in figure 5.

Elevator hinge moments were measured by means of an electric strain gage mounted in the stabilizer. The dynamic pressure and downwash angles in the region of the tail were measured with a bank of pitot-pitch tubes connected to a direct-reading multiple-tube manometer.

TESTS AND RESULTS

Test Conditions

The tests were made in the Langley 7- by 10-foot tunnel at dynamic pressures of 12.53 pounds per square foot for the power-on tests with the double slotted flap and of 16.37 pounds per square foot for all other tests, which correspond to air-speeds of about 70 and 80 miles per hour, respectively. The test Reynolds numbers were about 875,000 and 1,000,000 based on the wing mean aerodynamic chord of 1.36 feet. Because of the turbulence factor of 1.6 for the tunnel, the effective Reynolds numbers (for maximum lift coefficients) were about 1,400,000 and 1,600,000.

Corrections

All power-on data have been corrected for tares caused by the model support strut. No tare corrections were obtained for the power-off tests because they have been found to be relatively small and erratic on similar models with flaps deflected; thus omission

of the power-off tare corrections is not believed to change seriously the results. The test results for the isolated horizontal tail were corrected for tares obtained by testing the tail assembly with the horizontal tail removed. Jet-boundary corrections have been applied to the angles of attack, the longitudinal-force coefficients, the tail-on pitching-moment coefficients, and the downwash angles measured by surveys.

The corrections were computed as follows:

$$\Delta\alpha = 57.3 \delta_w \frac{S}{C} C_L \quad (\text{deg})$$

$$\Delta C_X = -\delta_w \frac{S}{C} C_L^2$$

$$\Delta C_m = -57.3 \left(\frac{\delta_T}{\sqrt{q_t/q}} - \delta_w \right) \frac{S}{C} \frac{\partial C_m}{\partial \delta_t} C_L$$

$$\Delta \epsilon = 57.3 \frac{\delta_T}{\sqrt{q_t/q}} \frac{S}{C} C_L$$

where

δ_w jet-boundary correction factor at wing (0.1125)

δ_T total jet-boundary correction at tail (varies between 0.200 and 0.210)

S model wing area (9.44 sq ft)

C tunnel cross-sectional area (69.59 sq ft)

$\frac{\partial C_m}{\partial \delta_t}$ change in pitching-moment coefficient per degree change in stabilizer setting as determined in tests

q_t/q ratio of effective dynamic pressure over the horizontal tail to free-stream dynamic pressure

All corrections were added to the test data. The equations for the pitching-moment and downwash corrections are explained in reference 9.

Procedure

Propeller calibrations were made by measuring the longitudinal force with the model at zero angle of attack, the flap neutral, and the tail removed for a range of propeller speeds. The effective thrust coefficient was then computed from the relation

$$T_c' = C_x(\text{propeller operating}) - C_x(\text{propeller removed})$$

Motor torque was also measured and propeller efficiency was computed. The propeller calibration is shown in figure 6.

Power-on tests were made with T_c' varying with C_L according to figure 7. A straight-line variation of T_c' with C_L was used because this variation approximates the variation for airplanes with constant-speed propellers operating under conditions of constant power. Preliminary tests were made by setting the propeller speed to obtain a given value of T_c' and then varying the angle of attack α until the value of C_L corresponding to the set value of T_c' , indicated in figure 7, was read on the scale. Subsequent power-on tests with the same flap setting were made at the same propeller speeds and angles of attack as the preliminary tests.

The approximate amount of airplane engine horsepower represented is given in figure 8 for various model scales and wing loadings. The amount of power represented was limited by the maximum output of the model motor and the desire to keep the tunnel air velocity as high as practical so that a reasonable value of Reynolds number could be maintained. The amount of airplane power represented will be found low for many cases.

The value of T_c' for the tests with the propeller windmilling was about -0.005.

Presentation of Results

An outline of the figures presenting the test results is as follows:

| | Figure |
|---|--------|
| Stabilizer tests | 9 - 11 |
| Tuft studies (double slotted flap only) | 12 |
| Effect of removing flap sections | 13 |
| Landing characteristics: | |
| Effect of power and flaps | 14 |
| Effect of scale and wing loading | 15 |

Figure

| | |
|--|---------|
| Neutral points: | |
| Effect of flaps | 16 |
| Effect of power | 17 |
| Increments due to power | 18 |
| Stability parameters: | |
| Effect of flaps | 19 |
| Effect of power | 20 |
| Increments due to power | 21 |
| Air flow at tail (double slotted flap only): | |
| Dynamic-pressure contours | 22 - 23 |
| Downwash contours | 24 - 25 |
| Isolated-tail tests | 26 |
| Elevator tests | 27 - 29 |
| Illustrative solution of q_t/q and ϵ : | |
| Stabilizer tests | 30 |
| Chart for graphical method | 31 |
| Vector diagrams for neutral-point equation | 32 |

DISCUSSION

Lift Characteristics

The following table shows the effect of flaps and power on lift characteristics (figs. 9 to 11):

| Flap | Operating condition | C_L tail off ($\alpha = 0^\circ$) | ΔC_L tail off ($\alpha = 0^\circ$) | $C_{L\alpha}$ ($\alpha = 0^\circ$) |
|----------------|-----------------------|---|--|---|
| Neutral | | 0.27 | ---- | 0.072 |
| Single slotted | Propeller off | 1.34 | 1.07 | .086 |
| Double slotted | | 2.14 | 1.87 | .074 |
| Neutral | | .27 | ---- | .074 |
| Single slotted | Propeller windmilling | 1.33 | 1.06 | .085 |
| Double slotted | | 2.14 | 1.87 | .074 |
| Neutral | | .25 | ---- | .087 |
| Single slotted | Power on | 1.47 | 1.22 | .097 |
| Double slotted | | 2.54 | 2.29 | .108 |

Maximum lift was not attained for all conditions; hence comparison is not possible. Values of trim lift increments not presented in the preceding table will be lower than untrimmed lift increments because of the large down loads required of the tail.

From the foregoing table it can be seen that with flaps deflected, the application of power caused a marked increase in lift-coefficient increment (0.16 with the single slotted flap and 0.42 with the double slotted flap). Power also produced a considerable increase in the slope of the untrimmed lift curves, especially for the double-slotted-flap condition. The noticeable effect of power with full-span single and double slotted flaps deflected can be explained, in part, by the increased dynamic pressure over the wing associated with the high lift coefficients and by the improved flow over the rear flap as shown by the tuft studies of figure 12. With power off, large parts of the rear flap are stalled throughout the angle-of-attack range although the rear flap unstalls when the main part of the wing begins to stall. The effects of the model scale are such that the full-scale airplane may not experience a stalled rear flap.

The tunnel-wall effect and the Reynolds number may be contributing factors in making the wing tips stall first. Computations indicate that the induced upwash at the wing caused by the tunnel walls increased the effective angle of attack of the tip about $0.3C_L$ degrees thus giving the wing an effective washin.

Tests were made with the single slotted flap to determine the effect of removing the section of flap beneath the fuselage (fig. 13). The sketches included in this figure show the flap configurations used. An appreciable loss in lift at a given angle of attack occurs with the gap of 8.1 inches. Although $12\frac{1}{2}$ percent of the wing area is included in the removed part of the flap and of the wing immediately ahead of this flap, the observed loss in flap lift increment is only about $5\frac{1}{2}$ percent; thus apparently over 50 percent of the flap lift increment is carried across the gap. For the gap of 0.6 inch no change was observed in lift.

Landing Characteristics

Landing characteristics were computed for the model based on an effective Reynolds number of 8,000,000 (approximately full size). It was found that a wing loading of approximately 90 pounds per square foot could be attained without exceeding the recommended maximum rate of descent of 25 feet per second (reference 10) with power off and either with flap neutral or single slotted flap deflected (fig. 14). With the double slotted flap deflected, a wing loading of approximately 40 pounds per square foot may be attained without exceeding a rate of descent of 25 feet per second.

With the application of power corresponding to the horsepower in figure 8, with flap neutral, and with single slotted flap deflected, the airplane will tend to gain altitude over most of the lift range.

The power required to maintain an indicated rate of descent of 25 feet per second at $0.85 CL_{max}$ (reference 10) and at various wing loadings is shown in figure 15 for three different model scales ($1/4$, $1/5$, and $1/8$ scales). This figure, derived from the model data of figure 14, also shows the wing loadings that may be attained without exceeding a maximum rate of descent of 25 feet per second with power off. With the application of flaps the power must be increased to maintain an indicated rate of descent of 25 feet per second at a given wing location.

Longitudinal Stability

Method of analysis. - The static longitudinal stability of the model is indicated by the plots of the variation of neutral-point location with CL (figs. 16 and 17). The neutral points were obtained by the methods given in references 11 and 12 from data shown in figures 9 to 11 and 27 to 29.

From the aforementioned references it can be seen that the hinge-moment characteristics of the tail are determining factors in calculating stick-free stability. Because hinge-moment parameters can vary widely for similar tail plan forms, details of the stability computations will be concentrated on the stick-fixed condition.

The quantities which affect the static longitudinal stability (stick fixed) have been separated into the various components of the following equation:

$$n_p = n_o + \frac{v_{t_b} \frac{dC_{L_t}}{da_t} \frac{q_t}{q} \left(1 - \frac{de}{da}\right)}{+ \frac{c_{m_e}}{\left(\frac{dc_L}{da}\right)_b \left[1 - \frac{\frac{d(q_t/q)}{dc_L}}{\frac{q_t/q}{c_L}}\right]}} \quad (1)$$

The derivation of equation (1) is given in the appendix. The terms of the equation, which have been found useful in analysis, are

referred to herein as static-longitudinal-stability parameters. The longitudinal stability parameters were obtained from the tail-off and stabilizer tests and isolated tail tests presented herein. As the slope of the lift curve for the tail is nonlinear, a special method was used to compute q_t/q and ϵ at the tail. (See appendix.) The effect of flap deflection and power on the parameters are presented in figure 19. The same results have been replotted in figure 20 to show the effect of power at various flap deflections. Results of surveys of dynamic pressure and downwash angles made with the double slotted flap are shown by points in the plots of figures 19(c) and 20(c) for comparison. The surveys, however, were made in only two vertical planes 6 inches on either side of the model center line and thus do not represent averages across the span as do the values obtained from stabilizer tests. In the subsequent discussion the effect of flap deflection and power on the neutral-point location will be explained by means of the parameters.

Considerations involved in tail location. - Preliminary estimates obtained from the air-flow surveys of figures 22 to 25 showed that the model with the double slotted flap would be very unstable with power on at all lift coefficients if the tail were placed in the conventional low position. The main destabilizing influence is shown by the third term of the right-hand side of equation (1) which would produce instability at all lift coefficients instead of only at high lift coefficients. The large negative value of C_{m_e} combined with a normal positive value of $\frac{d(q_t/q)}{dC_L}$ when the tail is in the slipstream results in a large destabilizing effect. For this reason the tail was placed as high as practical in an attempt to remove it from the slipstream and thus to reduce $\frac{d(q_t/q)}{dC_L}$ to a low value. (See $\frac{\Delta(q_t/q)}{\Delta C_L}$ in fig. 23.) As shown in figure 20(c), $\frac{d(q_t/q)}{dC_L}$ was reduced to a low value and stability was maintained up to a fairly large value of lift coefficient. Lower and more favorable values of $\Delta\epsilon/\Delta\alpha$ would also be encountered at the higher tail location (fig. 25).

Effect of tail slot. - The use of a slot on the nose of the horizontal tail improved the stability as shown in figure 11 by the increased slope of the C_m curve over that for the tail with the slot filled. This stabilizing effect is explained by the isolated-tail data (fig. 26) which show a higher value of dC_{L_t}/dq_t for the slot-open condition. The neutral points presented for flap neutral and single slotted flap were obtained with the tail slot filled but the neutral points for the double slotted flap were obtained with the tail slot open.

Effect of flap deflection. - With power off, deflecting the flap shifts the neutral point rearward so that the stability is slightly increased. One cause of the rearward shift is shown in figures 19(a) and 19(b) to be the shift in n_o with flap deflection. In the case of the double slotted flap another factor which contributes to the rearward shift of n_o is the fact that the tail slot was open and the slope of the tail lift curve was thus increased. The large value of C_{m_e} is of little significance with power off because $\frac{d(q_t/q)}{dC_L}$ is small. With power on, the same

stabilizing trend of flap deflection is shown except that a peculiar neutral-point variation is shown for the single slotted flap (fig. 16(c)). The neutral-point variation with single slotted flap was traced to the variation of $d\epsilon/d\alpha$ (fig. 19(c)) with C_L . Although the stabilizing influence of n_o became greater as the flaps were deflected with power on, the increase in $dC_L/d\alpha$ reduced the rearward shift of neutral point caused by the flaps to about the same order of magnitude as the shift with power off (fig. 19(c) and equation (1)).

Effect of power. - When the propeller is added and allowed to windmill, the neutral point shifts forward between 1 and 5 percent mean aerodynamic chord (fig. 17). About 1 percent of this shift in neutral point was traced to the forward shift of n_o when the propeller was added. The remainder of this shift can be accounted for by the slight increases in $d\epsilon/d\alpha$ and $(dC_L/d\alpha)_b$ with propeller windmilling (fig. 20).

The application of power with flap neutral shifts the neutral point no more than 1 percent mean aerodynamic chord over the windmilling condition (figs. 17 and 18). The destabilizing influence of the increased $d\epsilon/d\alpha$ and $dC_L/d\alpha$ apparently is offset by the stabilizing influence of n_o , q_t/q , and $\frac{d(q_t/q)}{dC_L}$ (figs. 20(a)

and 21). With the single slotted flap the variation of neutral point with power on, as previously discussed, makes the increment due to power very erratic. With the double slotted flap the effect of power is very small up to a C_L of about 2.3 beyond which the power-on neutral point moves rapidly forward (figs. 17(c) and 18). As is the case with flap neutral, there is a balancing of the stabilizing and destabilizing effects. The tail-off center of gravity n_o shifts rearward about 15 percent mean aerodynamic chord but this shift is offset primarily by the destabilizing effects of the increase in $d\epsilon/d\alpha$ and $(dC_L/d\alpha)_b$ with power

(figs. 20(c) and 21). At high values of C_L the rapid forward movement of the neutral point seems to be caused by several of the parameters. The value of n_o moves forward quite rapidly; $d(q_t/q)$

$\frac{dC_L}{dC_L}$ increases and, in combination with the large negative value of C_{m_e} , produces a large destabilizing effect as shown by the last term of equation (1).

Longitudinal Control and Trim

Since the tail-off pitching-moment coefficients are highly negative, especially with the full-span double slotted flap (fig. 11), the tail load for trim is very large. Preliminary calculations showed that with the conventional tail size used, the tail would stall when the value of C_L with flap down was reduced to a moderately low value. In order to prevent the early tail stall a leading-edge slot was installed in the tail. According to available data, a slot is more effective on cambered sections. For this reason a cambered section (Clark Y) was used for the tail. Tests of the tail with and without the nose slot filled showed that a large negative angle of attack and lift coefficient were obtainable with the slot open (fig. 26). The Clark Y section was mounted inverted since the tail load with flap deflected is down. An airplane having a slotted tail would probably also require an adjustable stabilizer to obtain the advantage of the slot. In addition, the slot was assumed to be retractable so that the slot could be closed when the airplane was cruising with flaps neutral.

The angle of attack of the horizontal tail can be obtained from the following equation:

$$\alpha_t = \alpha + i_t - \epsilon$$

For the double slotted flap with power on at $\alpha = -8^\circ$ and $C_{Lb} = 1.46$, α_t is computed by using figures 11 and 19(c).

Thus,

$$\alpha_t = -8^\circ - 1.3^\circ - 8^\circ = -17.3^\circ$$

Reference to the isolated-tail data of figure 26 shows that a tail angle of attack of -17.3° is beyond the stall for the slot-filled case but not for the slot-open case. Although the tail stall is not apparent in the C_m of figure 11, tail stall is indicated by the

sharp rise of elevator hinge moments with the nose slot filled. Of course, at a value of C_L lower than the value tested, the tail with the nose slot open would also stall. Tail stall would be indicated to the pilot by a sudden uncontrollable tendency of the airplane to dive. Even with the slot open, forward movement of the center of gravity would be seriously limited with the double slotted flap because of excessive tail loads required for trim. A larger tail volume would improve this situation.

Elevator effectiveness (figs. 27 to 29) is normal and about the same for each flap deflection except the double slotted flap with the tail slot open. The low elevator effectiveness with the double slotted flap is explained by comparing the isolated tail data with tail slot open and filled. (See fig. 26.) The parameters $dC_{L_t}/d\delta_e$ and $d\alpha_t/d\delta_e$ are smaller with slot open in the α_t range through which the tail is operating. Elevator effectiveness increases for the power-on conditions at the higher values of C_L where the tail enters the edge of the slipstream.

In summarizing the importance of the tail in regard to both stability and control, it appears that raising the tail to provide adequate stability removes it from regions of higher dynamic pressures which are necessary for providing control in the case of the tail tested. Control is possible with the tail as tested, provided that the flaps are deflected gradually to avoid a possible tail stall.

CONCLUSIONS

The following conclusions were reached with regard to the longitudinal characteristics of a low-wing, single-engine model with full-span flaps and an elevated horizontal tail:

1. With flaps deflected, the application of power caused a marked increase in lift coefficient increment (0.16 for the single slotted flap and 0.42 for the double slotted flap).
2. Power increased the slope of the untrimmed lift curves (0.03⁴ increase for the double-slotted-flap case).
3. Deflecting either the single or double slotted flap increased the stability slightly with power off.

4. Adding the windmilling propeller shifted the neutral point forward between 1 and 5 percent mean aerodynamic chord. Power shifted the neutral point no more than 1 percent mean aerodynamic chord with flaps neutral.

5. With the single slotted flap, power was, in general, destabilizing and the effect varied greatly with lift coefficient. With the double slotted flap, power had only a very small effect on stability up to a lift coefficient of about 2.3 when the neutral point moved rapidly forward. The success in obtaining power-on stability for most of the lift coefficient range was attributed to the tail being out of the slipstream.

6. Elevator effectiveness was adequate and normal with flaps neutral and with the single slotted flap. The stabilizer nose slot, which was open with the double slotted flap deflected, caused a low elevator effectiveness.

7. The stabilizer nose slot delayed the tail stall with the double slotted flap. Forward center-of-gravity travel would be seriously limited, however, even with the stabilizer slot open because of excessive tail loads required for trim.

8. A larger tail volume would provide a more satisfactory control for the particular airplane model, especially at the forward center-of-gravity locations where larger downloads will be required by the tail for trim.

Langley Memorial Aeronautical Laboratory
National Advisory Committee for Aeronautics
Langley Field, Va., October 29, 1946

APPENDIX

METHOD OF OBTAINING DYNAMIC PRESSURE AND DOWNWASH AT THE TAIL
 WHEN THE TAIL LIFT CURVE IS NONLINEAR AND DERIVATION
 OF NEUTRAL-POINT EQUATION

Tabular procedure for determining q_t/q and ϵ .- A simple and commonly used method for obtaining the effective dynamic-pressure ratio q_t/q , especially when isolated-horizontal-tail data are lacking, is as follows

$$\frac{q_t}{q} = \frac{\frac{dC_m}{di_t}}{\left(\frac{dC_m}{di_t}\right)_{\max}} = \frac{\frac{C_{m2} - C_{m1}}{i_{t2} - i_{t1}}}{\left(\frac{C_{m2} - C_{m1}}{i_{t2} - i_{t1}}\right)_{\max}} \quad (A1)$$

where $\left(\frac{dC_m}{di_t}\right)_{\max}$ is the maximum value obtained by use of propeller-off stabilizer curves (propeller-windmilling stabilizer curves may be used in the absence of propeller-off data). The value

of $\left(\frac{dC_m}{di_t}\right)_{\max}$ may be estimated from the slope of the tail lift curve

obtained from tests of the isolated tail or estimated from the aspect ratio of the tail. The effective downwash angle ϵ , in the absence of isolated-horizontal-tail data, may be obtained from the following equations:

$$\alpha_{t1} = \frac{C_{m_{t1}}}{\frac{dC_m}{di_t}} = \frac{C_{m1} - C_{m0}}{\frac{C_{m2} - C_{m1}}{i_{t2} - i_{t1}}} \quad (A2)$$

$$\epsilon = \alpha + i_{t1} - \alpha_{t1} \quad (A3)$$

When this method was applied to the present model, the agreement between q_t/q and ϵ obtained by surveys made with pitot-pitch tubes and computed values of q_t/q and ϵ was found to be very poor. This discrepancy was traced to the fact that the slope of the tail lift curve was not linear, especially with the tail slot open (fig. 26), as was assumed with the foregoing method of computation. In order to deal with this situation a method of computation was developed for which good agreement was obtained with the surveys (fig. 19). In addition to test data obtained with tail off and with two stabilizer settings, test data are required of the tail lift coefficient against tail angle of attack.

At any one angle of attack the pitching-moment coefficient C_{m_t} provided by the tail is a function of the tail volume v_t , the effective dynamic-pressure ratio q_t/q , and the tail lift coefficient C_{L_t} . This relation is expressed as

$$\begin{aligned} C_{m_{t1}} &= C_{m1} - C_{m0} \\ &= -C_{L_{t1}} \frac{q_t}{q} v_t \end{aligned}$$

from which

$$C_{L_{t1}} = -\frac{C_{m_{t1}}/v_t}{q_t/q} \quad (A4)$$

Likewise, at any one angle of attack, a change in stabilizer incidence will result in a change in tail lift coefficient ΔC_{L_t} and a corresponding change in pitching-moment coefficient ΔC_m , or

$$\begin{aligned} \Delta C_m &= C_{m2} - C_{m1} \\ &= -\Delta C_{L_t} \frac{q_t}{q} v_t \end{aligned}$$

from which

$$\frac{q_t}{q} = -\frac{\Delta C_m/v_t}{\Delta C_{L_t}} \quad (A5)$$

where

$$\Delta C_{L_t} = C_{L_{t_2}} - C_{L_{t_1}}$$

When the isolated horizontal tail possesses a constant lift-curve slope, the effective dynamic-pressure ratio q_t/q may be determined directly by dividing both sides of equation (A5) by Δi_t and transposing; thus

$$\frac{q_t}{q} = \frac{\frac{dC_m/di_t}{dC_{L_t}}}{\frac{d\alpha_t}{d\alpha_t} v_t} \quad (A6)$$

where dC_m/di_t is determined from stabilizer tests and $dC_{L_t}/d\alpha_t$ is determined from isolated-tail tests. Equation (A6) is an improvement over equation (A1) but is based on the assumption that the slope of the lift curve is linear throughout the tail-angle-of-attack range. In cases where the horizontal tail does not possess linear lift-curve characteristics the solution is not so direct. In attempting to use equations (A4) and (A5), the tail volume v_t may be obtained from dimensions of the model, and the values of ΔC_m and C_{m_t} may be determined from the wind-tunnel data at any one angle of attack; however, three quantities remain unknown, namely, the related values C_{L_t} , ΔC_{L_t} , and q_t/q . Since there are only two equations, a direct solution is not feasible. The following successive approximations are therefore made:

(1) If v_t , C_{m_t} , and ΔC_m have been obtained for some one angle of attack, a first approximation of q_t/q is obtained from equation (A6) by using an average value of $dC_{L_t}/d\alpha_t$ from isolated-tail data.

(2) Upon substituting q_t/q into equation (A4), solving for $C_{L_{t_1}}$, and referring to the isolated-tail lift curve (fig. 26) to determine the corresponding tail angle of attack α_t , the tail angle of attack at i_{t_2} may be obtained from the relationship

$$\alpha_{t_2} = \alpha_{t_1} + (i_{t_2} - i_{t_1}) \quad (A7)$$

(3) By referring to the isolated-tail lift curve, the value of $C_{L_{t_2}}$ that corresponds to α_{t_2} is determined; the evaluation of

$$\Delta C_{L_t} = C_{L_{t_2}} - C_{L_{t_1}}$$

is then made possible.

(4) Upon substituting the value of ΔC_{L_t} into equation (A5), the value of q_t/q is obtained. If this value of q_t/q is numerically equal to the value obtained in step 1, the effective value of q_t/q has been found.

(5) If, on the other hand, the values of q_t/q are not in agreement, the value of q_t/q found in step 4 is used in repeating steps 2 through 4. A more rapid convergence is sometimes found to occur if the average of the last two values of q_t/q are used for the next approximation.

(6) Steps 2 through 5 are repeated until two successive values of q_t/q are in agreement within the accuracy of the data. The effective dynamic-pressure ratio has then been determined.

(7) When the effective dynamic-pressure ratio has been determined and the value of α_{t_1} can then be obtained from

figure 26(c) the downwash angle is obtained from the relation

$$\epsilon = \alpha + i_{t_1} - \alpha_{t_1} \quad (A8)$$

Table III presents a solution for q_t/q and ϵ for one angle of attack of the model (fig. 1) with double slotted flaps down and power on. The pertinent aerodynamic data are presented in figures 11 and 26. The procedure for obtaining additional data needed to determine q_t/q and ϵ is illustrated in figure 30. The initial approximation of q_t/q was obtained by using equation (A6).

Graphical procedure for determining q_t/q and ϵ . - The use of a tabular procedure such as exemplified by the illustrative solution of table III will be found rather tedious when a range of angle of attack and flight conditions is being investigated. In order to reduce appreciably the time and to simplify the solution to some

extent, a chart has been prepared for determining the values of q_t/q and tail angle of attack graphically. This chart, shown as two separate parts by figures 31(a) and 31(b), has been found to be very effective when placed side by side with the families of curves laid out to about twice the scale of figure 31.

The family of curves in the upper part of figure 31(a) is the graphical representation of equation (A4); the lone curve in the lower part of figure 31(a) is a specific isolated-tail lift curve for the model in question. The family of curves in figure 31(b) is the graphical representation of equation (A5).

In order to use the chart it will be found desirable to set up a table such as table IV in which the first seven columns are the same as those of table III. For a given angle of attack, horizontal reference lines corresponding to the values of $\frac{C_{m_t}}{v_t}$ and $\frac{\Delta C_m}{v_t}$

given in table IV should first be drawn as shown in figures 31(a) and 31(b). These two lines form the reference lines for the successive approximations for the model angle of attack concerned.

By use of the model data considered in illustrating the tabular approach of table IV, the intersection of the first approximation of q_t/q (1.494) with $\frac{C_{m_t}}{v_t}$ (0.985) should now be located

in figure 31(a); the first approximation of C_{L_t} is thus determined.

By projecting this intersection down to the isolated tail lift curve and using a specially devised cardboard or celluloid scale (shown in fig. 31) having sides at right angles to each other and graduated to conform to the ordinates and abscissa of the lift curve, the value of ΔC_{L_t} (0.403) resulting from Δi_t (8.3°) (see fig. 30) is readily determined (fig. 31(a)).

At the intersection of this first approximation of ΔC_{L_t} (0.403) with $\frac{\Delta C_m}{v_t}$ (-0.496) in figure 31(b), the second approximation of q_t/q may be read from the bottom scale. Since this second approximation of q_t/q is not in agreement with the first approximation, the entire procedure is repeated as many times as is necessary to obtain agreement between two consecutive values of q_t/q . When the procedure is continued, the last value of q_t/q obtained should be used for the next successive approximation. Although figures 31(a) and 31(b) merely show by means of the dashed lines the work for

obtaining the second approximation of q_t/q , table IV gives the successive values of q_t/q and ΔC_{L_t} obtained as well as the final answer for q_t/q and ϵ . The value of ϵ is obtained from a_t , which should be read from the tail lift curve (fig. 31(a)) during the final approximation.

The solution of q_t/q in table IV illustrates the discrepancy resulting from the use of the approximate method formerly used to obtain q_t/q by assuming a linear tail lift curve. The present refined method gives a value of $q_t/q = 1.115$ (column (19), table IV) whereas the approximate method gives a value of $q_t/q = 1.494$ (column (7), table IV) or about 38-percent error.

Comparison of the tabular and graphical procedures for determining q_t/q and ϵ . - The graphical solution as presented provides a very good degree of accuracy. Comparisons between the tabular approach, such as table III, and the graphical approach to the solution of q_t/q and ϵ at the tail for various models has shown consistent agreement through the second decimal place. The use of the graphical approach permits a better than 60-percent saving in time when compared to a tabular solution using a slide rule, and about a 40-percent saving in time when compared to a tabular solution using a calculating machine, particularly when the tail lift curve is nonlinear.

Neutral-point equation. - A neutral point is defined as a center-of-gravity location for which the curve of C_m against C_L has zero slope at the trim lift coefficient C_{L_b} . The measurement of the slope C_m/C_L with tail off C_{m_e} gives the tail-off aerodynamic center n_o ; with tail on, C_m gives the neutral point n_p . (See fig. 32(a).)

At trim, the wing-fuselage pitching-moment coefficient equals the negative of the pitching-moment coefficient contributed by the tail. For the center of gravity at the neutral point this relation may be expressed by

$$C_{m_e} + C_{L_b} (n_p - n_o) = v_{t_b} C_{L_t} (q_t/q) \quad (A9)$$

The term C_{m_e} represents the pitching moment of the wing-fuselage about the tail-off neutral point n_o at trim. (This term may be evaluated from the tail-off pitching-moment data obtained from figure 32(b).)

Differentiating equation (A9) with respect to C_L gives

$$n_p - n_o = v_{t_b} C_{L_t} \left(\frac{d \frac{q_t}{q}}{d C_L} \right)_b + \frac{v_{t_b} \frac{d C_{L_t}}{d \alpha_t} \left(1 - \frac{d \epsilon}{d \alpha} \right) \frac{q_t}{q}}{\left(\frac{d C_L}{d \alpha} \right)_b} \quad (A10)$$

The derivatives are to be evaluated with the trim variation of T_c with C_L . Solving equation (A9) for $v_{t_b} C_{L_t}$ and substituting in equation (A10) yields

$$n_p - n_o = \frac{C_{m_e} + C_{L_b} (n_p - n_o)}{q_t/q} \left(\frac{d \frac{q_t}{q}}{d C_L} \right)_b + \frac{v_{t_b} \frac{d C_{L_t}}{d \alpha_t} \left(1 - \frac{d \epsilon}{d \alpha} \right) \frac{q_t}{q}}{\left(\frac{d C_L}{d \alpha} \right)_b} \quad (A11)$$

Solving for n_p gives

$$n_p = n_o + \frac{v_{t_b} \frac{d C_{L_t}}{d \alpha_t} \frac{q_t}{q} \left(1 - \frac{d \epsilon}{d \alpha} \right)}{\left(\frac{d C_L}{d \alpha} \right)_b \left[1 - \frac{d(q_t/q)}{d C_L} \right]} + \frac{C_{m_e}}{C_L \left[\frac{1}{d(q_t/q)/q_t/q} - 1 \right]} \quad (A12)$$

Derivation of $(d C_L/d \alpha)_b$.- The term $(d C_L/d \alpha)_b$ is derived as follows (see fig. 32(c)):

$$C_{L_b} = C_{L(\text{tail off})} + C_{L_t}$$

$$C_{L(\text{tail off})}(n_p - n_o) = C_{L_t}(\iota_t/c)$$

$$C_{I_b} = C_{L(\text{tail off})} + C_{L(\text{tail off})} \left(\frac{n_p - n_o}{l_t/c} \right)$$

$$C_{I_b} = C_{L(\text{tail off})} \left(1 + \frac{n_p - n_o}{l_t/c} \right)$$

$$(24) \quad \left(\frac{dC_L}{d\alpha} \right)_b = \frac{dC_{I_b(\text{tail off})}}{d\alpha} \left(1 + \frac{n_p - n_o}{l_t/c} \right)$$

In order to use the preceding equation, the neutral point must be known.

REFERENCES

1. Millikan, Clark B.: The Influence of Running Propellers on Airplane Characteristics. *Jour. Aero. Sci.*, vol. 7, no. 3, Jan. 1940, pp. 85-103. (Discussion, pp. 103-106.)
2. Recant, Isidore G., and Swanson, Robert S.: Determination of the Stability and Control Characteristics of Airplanes from Tests of Powered Models. *NACA ARR*, July 1942.
3. Sherman, Albert: Interference of Tail Surfaces and Wing and Fuselage from Tests of 17 Combinations in the N.A.C.A. Variable-Density Tunnel. *NACA Rep. No. 678*, 1939.
4. Wallace, Arthur R., and Turner, Thomas R.: Wind-Tunnel Investigation of Effect of Yaw on Lateral-Stability Characteristics. V - Symmetrically Tapered Wing with a Circular Fuselage Having a Horizontal and a Vertical Tail. *NACA ARR No. 3F23*, 1943.
5. Harris, Thomas A.: The 7 by 10 Foot Wind Tunnel of the National Advisory Committee for Aeronautics. *NACA Rep. No. 412*, 1931.
6. Wenzinger, Carl J., and Harris, Thomas A.: Wind-Tunnel Investigation of an N.A.C.A. 23012 Airfoil with Various Arrangements of Slotted Flaps. *NACA Rep. No. 664*, 1939.
7. Harris, Thomas A., and Recant, Isidore G.: Wind-Tunnel Investigation of NACA 23012, 23021, and 23030 Airfoils Equipped with 40 Percent-Chord Double Slotted Flaps. *NACA Rep. No. 723*, 1941.
8. Weick, Fred E., and Wenzinger, Carl J.: The Characteristics of a Clark Y Wing Model Equipped with Several Forms of Low-Drag Fixed Slots. *NACA Rep. No. 407*, 1932.
9. Swanson, Robert S., and Schuldenfrei, Marvin J.: Jet-Boundary Corrections to the Downwash behind Powered Models in Rectangular Wind Tunnels with Numerical Values for 7- by 10-Foot Closed Wind Tunnels. *NACA ARR*, Aug. 1942.

10. Gustafson, F. B., and O'Sullivan, William J., Jr.: The Effect of High Wing Loading on Landing Technique and Distance, with Experimental Data for the B-26 Airplane. NACA ARR No. L4K07, 1945.
11. Schuldenfrei, Marvin: Some Notes on the Determination of the Stick-Fixed Neutral Point from Wind-Tunnel Data. NACA RB No. 3I20, 1943.
12. Schuldenfrei, Marvin: Some Notes on the Determination of the Stick-Free Neutral Point from Wind-Tunnel Data. NACA RB No. 4B21, 1944.

TABLE I
MODEL WING AND TAIL-SURFACE DATA

| | Wing | Horizontal tail | Vertical tail |
|---|-----------|--------------------|---------------|
| Area, sq ft | 9.440 | 1.920 | 1.250 |
| Span, ft | 7.458 | 2.542 | 1.505 |
| Aspect ratio | 5.91 | 3.36 | 1.81 |
| Taper ratio | 0.445 | 0.438 | ---- |
| ^a Dihedral, deg | 5.8 | 0 | ---- |
| Sweepback, quarter chord line, deg | 1.9 | ---- | ---- |
| Root section | NACA 2215 | Clark Y (inverted) | NACA 0009 |
| Tip section | NACA 2209 | Clark Y (inverted) | NACA 0004.5 |
| ^b Angle of incidence at root, deg | 1.00 | -1.3 or 7 | -1.50 |
| ^b Angle of incidence at tip, deg | 1.00 | -1.3 or 7 | -1.50 |
| Mean aerodynamic center, ft | 1.36 | ---- | ---- |
| Root chord, ft | 1.80 | 1.141 | 1.272 |
| Theoretical tip chord, ft | 0.80 | 0.500 | ---- |

^aDihedral measured with respect to chord plane.

^bAngle of incidence measured with respect to fuselage center line.

TABLE II
AIRPLANE CONTROL-SURFACE DATA

| | Elevators | Rudder | Flaps |
|--|-----------|---------|-------|
| Percent span | 99.5 | 99.1 | 93.0 |
| Area behind hinge line, sq ft | 0.621 | 0.506 | ---- |
| Balance area, sq ft | 0.131 | Minimum | ---- |
| Root-mean-square chord behind hinge line, ft | 0.264 | 0.353 | ---- |
| Distance to hinge line from normal center of gravity, ft | 3.721 | 3.611 | ---- |

TABLE III
PROCEDURE FOR DETERMINATION OF EFFECTIVE DYNAMIC-PRESSURE RATIO AND
EFFECTIVE DOWNWASH ANGLE AT THE HORIZONTAL TAIL OF AN AIRPLANE MODEL

Configuration: Double slotted flap deflected and power on.

$$\alpha = 0^\circ; v_t = 0.532; i_{t_1} = -1.3^\circ; i_{t_2} = 7.0^\circ; \left(\frac{dc_{L_t}}{da_t} \right)_{\alpha=0} = 0.040$$

Aerodynamic data obtained from figures 10 and 11.

$$\text{Initial } \frac{q_t}{q} \text{ value approximated from } \left(\frac{q_t}{q} \right)_1 = - \frac{\frac{dc_{L_t}}{da_t}}{v_t \left(\frac{dc_{L_t}}{da_t} \right)_{\alpha=0}}$$

| (1) | (2) | (3) | (4) | (5) | (6) | (7) | (8) | (9) | (10) |
|---|----------------------------------|----------------------------------|----------------------------------|------------------------------|------------------------------|----------------------------------|----------------------------------|-----------------|-----------------------------|
| α | c_{m_1} | c_{m_2} | c_{m_0} | $\frac{\Delta c_m}{v_t}$ | $\frac{c_{m_{t_1}}}{v_t}$ | $\left(\frac{q_t}{q} \right)_1$ | $c_{L_{t_1}}$ | α_{t_1} | α_{t_2} |
| | $i_{t_1} = -1.3^\circ$ | $i_{t_2} = 7.0^\circ$ | Tail off | $\frac{(3) - (2)}{v_t}$ | $\frac{(2) - (4)}{v_t}$ | | $-\frac{(6)}{(7)}$ | From tail curve | $(9) + (i_{t_2} - i_{t_1})$ |
| 0 | -0.317 | -0.581 | -0.841 | -0.496 | 0.985 | 1.494 | -0.659 | -9.88 | -1.58 |
| (11) | (12) | (13) | (14) | (15) | (16) | (17) | (18) | | |
| $c_{L_{t_2}}$ | $(\Delta c_{L_t})_1$ | $\left(\frac{q_t}{q} \right)_2$ | $c_{L_{t_1}}$ | α_{t_1} | α_{t_2} | $c_{L_{t_2}}$ | $(\Delta c_{L_t})_2$ | | |
| From tail curve | $(11) - (8)$ | $-\frac{(5)}{(12)}$ | $-\frac{(6)}{(13)}$ | From tail curve | $(15) + (i_{t_2} - i_{t_1})$ | From tail curve | $(17) - (14)$ | | |
| -0.256 | 0.403 | 1.231 | -0.800 | -12.58 | -4.28 | -0.360 | 0.440 | | |
| (19) | (20) | (21) | (22) | (23) | (24) | (25) | (26) | (27) | |
| $\left(\frac{q_t}{q} \right)_3$ | $c_{L_{t_1}}$ | α_{t_1} | α_{t_2} | $c_{L_{t_2}}$ | $(\Delta c_{L_t})_3$ | $\left(\frac{q_t}{q} \right)_4$ | $c_{L_{t_1}}$ | α_{t_1} | |
| $-\frac{(5)}{(18)}$ | $-\frac{(6)}{(19)}$ | From tail curve | $(21) + (i_{t_2} - i_{t_1})$ | From tail curve | $(23) - (20)$ | $-\frac{(5)}{(24)}$ | $-\frac{(6)}{(25)}$ | From tail curve | |
| 1.127 | -0.874 | -13.99 | -5.69 | -0.432 | 0.442 | 1.123 | 0.878 | -14.02 | |
| (28) | (29) | (30) | (31) | (32) | (33) | (34) | (35) | | |
| α_{t_2} | $c_{L_{t_2}}$ | $(\Delta c_{L_t})_4$ | $\left(\frac{q_t}{q} \right)_5$ | $c_{L_{t_1}}$ | α_{t_1} | α_{t_2} | $c_{L_{t_2}}$ | | |
| $(27) + (i_{t_2} - i_{t_1})$ | From tail curve | $(29) - (26)$ | $-\frac{(5)}{(30)}$ | $-\frac{(6)}{(31)}$ | From tail curve | $(33) + (i_{t_2} - i_{t_1})$ | From tail curve | | |
| -5.72 | -0.434 | 0.444 | 1.117 | -0.882 | -14.05 | -5.75 | -0.437 | | |
| (36) | (37) | (38) | (39) | (40) | (41) | (42) | (43) | | |
| $(\Delta c_{L_t})_5$ | $\left(\frac{q_t}{q} \right)_6$ | $c_{L_{t_1}}$ | α_{t_1} | α_{t_2} | $c_{L_{t_2}}$ | $(\Delta c_{L_t})_6$ | $\left(\frac{q_t}{q} \right)_7$ | | |
| $(35) - (32)$ | $-\frac{(5)}{(36)}$ | $-\frac{(6)}{(37)}$ | From tail curve | $(39) + (i_{t_2} - i_{t_1})$ | From tail curve | $(41) - (38)$ | $-\frac{(5)}{(42)}$ | | |
| 0.445 | 1.115 | -0.883 | -14.07 | -5.77 | -0.438 | 0.445 | 1.115 | | |
| Effective $\frac{q_t}{q} = 1.115$, since $\alpha_{t_1} = -14.1^\circ$ $\epsilon = \alpha + i_{t_1} - \alpha_{t_1}$ $= 0 - 1.3 - (-14.1)$ $= 12.8^\circ$ | | | | | | | | | |

TABLE IV

TABLE FOR USE WITH THE GRAPHICAL SOLUTION OF EFFECTIVE DYNAMIC-PRESSURE RATIO
AND EFFECTIVE DOWNWASH ANGLE AT THE HORIZONTAL TAIL OF AN AIRPLANE MODEL

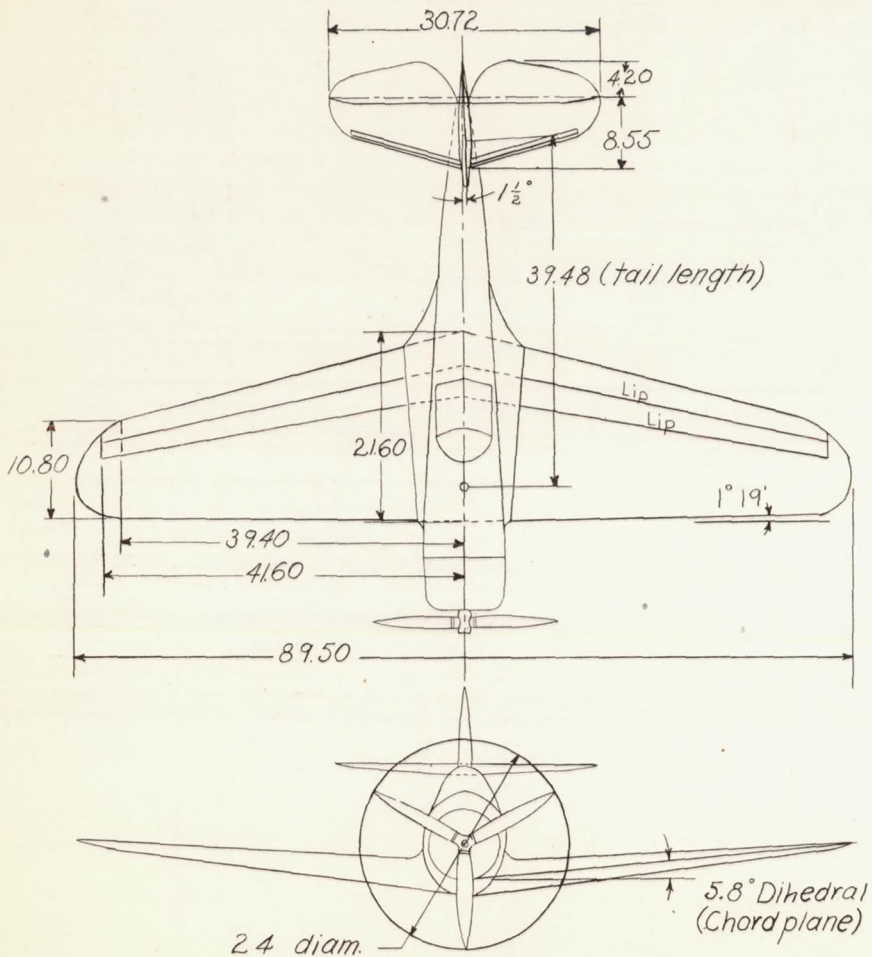
Configuration: Double slotted flap deflected and power on.

$$\alpha = 0^\circ; v_t = 0.532; i_{t_1} = -1.3^\circ; i_{t_2} = 7.0^\circ; \left(\frac{dc_{L_t}}{da_t} \right)_{a=0} = 0.040$$

Aerodynamic data obtained from figures 10 and 11.

$$\text{Initial } \frac{q_t}{q} \text{ value approximated from } \left(\frac{q_t}{q} \right)_1 = - \frac{\frac{dc_m}{di_t}}{v_t \left(\frac{dc_L}{da} \right)_{a=0}}$$

| (1) | (2) | (3) | (4) | (5) | (6) | (7) | (8) | (9) | (10) |
|--|----------------------|----------------------------------|----------------------|----------------------------------|-----------------------|----------------------------------|----------------------|----------------------------------|----------------------|
| α | c_{m_1} | c_{m_2} | c_{m_0} | $\frac{\Delta c_m}{v_t}$ | $\frac{c_{m_1}}{v_t}$ | $\left(\frac{q_t}{q} \right)_1$ | $(\Delta c_{L_t})_1$ | $\left(\frac{q_t}{q} \right)_2$ | $(\Delta c_{L_t})_2$ |
| 0 | -0.317 | -0.581 | -0.841 | -0.496 | 0.985 | 1.494 | 0.403 | 1.231 | 0.440 |
| (11) | (12) | (13) | (14) | (15) | (16) | (17) | (18) | (19) | |
| $\left(\frac{q_t}{q} \right)_3$ | $(\Delta c_{L_t})_3$ | $\left(\frac{q_t}{q} \right)_4$ | $(\Delta c_{L_t})_4$ | $\left(\frac{q_t}{q} \right)_5$ | $(\Delta c_{L_t})_5$ | $\left(\frac{q_t}{q} \right)_6$ | $(\Delta c_{L_t})_6$ | $\left(\frac{q_t}{q} \right)_7$ | |
| 1.127 | 0.442 | 1.122 | 0.444 | 1.117 | 0.445 | 1.115 | 0.445 | 1.115 | |
| <p>Effective $\frac{q_t}{q} = 1.115$, since $\alpha_{t_1} = -14.1$</p> $\epsilon = \alpha + i_{t_1} - \alpha_{t_1}$ $= 0 - 1.3 - (-14.1)$ $= 12.8^\circ$ | | | | | | | | | |



Geometric characteristics

| | |
|-------------------------------|-----------|
| Wing area, sq ft | 9.44 |
| MAC, ft | 1.36 |
| C.G. (percent MAC) | 26.70 |
| Wing section | |
| Root | NACA 2215 |
| Tip | NACA 2209 |
| Wing incidence, deg | 1.0 |

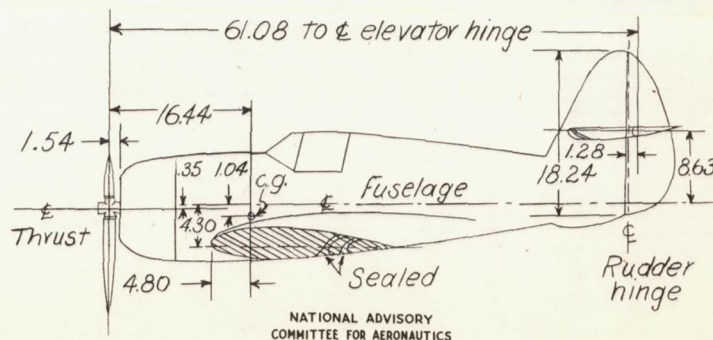
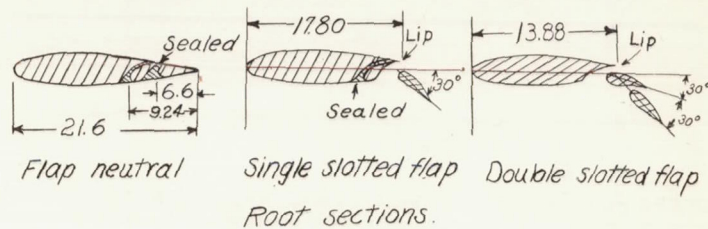


Figure 1.- Three-view drawing of model as a low-wing airplane. All dimensions are in inches.

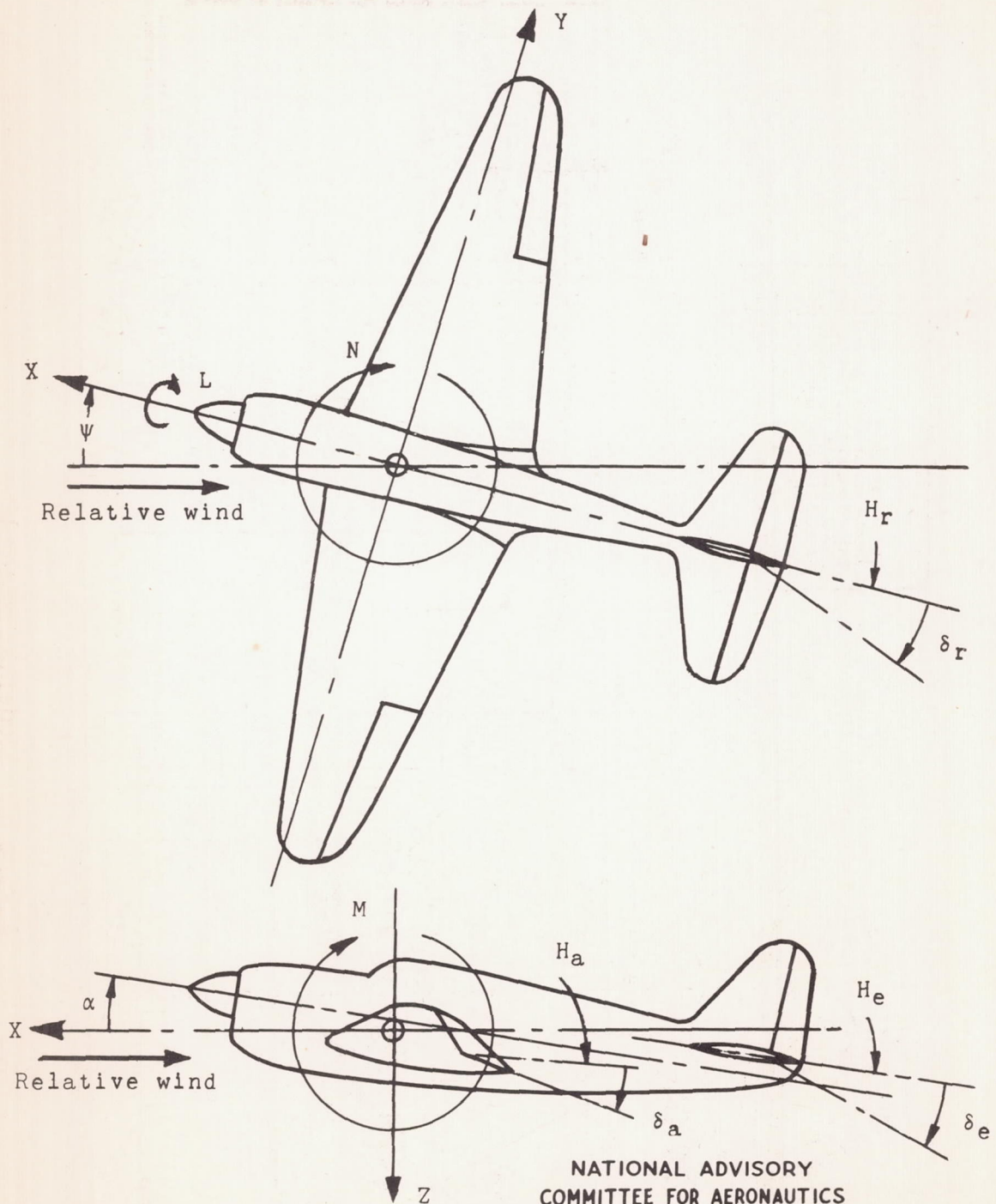
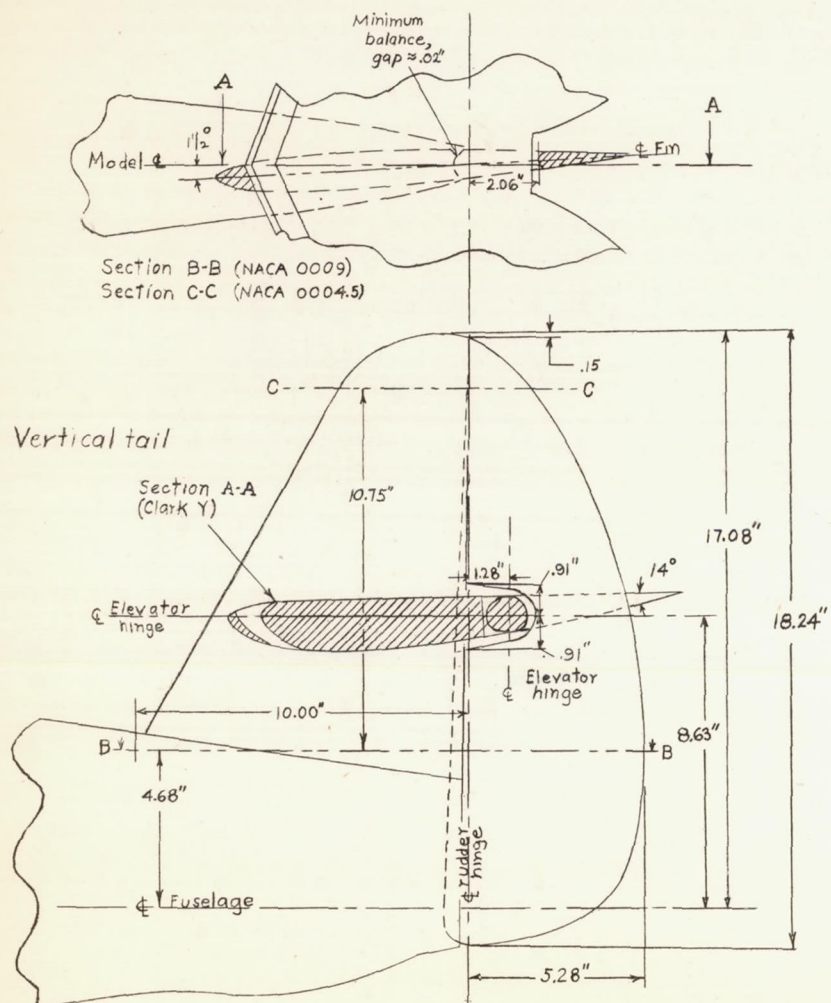


Figure 2.- System of axes and control-surface hinge moments and deflections. Positive values of forces, moments, and angles are indicated by arrows. Positive values of tab hinge moments and deflections are in the same directions as the positive values for the control surfaces to which the tabs are attached.

NATIONAL ADVISORY
COMMITTEE FOR AERONAUTICS



| | |
|-----------------------------|-------|
| Elevator area, sq ft | 0.621 |
| Elevator rms chord, ft | 0.264 |
| Rudder area, sq ft | 0.506 |
| Rudder rms chord, ft | 0.353 |
| Horizontal tail area, sq ft | 1.92 |
| Vertical tail area, sq ft | 1.25 |
| Elevator span, ft | 2.542 |
| Rudder span, ft | 1.508 |

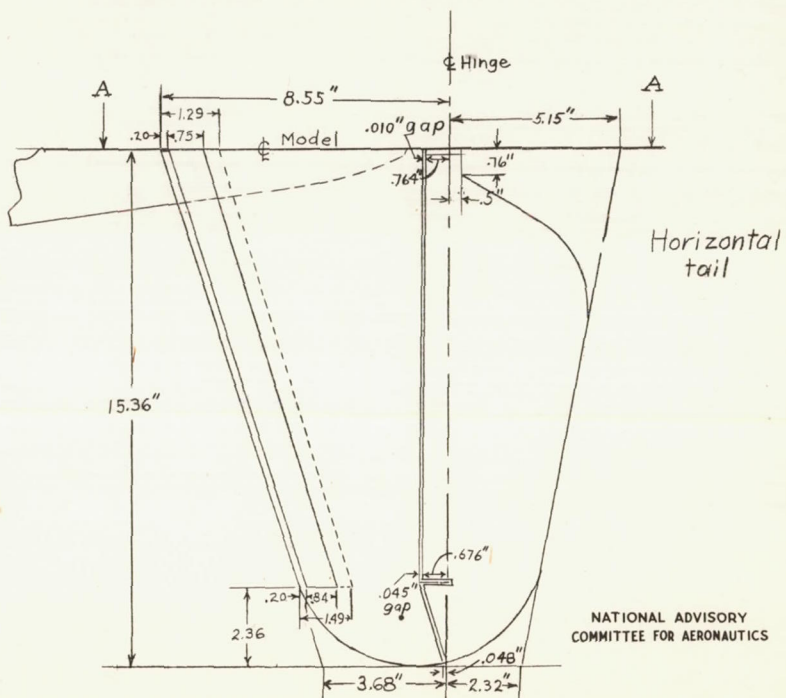


Figure 3.- Model tail assembly.

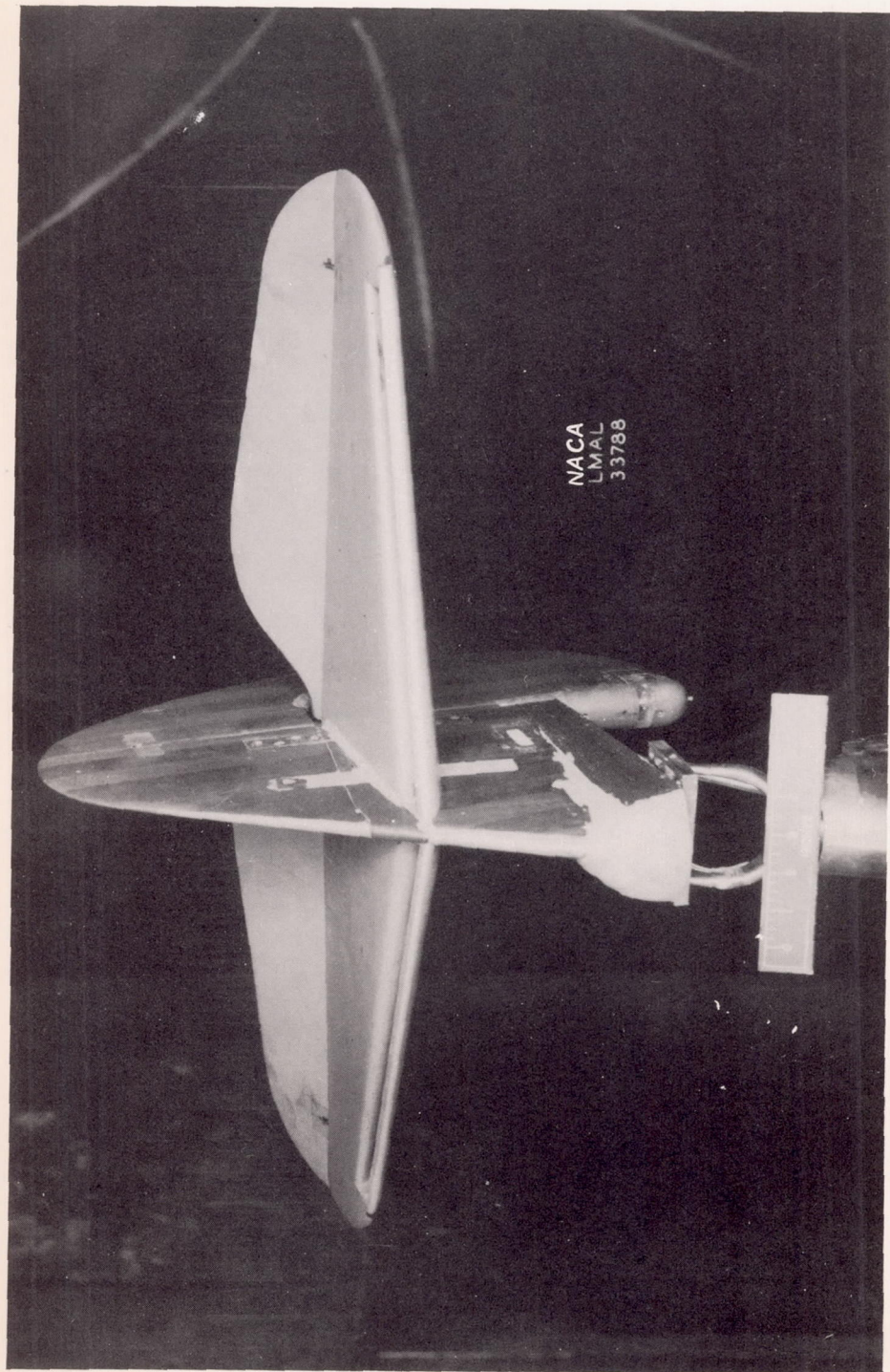
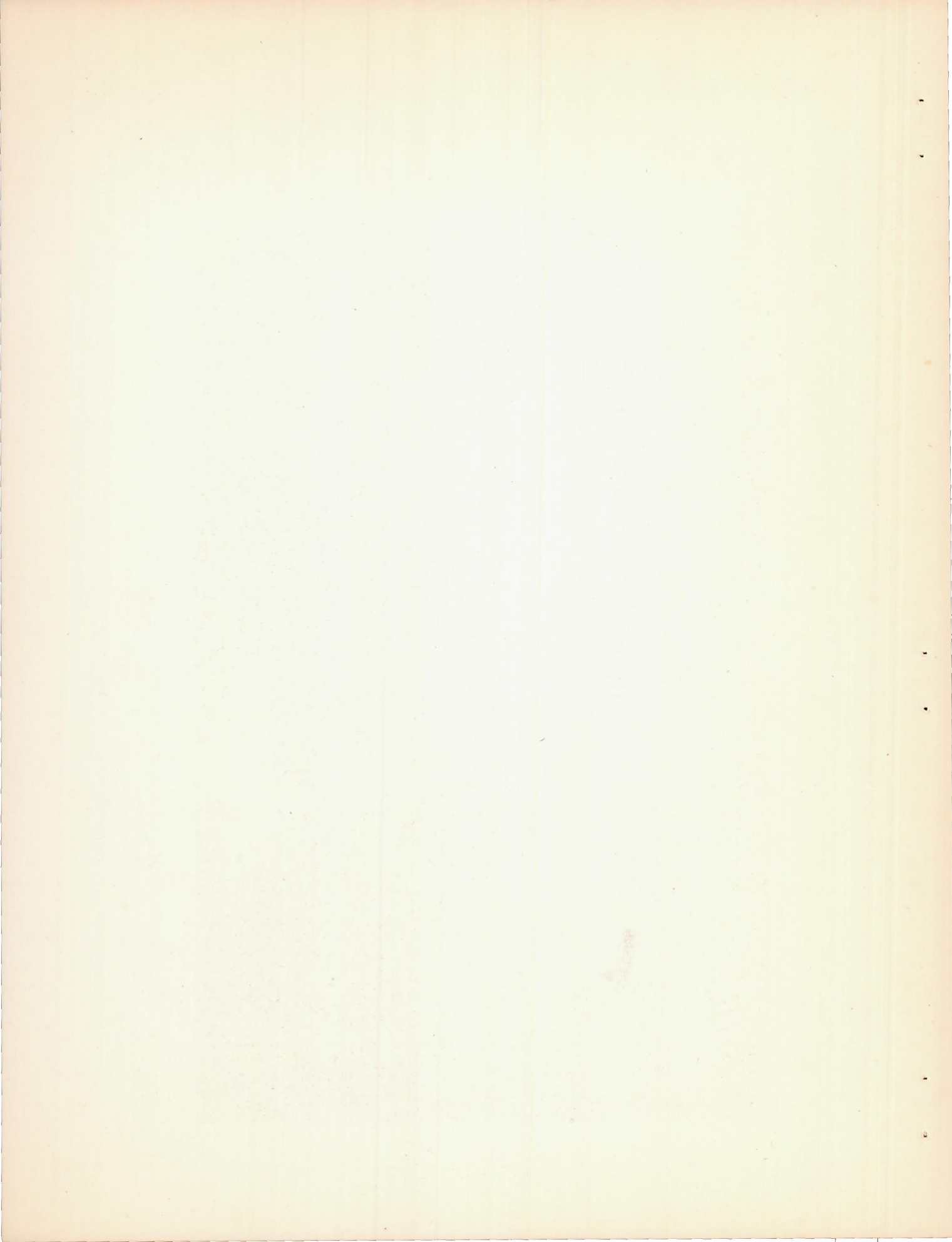


Figure 4.- Isolated tail assembly mounted in Langley 7- by 10-foot tunnel.



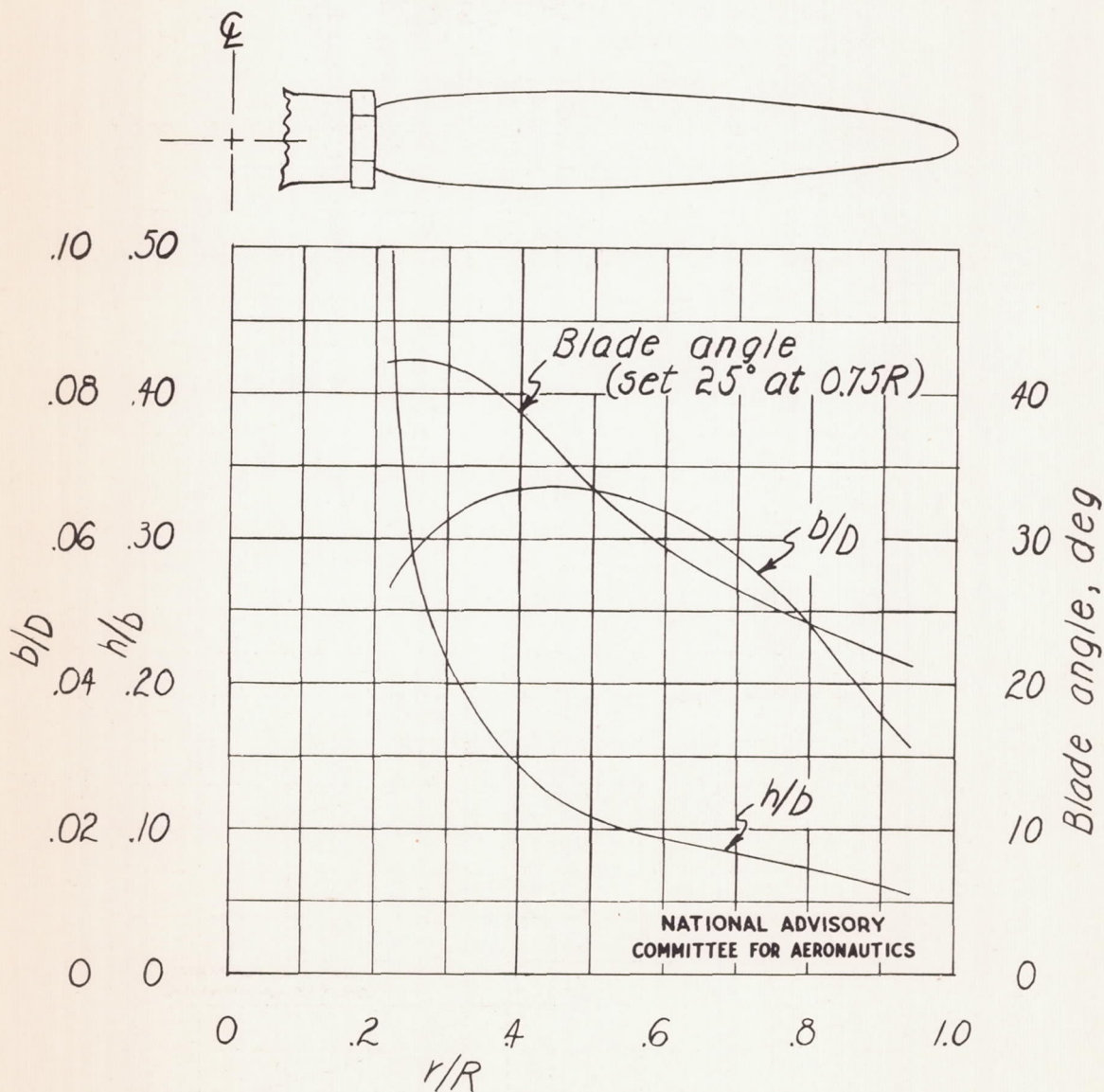


Figure 5.- Plan-form and blade-form curves for the model propeller.
 D , diameter; R , radius to tip; r , station radius; b , section chord;
 h , section thickness. RAF 6 airfoil section.

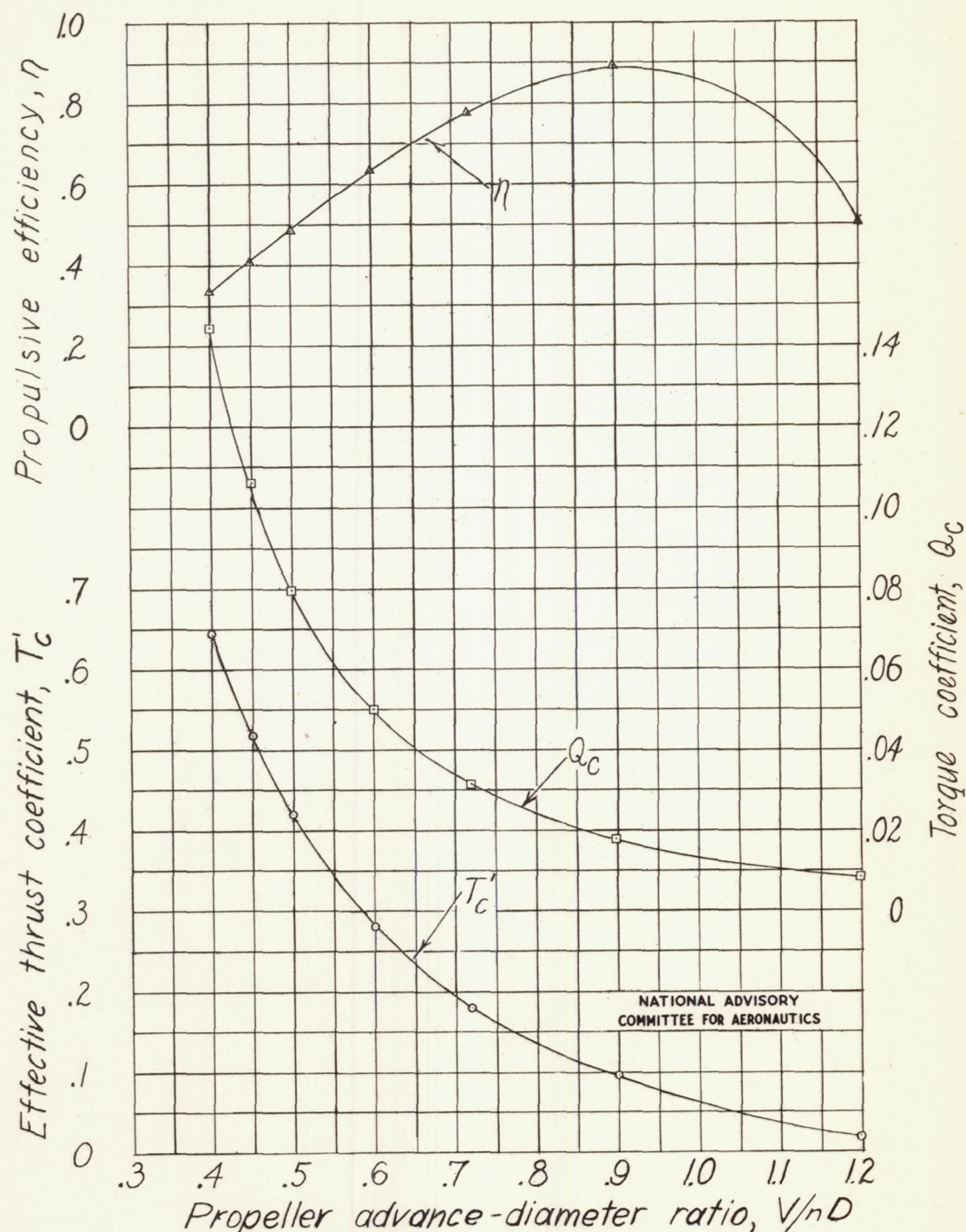


Figure 6.- Effective thrust coefficient, torque coefficient, and efficiency as functions of propeller advance-diameter ratio for the model of the low-wing airplane tested. $D = 2.0$ feet; $\beta = 25^\circ$.

Effective thrust coefficient, T_C'

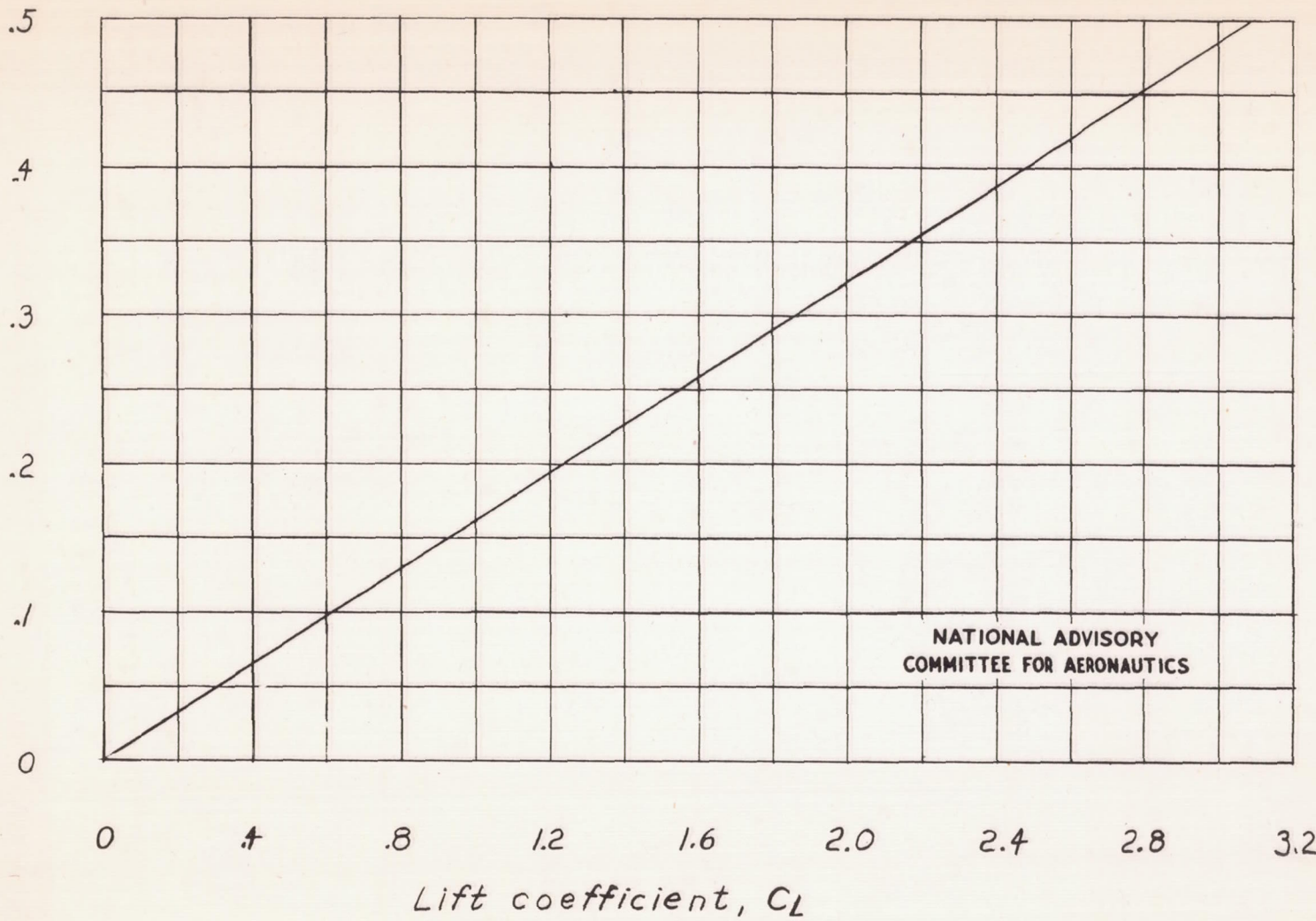


Figure 7.- Variation of effective thrust coefficient with lift coefficient for constant-power tests.

NACA TN No. 1239

Fig. 7

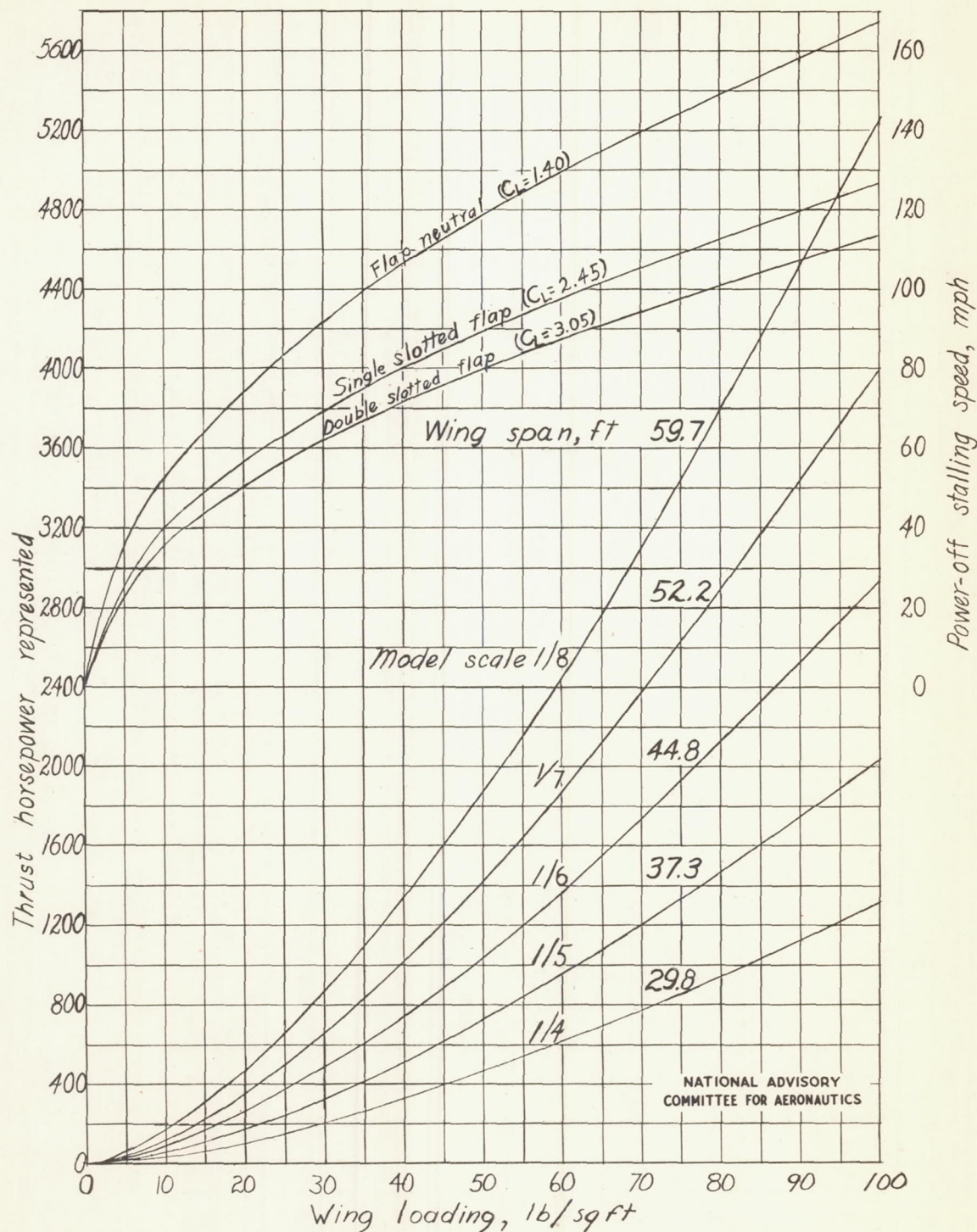
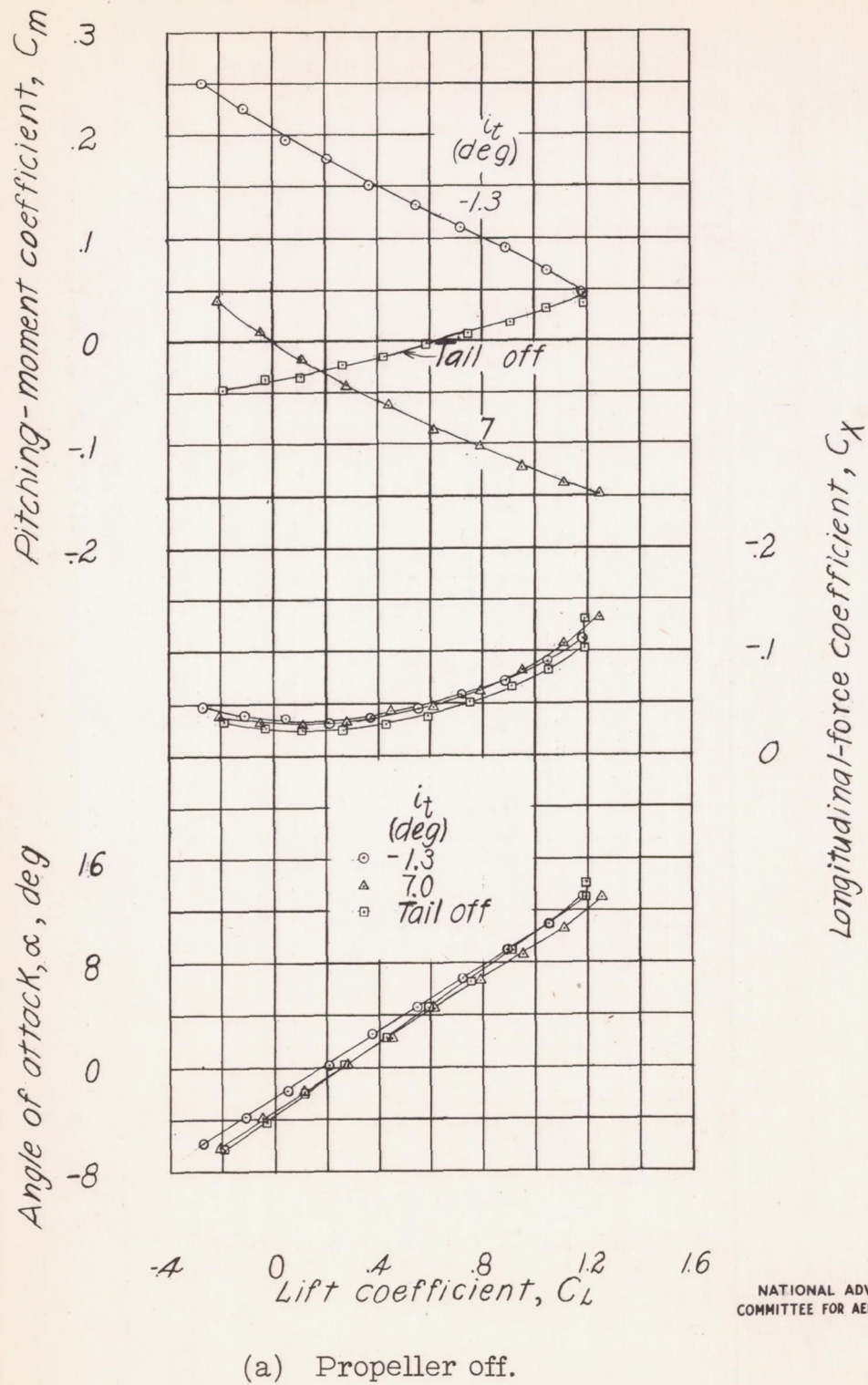


Figure 8.- Variation of approximate horsepower represented and stalling speeds with airplane wing loading.



(a) Propeller off.

Figure 9.- Effect of stabilizer setting on the aerodynamic characteristics of the model as a low-wing airplane with flap neutral.
 $\delta = 0^\circ$; tail slot filled.

Fig. 9a conc.

NACA TN No. 1239

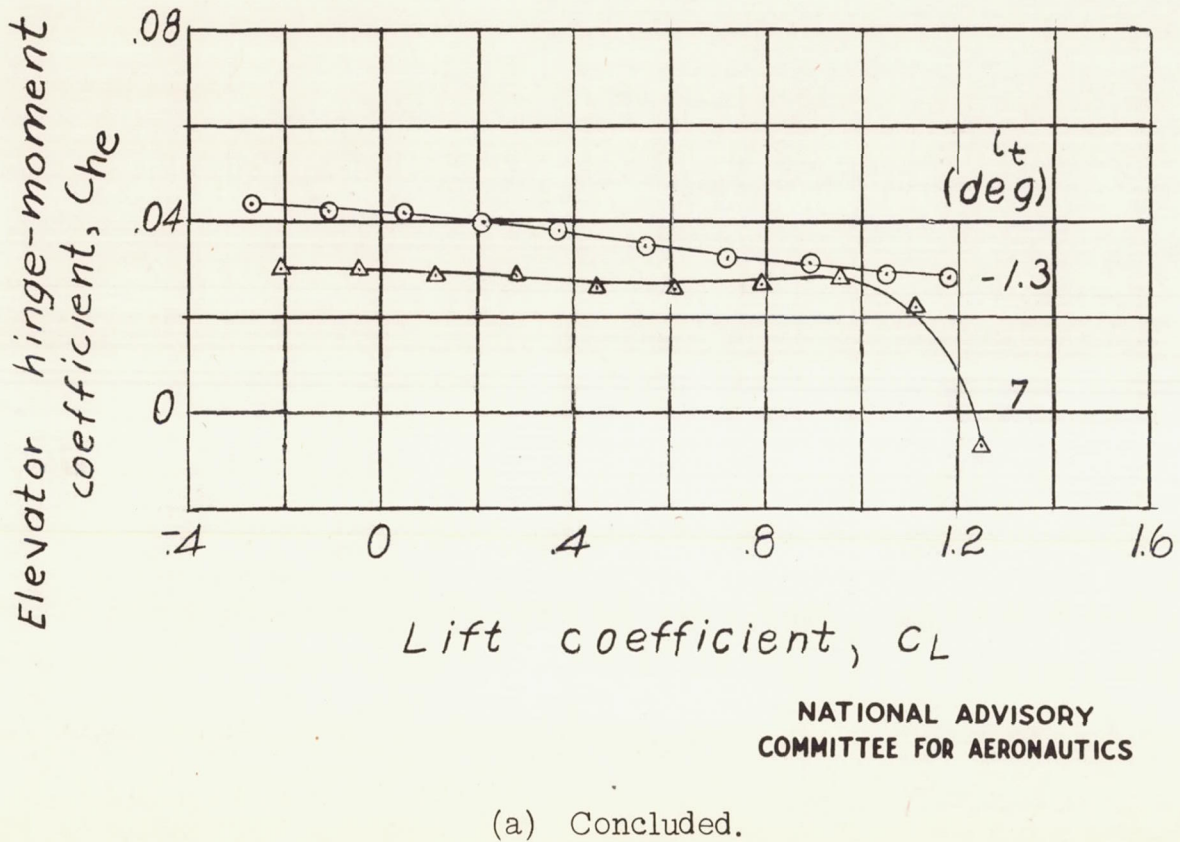


Figure 9.- Continued.

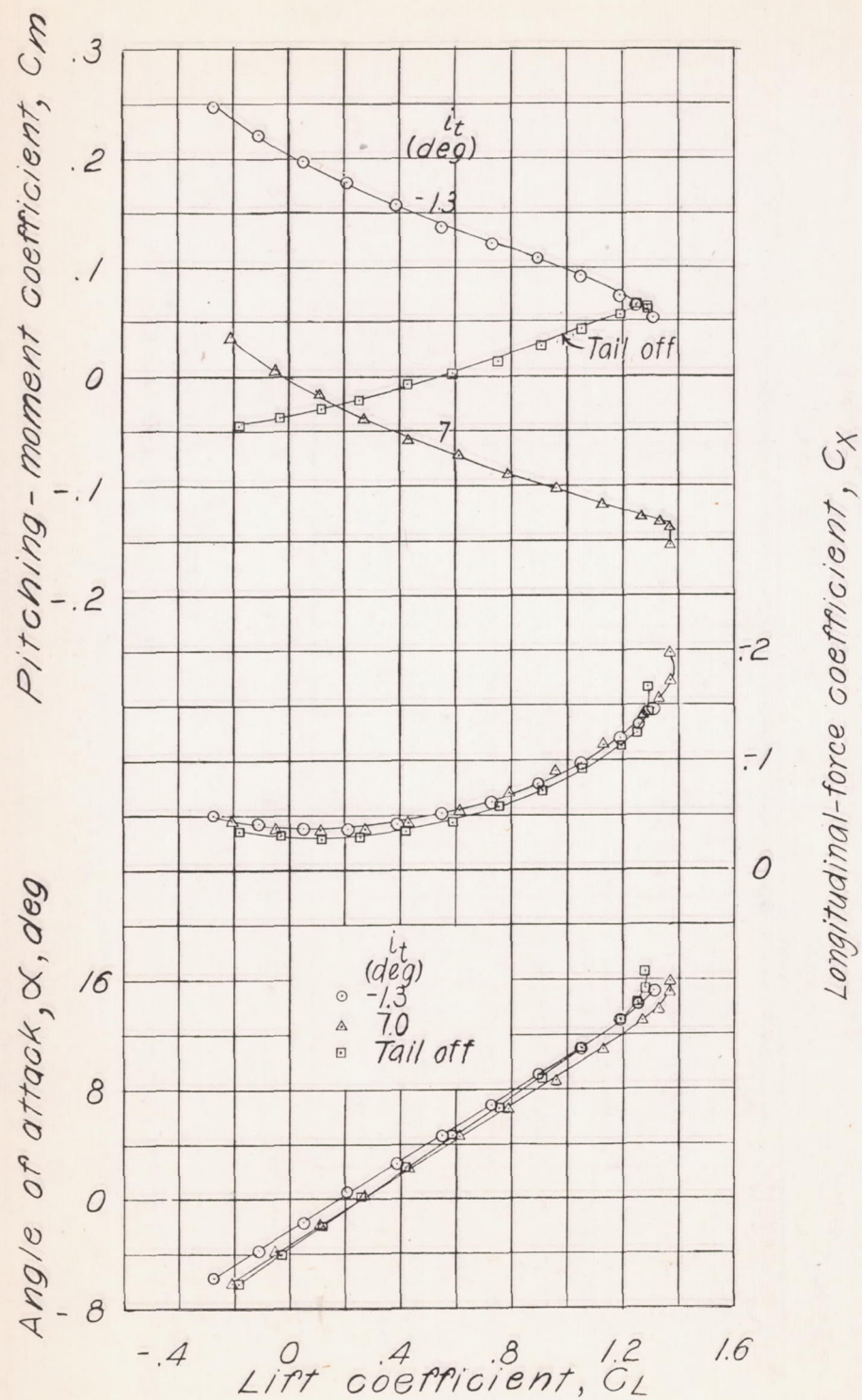
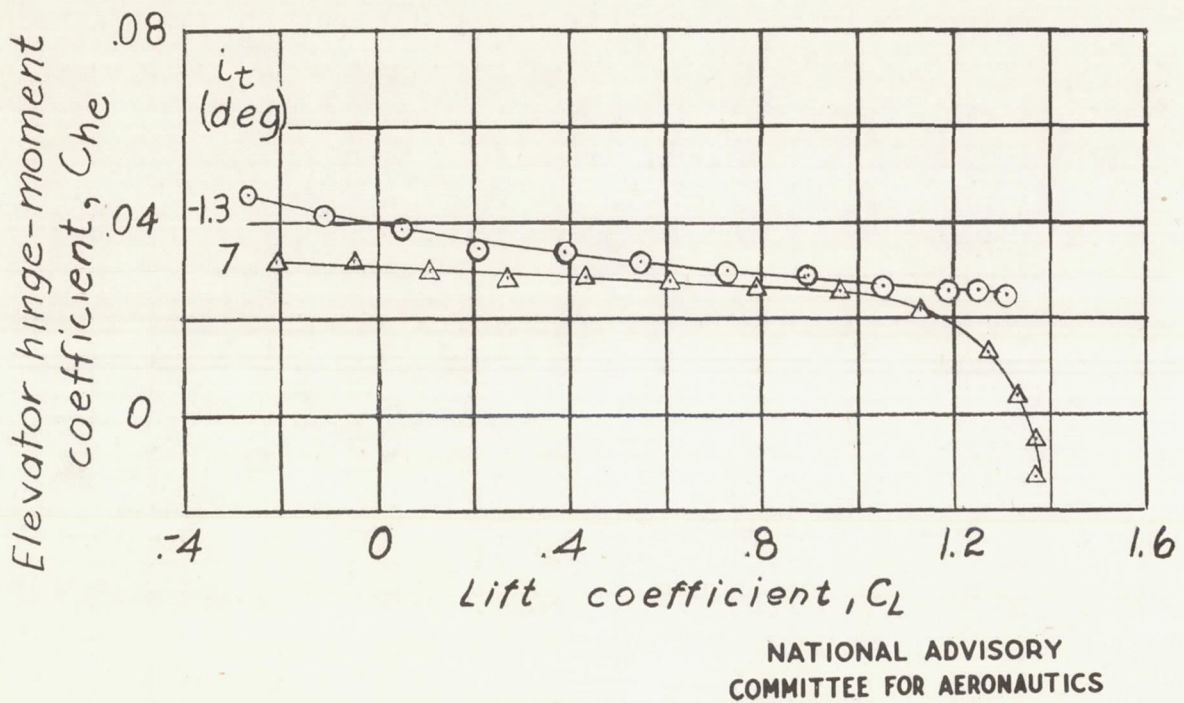


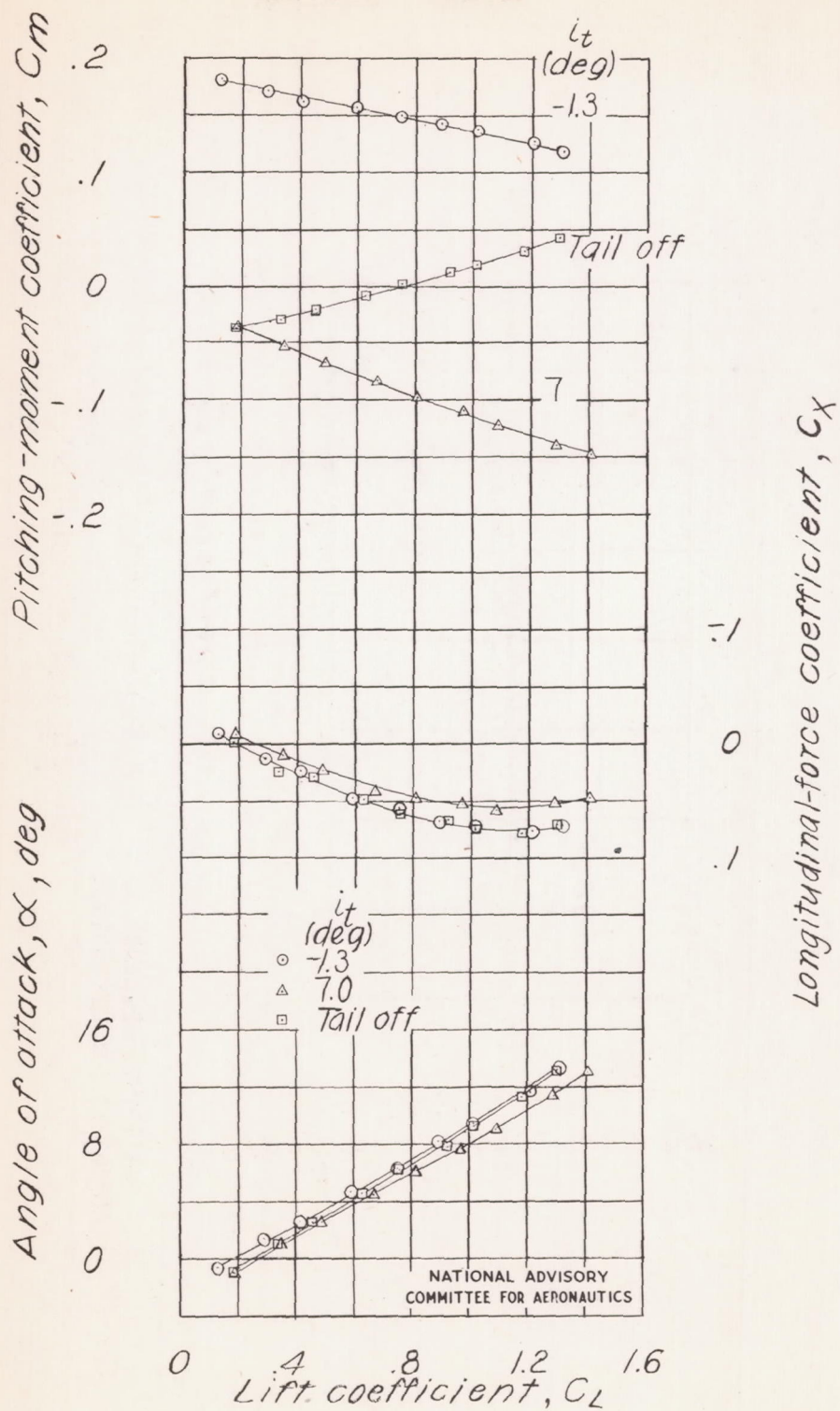
Fig. 9b conc.

NACA TN No. 1239



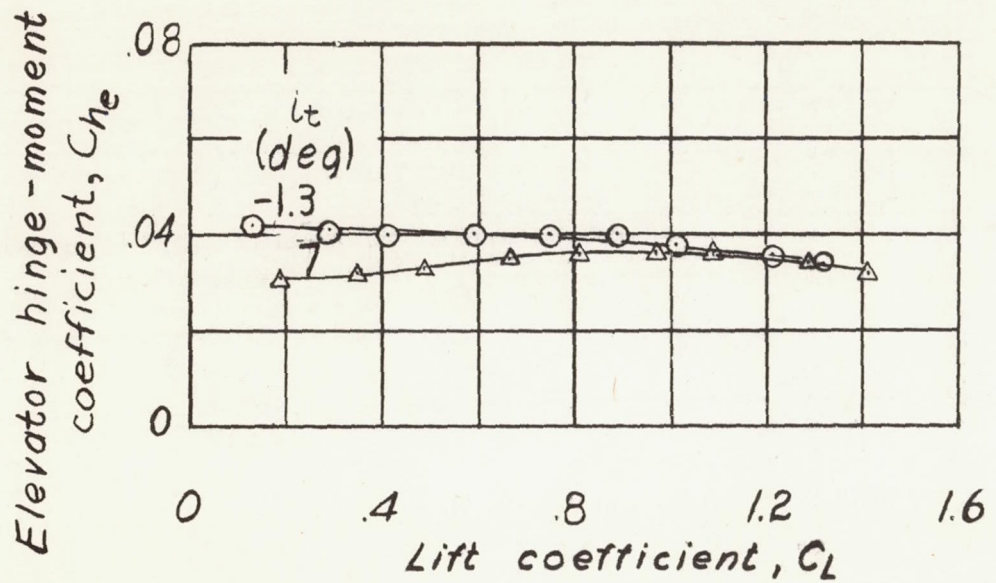
(b) Concluded.

Figure 9.- Continued.



(c) Power on.

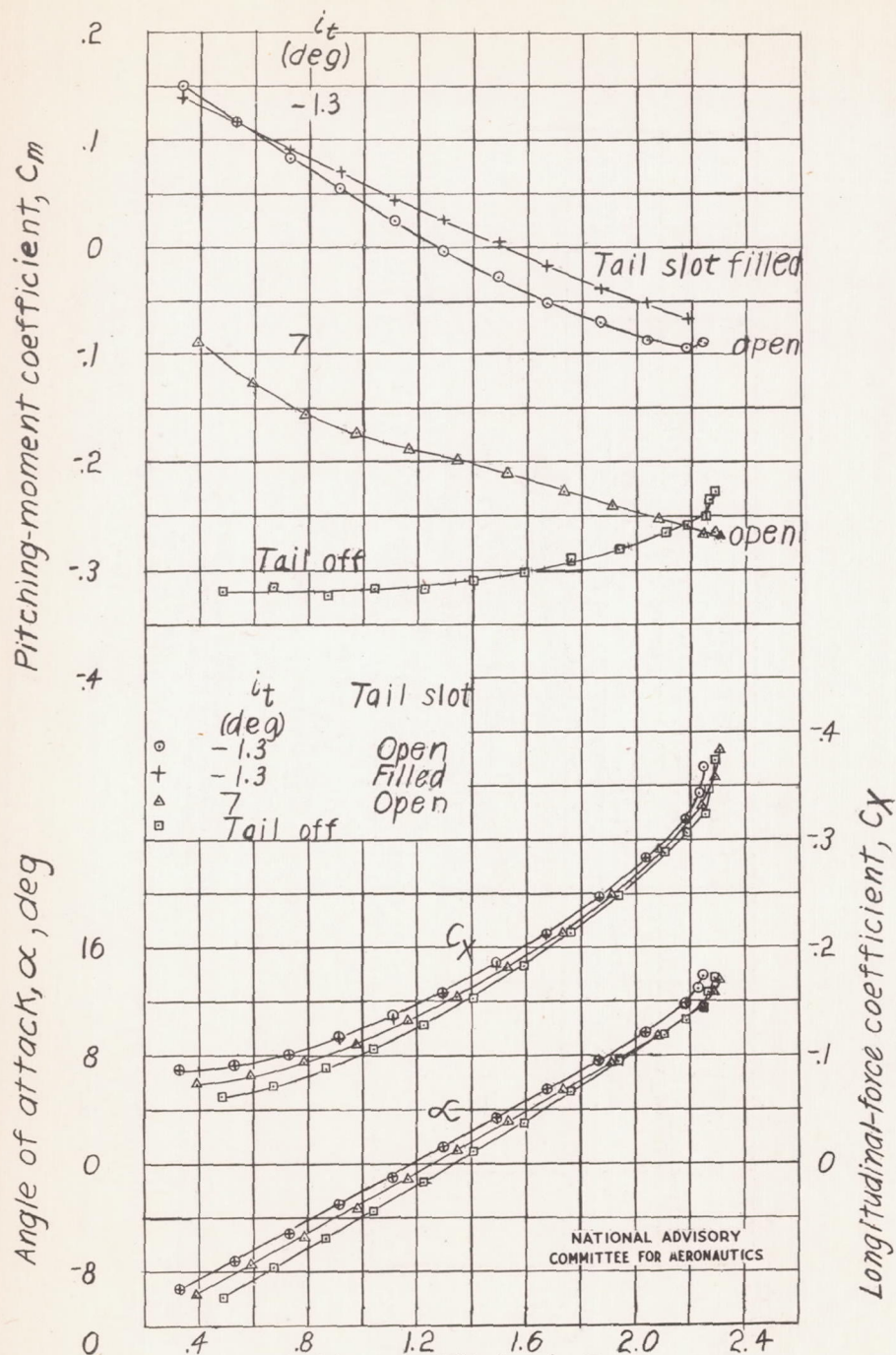
Figure 9.- Continued.



NATIONAL ADVISORY
COMMITTEE FOR AERONAUTICS.

(c) Concluded.

Figure 9.- Concluded.

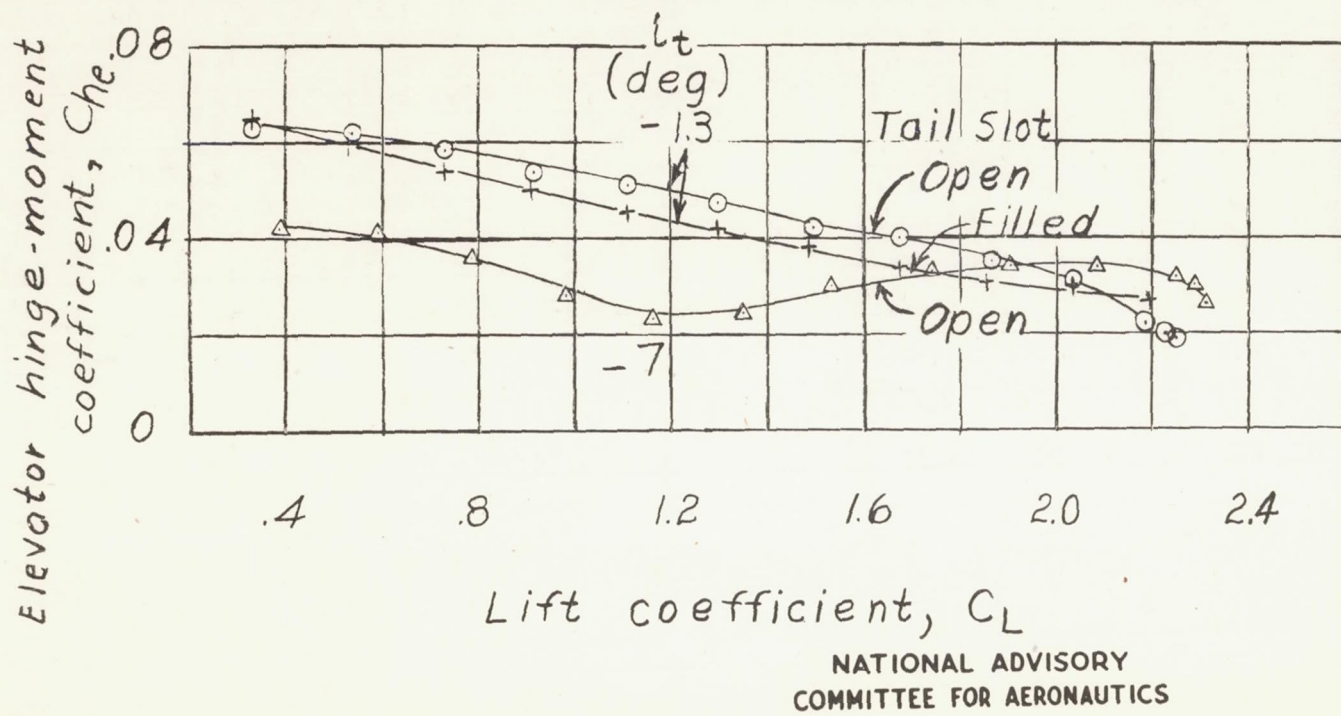


(a) Propeller off.

Figure 10.- Effect of stabilizer setting on the aerodynamic characteristics of the model as a low-wing airplane with a full-span single slotted flap. $\delta_e = 0^\circ$.

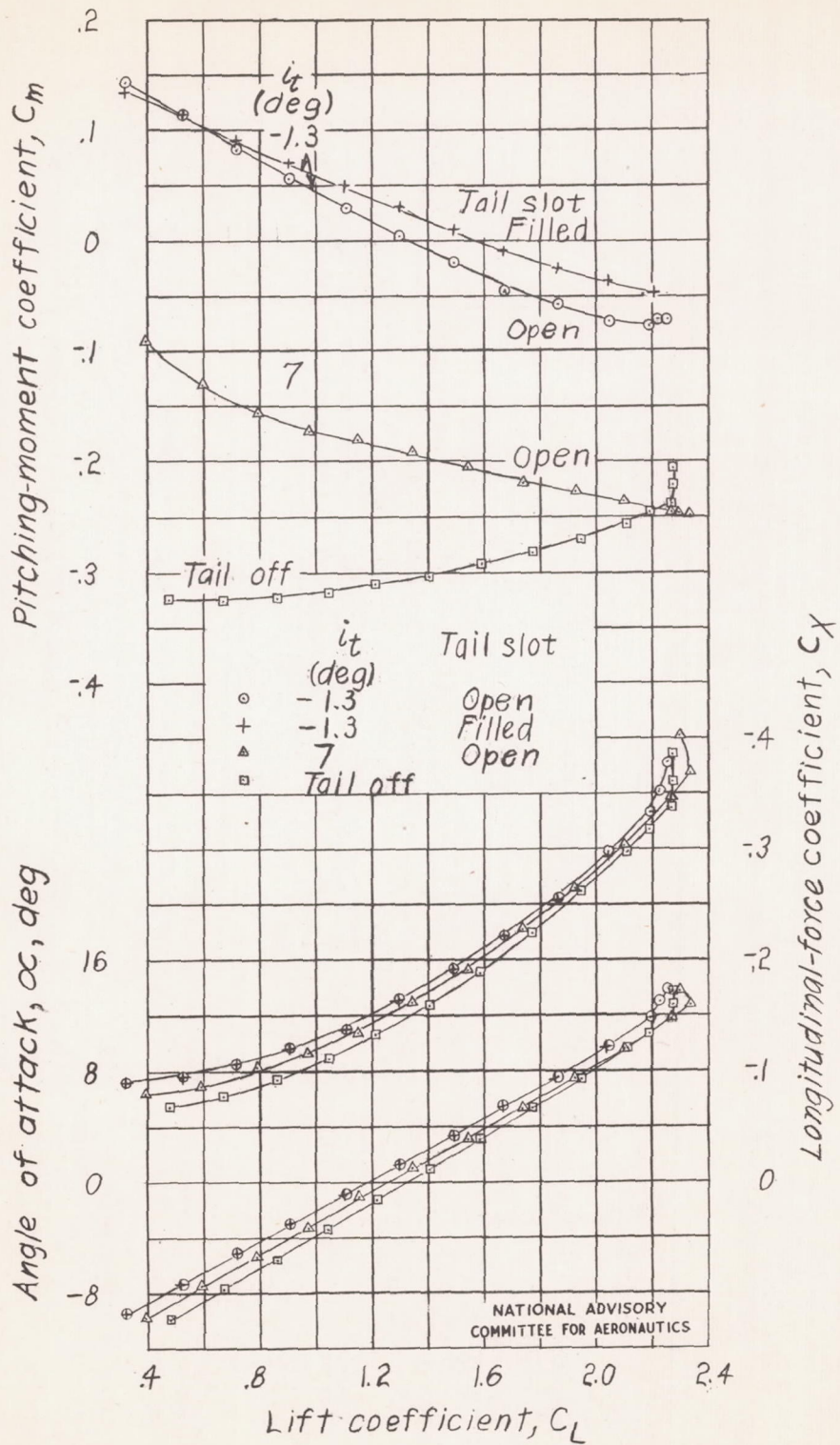
Fig. 10a conc.

NACA TN No. 1239



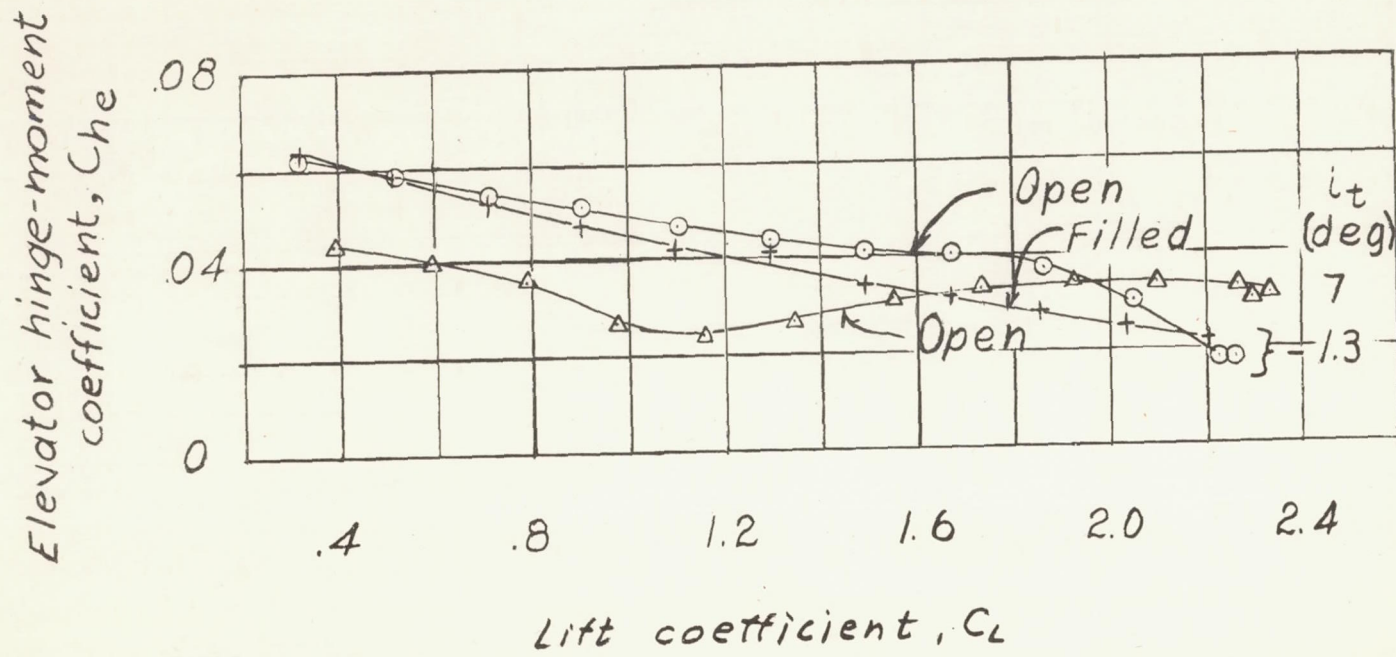
(a) Concluded.

Figure 10.- Continued.



(b) Propeller windmilling.

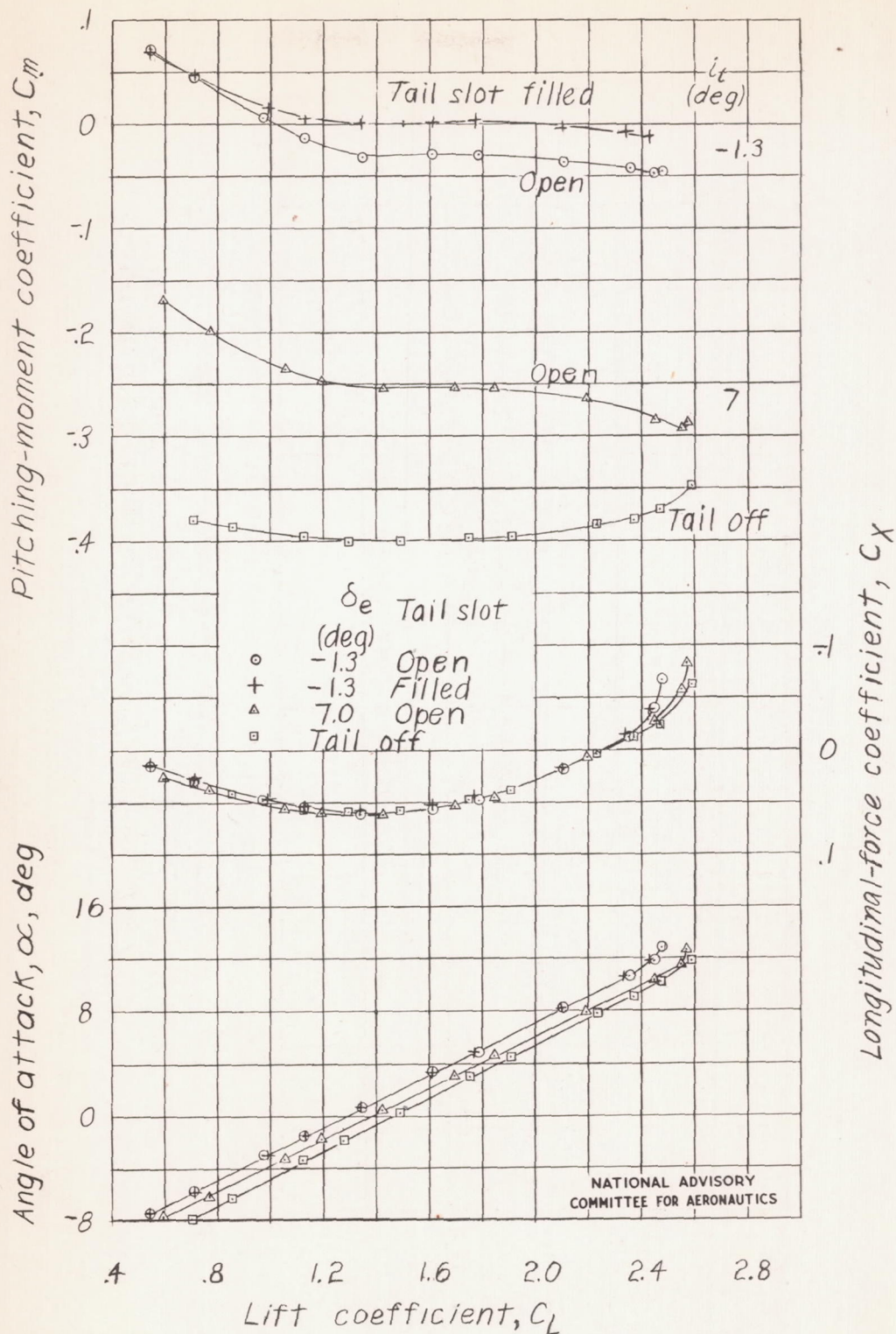
Figure 10.- Continued.



NATIONAL ADVISORY
COMMITTEE FOR AERONAUTICS.

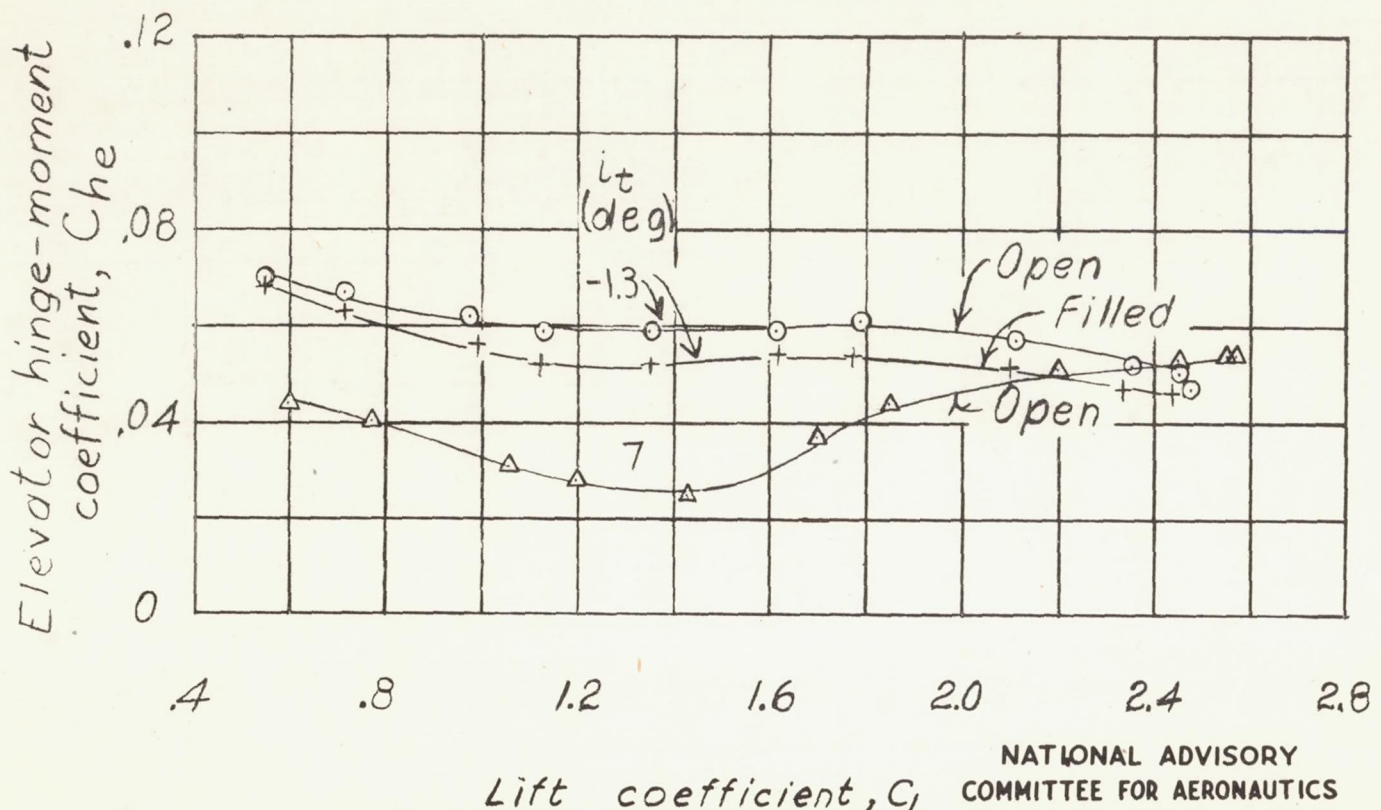
(b) Concluded.

Figure 10.- Continued.



(c) Power on.

Figure 10.- Continued.



(c) Concluded.

Figure 10.- Concluded.

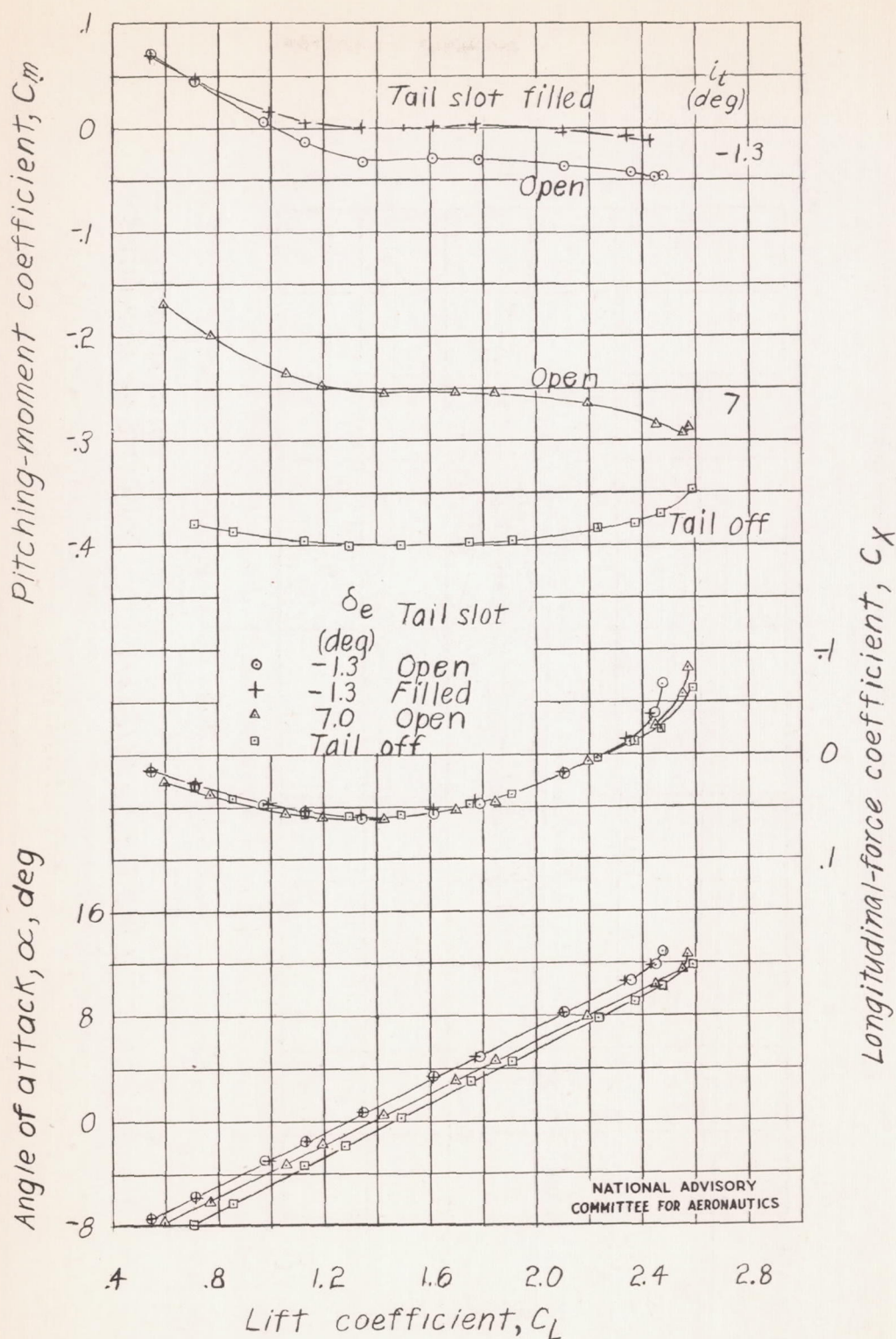
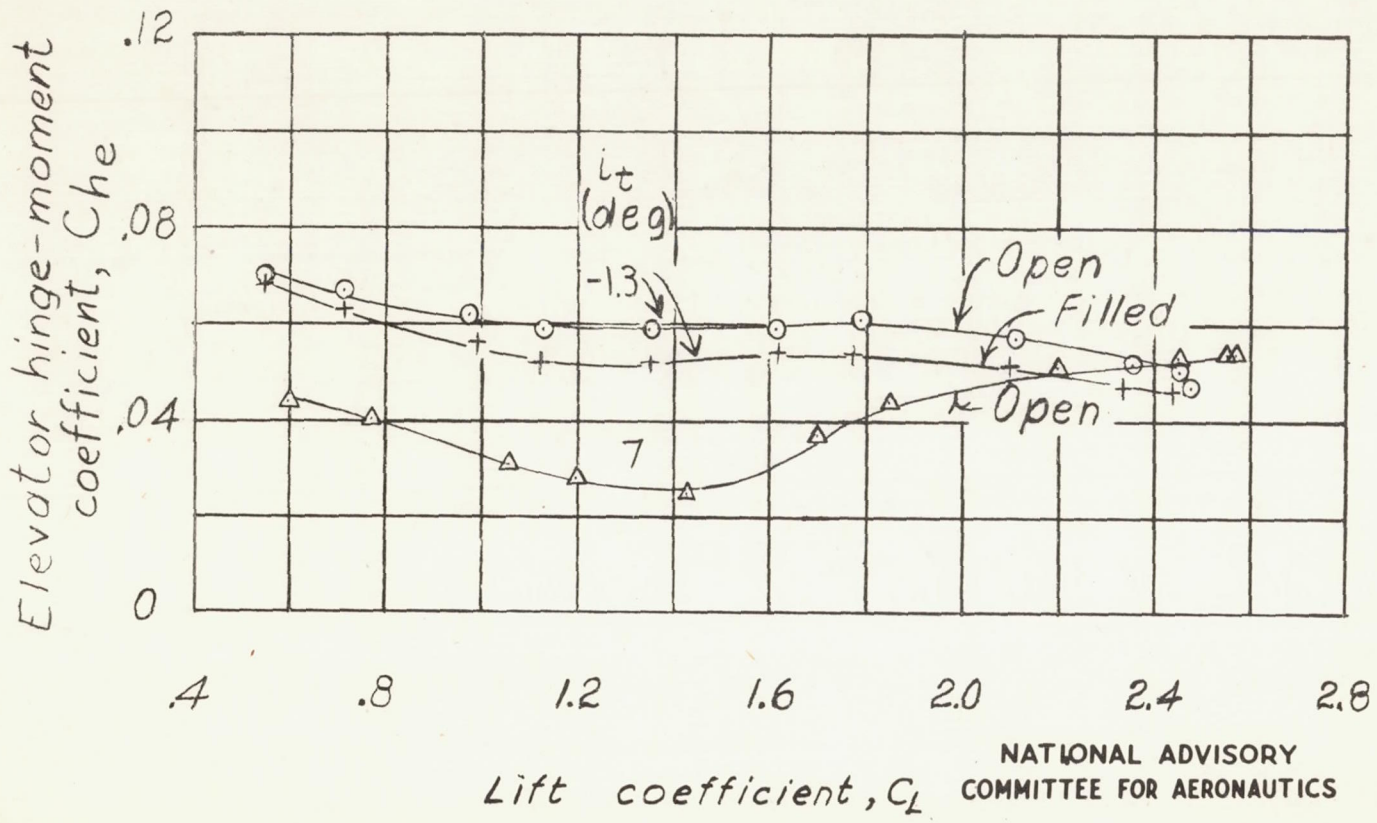


Figure 10.- Continued.

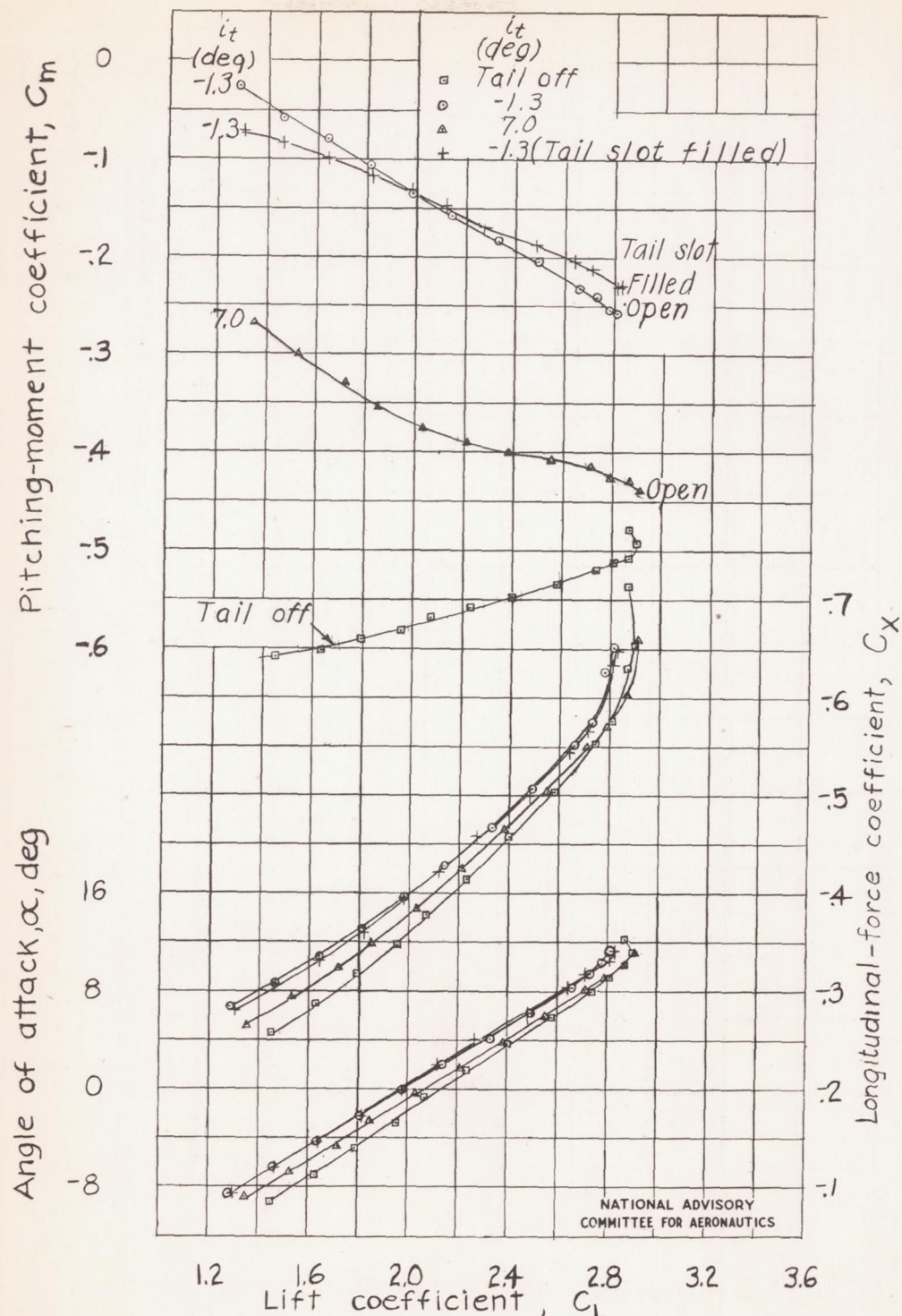
Fig. 10c conc.

NACA TN No. 1239



(c) Concluded.

Figure 10.- Concluded.



(a) Propeller off.

Figure 11.- Effect of stabilizer setting on the aerodynamic characteristics of the model as a low-wing airplane with full-span double slotted flap. $\delta_e = 0^\circ$.

Fig. 11a conc.

NACA TN No. 1239

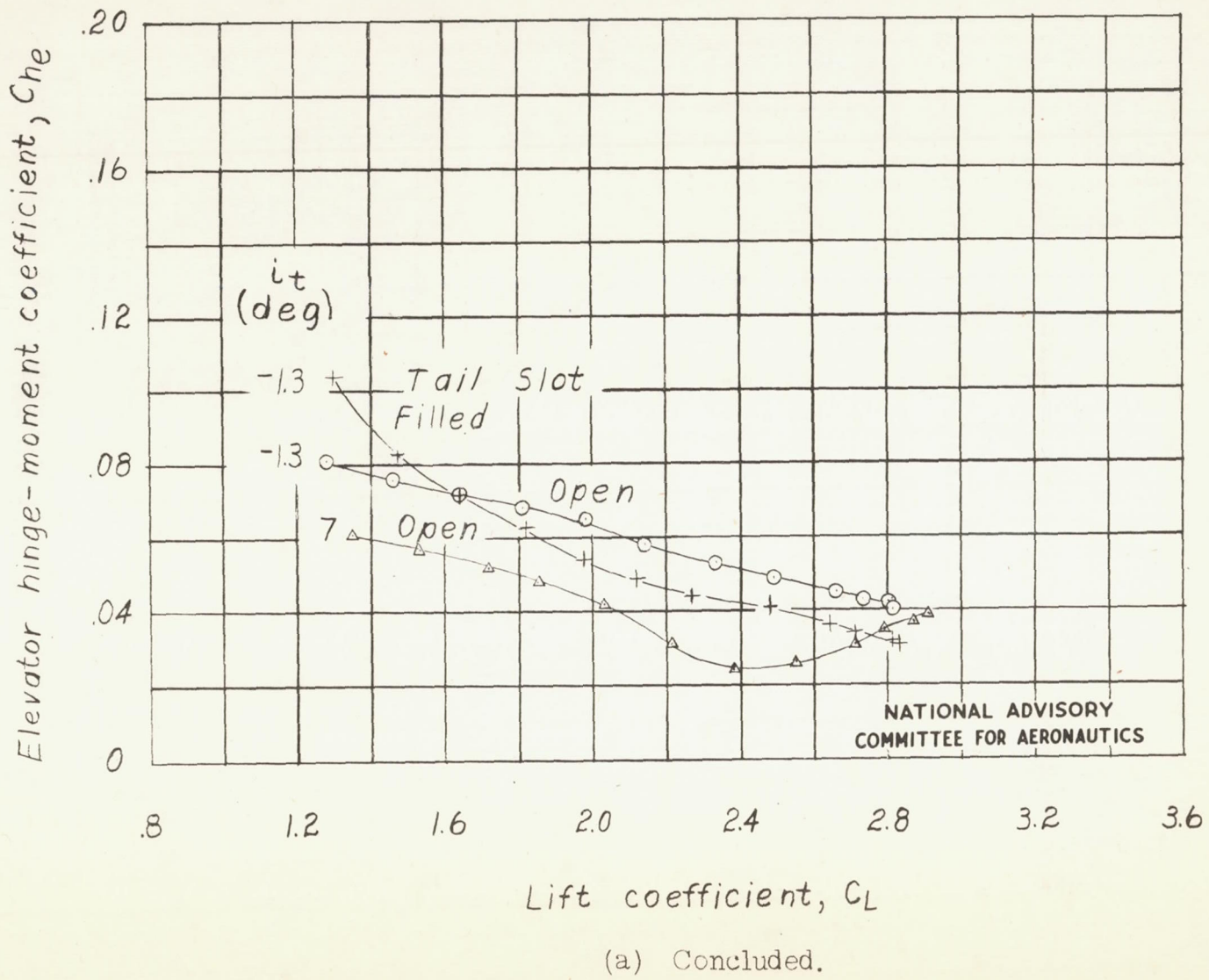
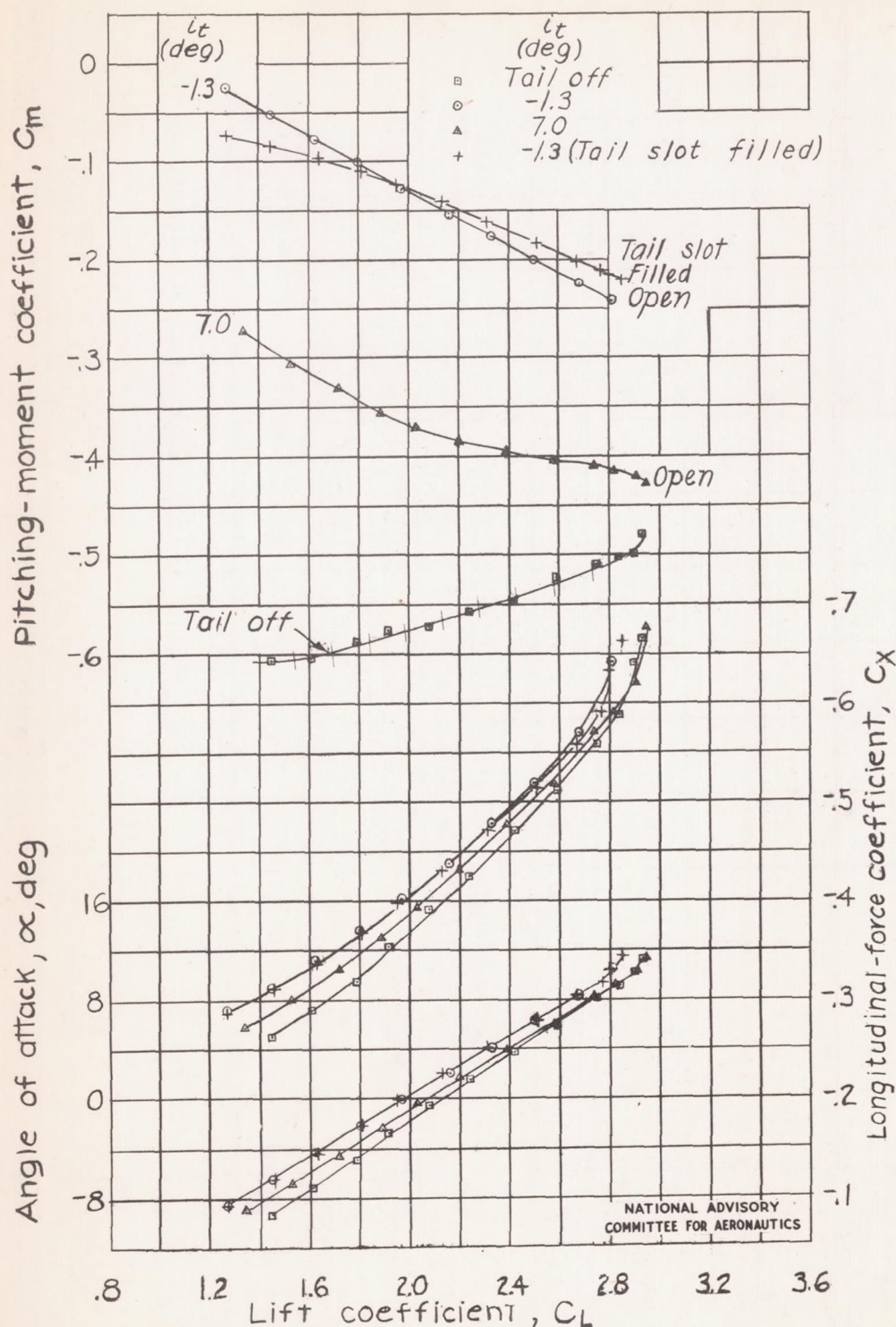


Figure 11.- Continued.

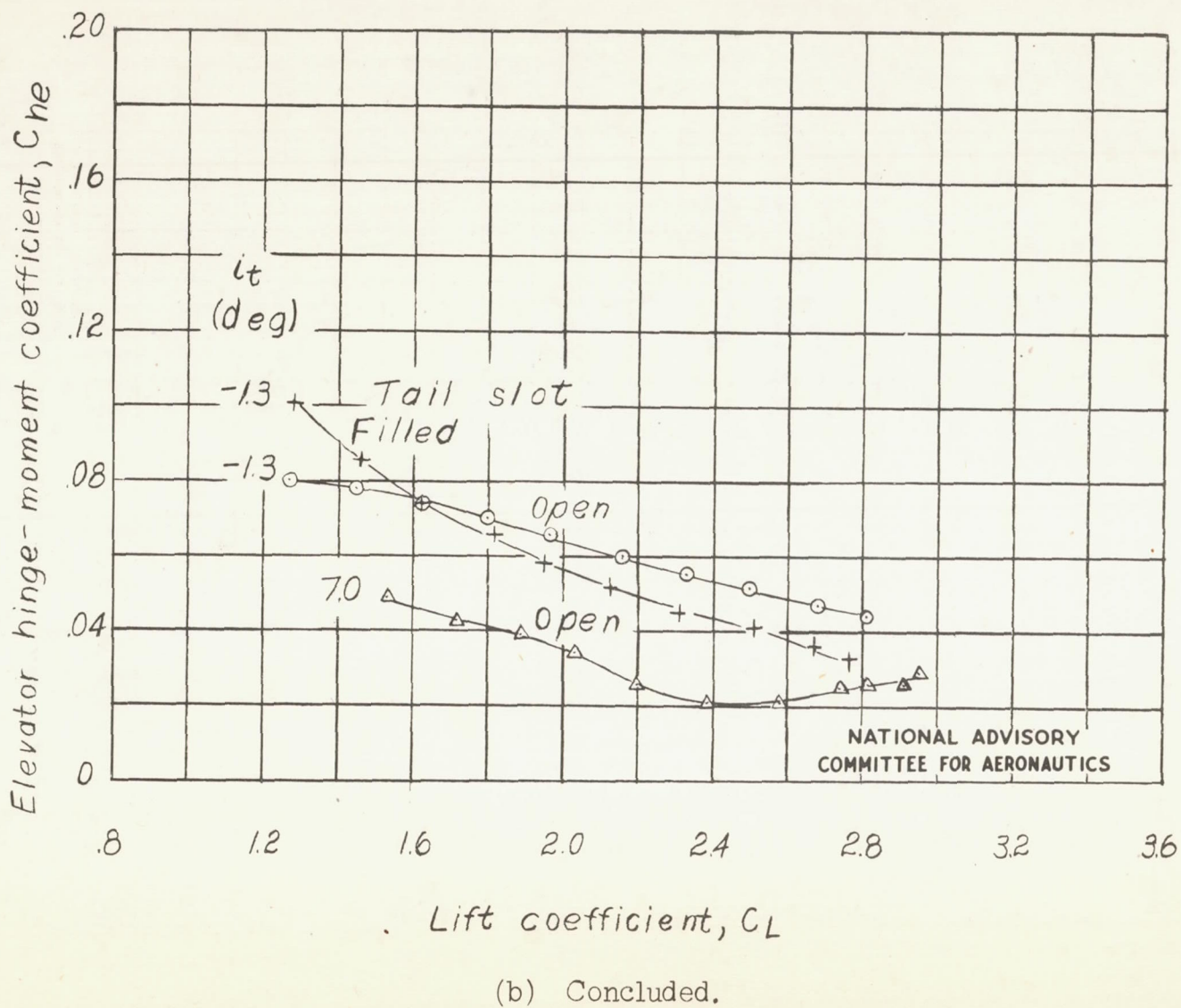


(b) Propeller windmilling.

Figure 11.- Continued.

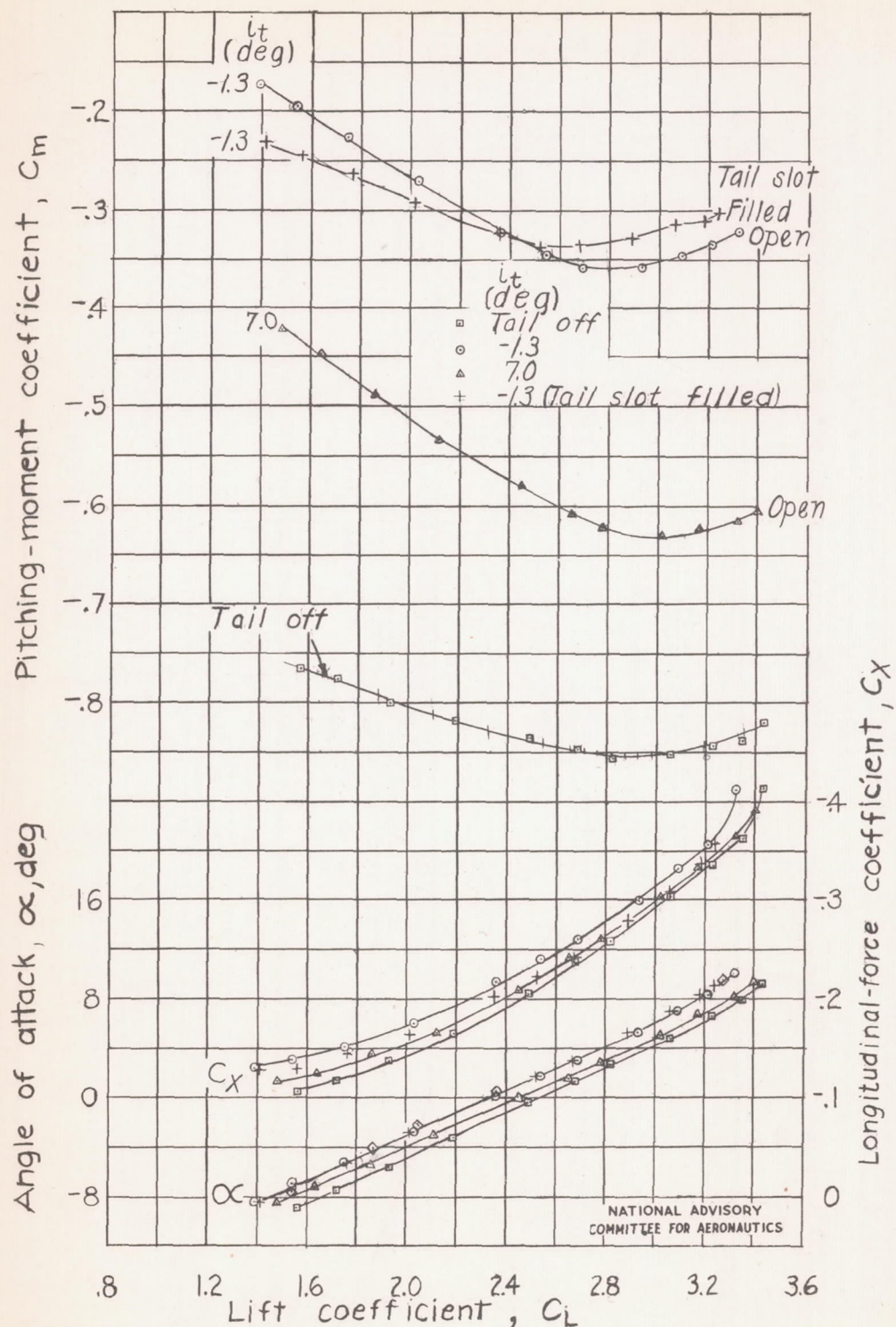
Fig. 11b conc.

NACA TN No. 1239



(b) Concluded.

Figure 11.- Continued.

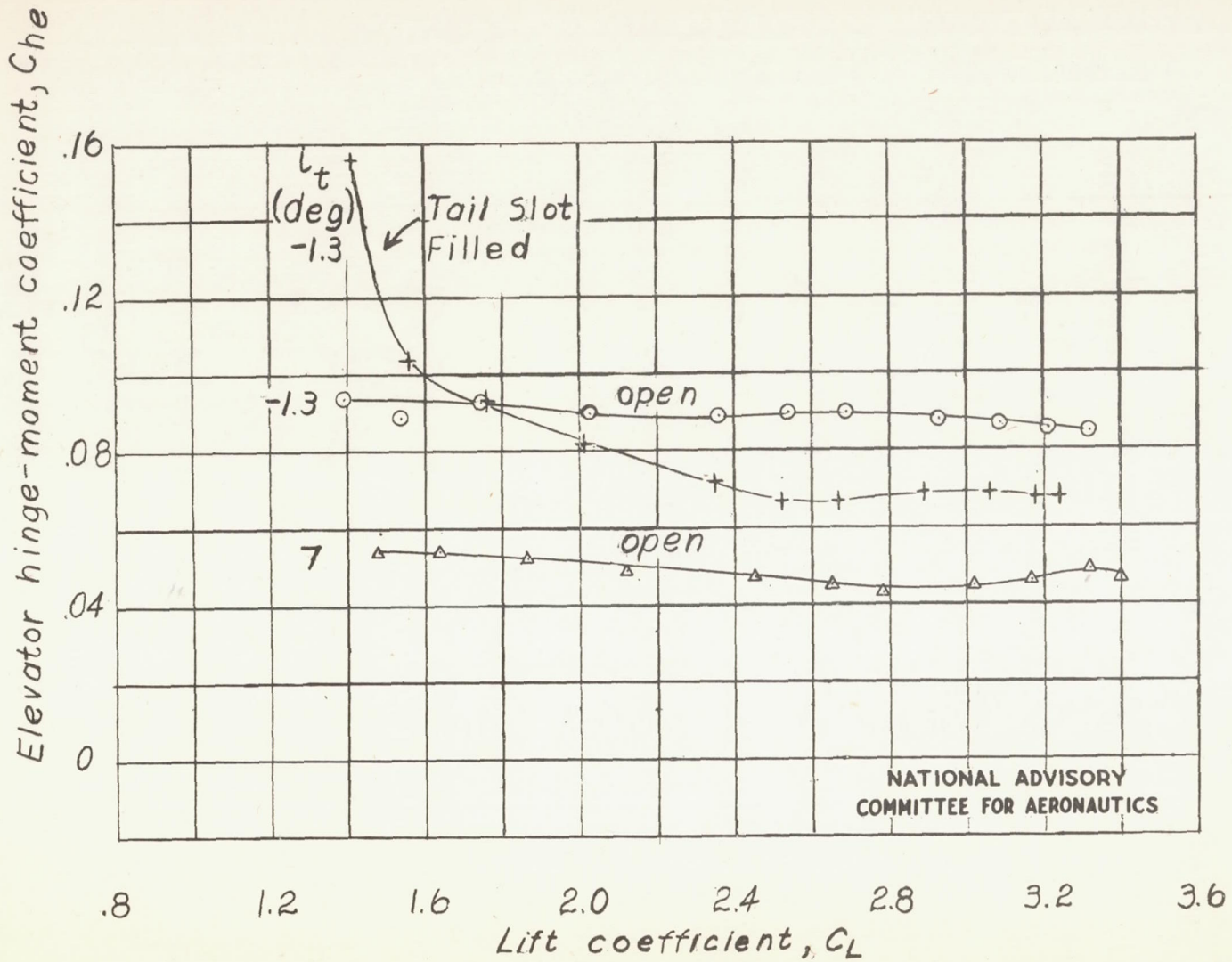


(c) Power on.

Figure 11.- Continued.

Fig. 11c conc.

NACA TN No. 1239



(c) Concluded.

Figure 11.- Concluded.

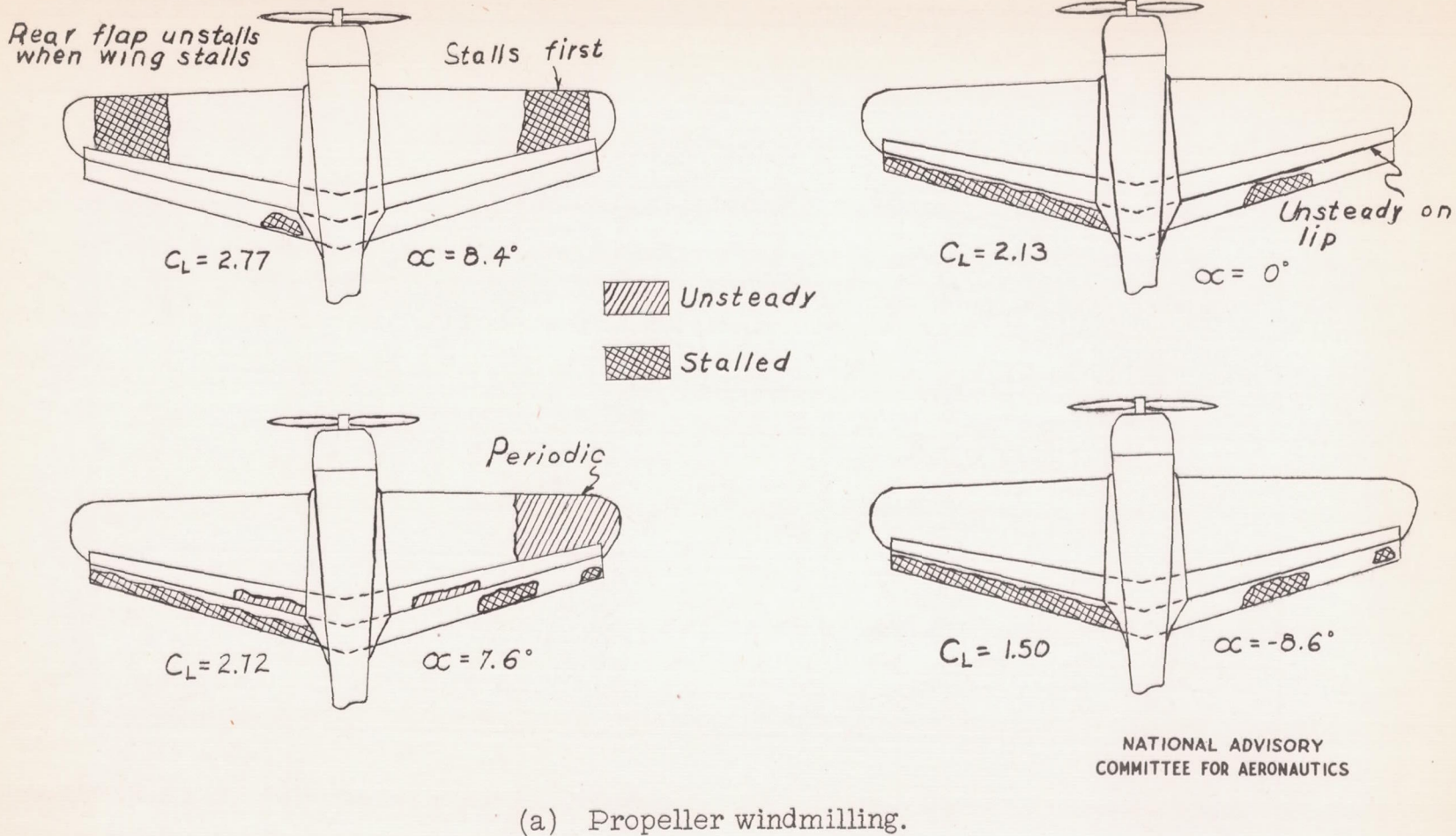
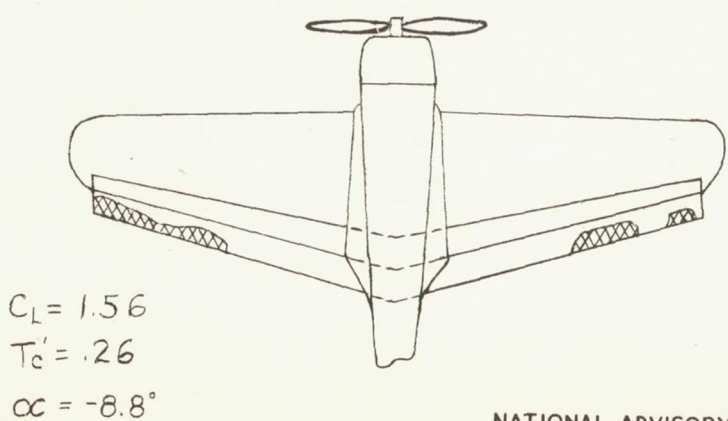
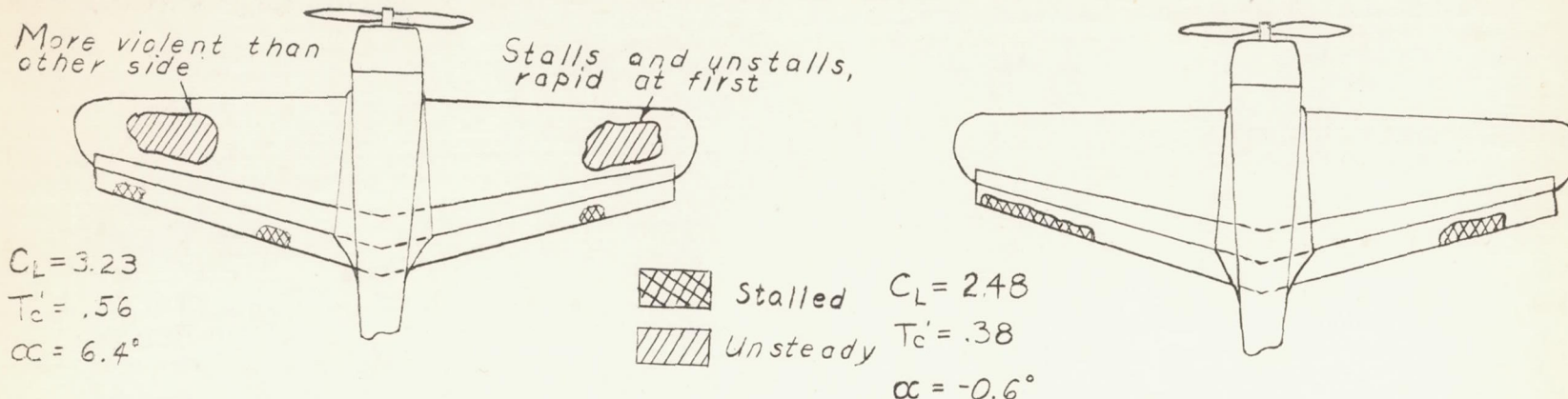


Figure 12.- Tuft studies of the model as a low-wing airplane with full-span double slotted flaps.

$$\delta_{f1} = \delta_{f2} = 30^\circ; q = 12.53 \text{ pounds per square foot.}$$

Fig. 12b



NATIONAL ADVISORY
COMMITTEE FOR AERONAUTICS

(b) Power on.

Figure 12.- Concluded.

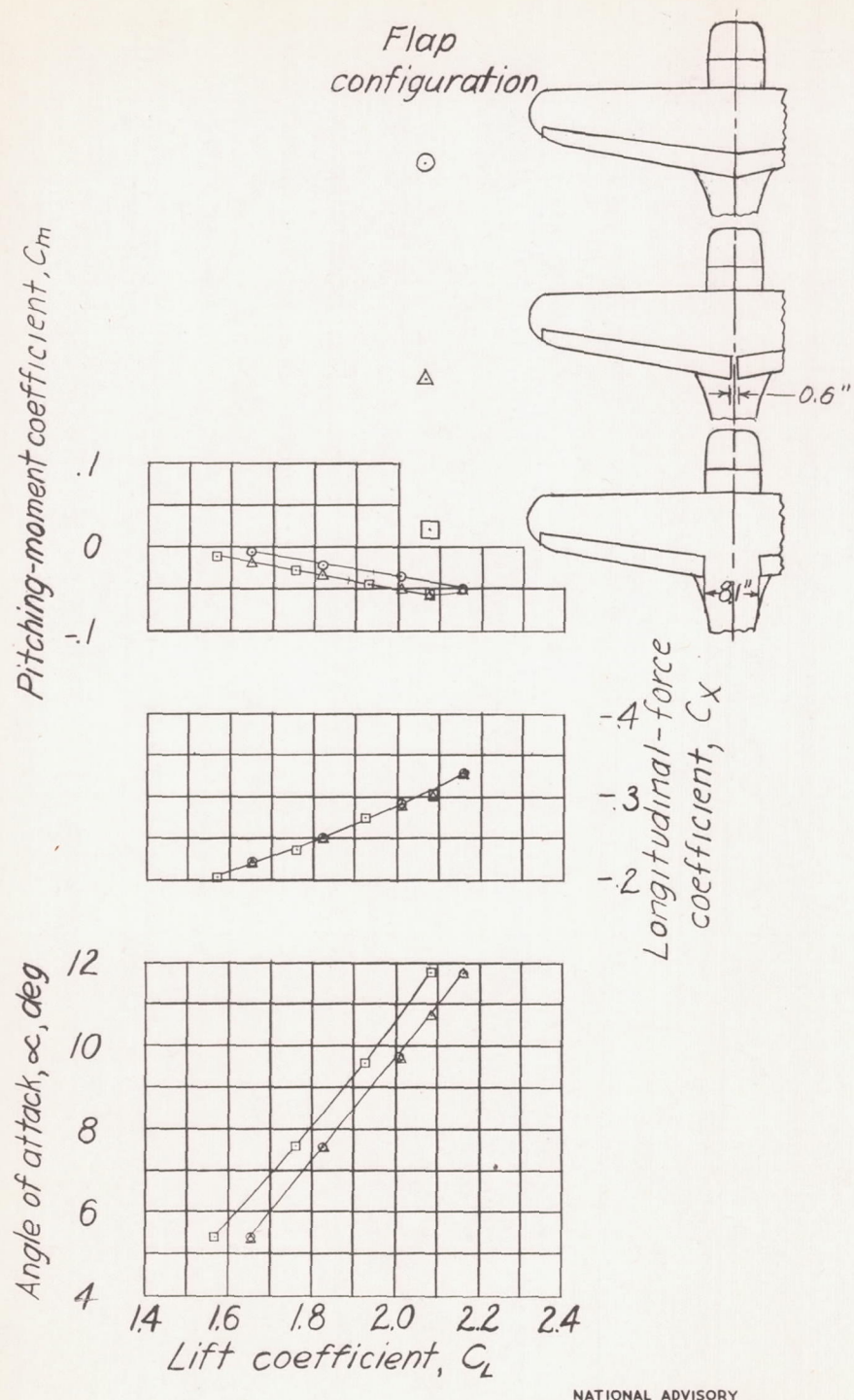


Figure 13.- Effect of removing flap sections beneath fuselage on the aerodynamic characteristics of the model as a low-wing airplane. $\delta_{f_2} = 30^\circ$; $\delta_e = 0^\circ$; $i_t = -1.3^\circ$; propeller windmilling; tail slot filled.

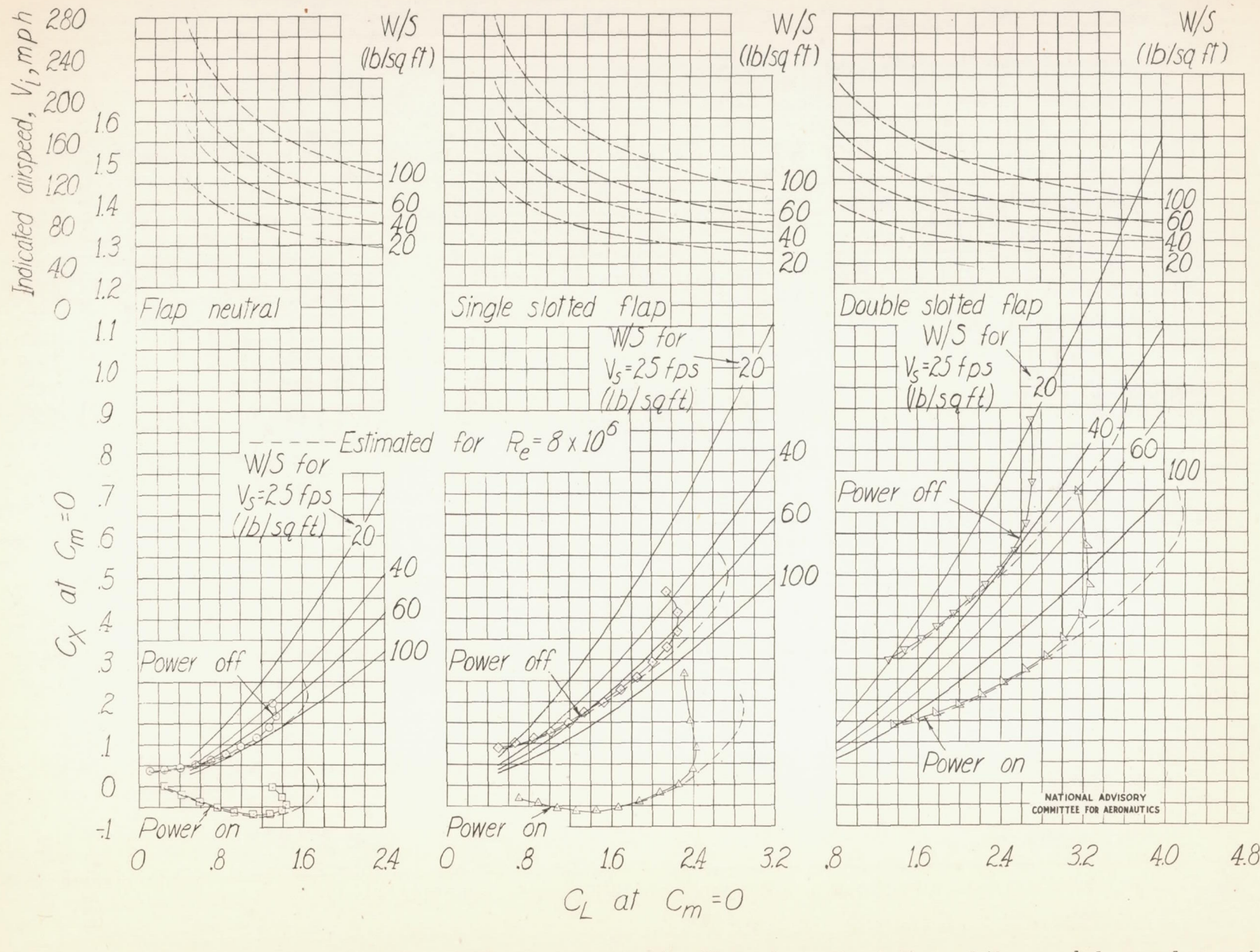


Figure 14.- Effect of power and flap deflection on the landing characteristics of the model as a low-wing single-engine airplane.

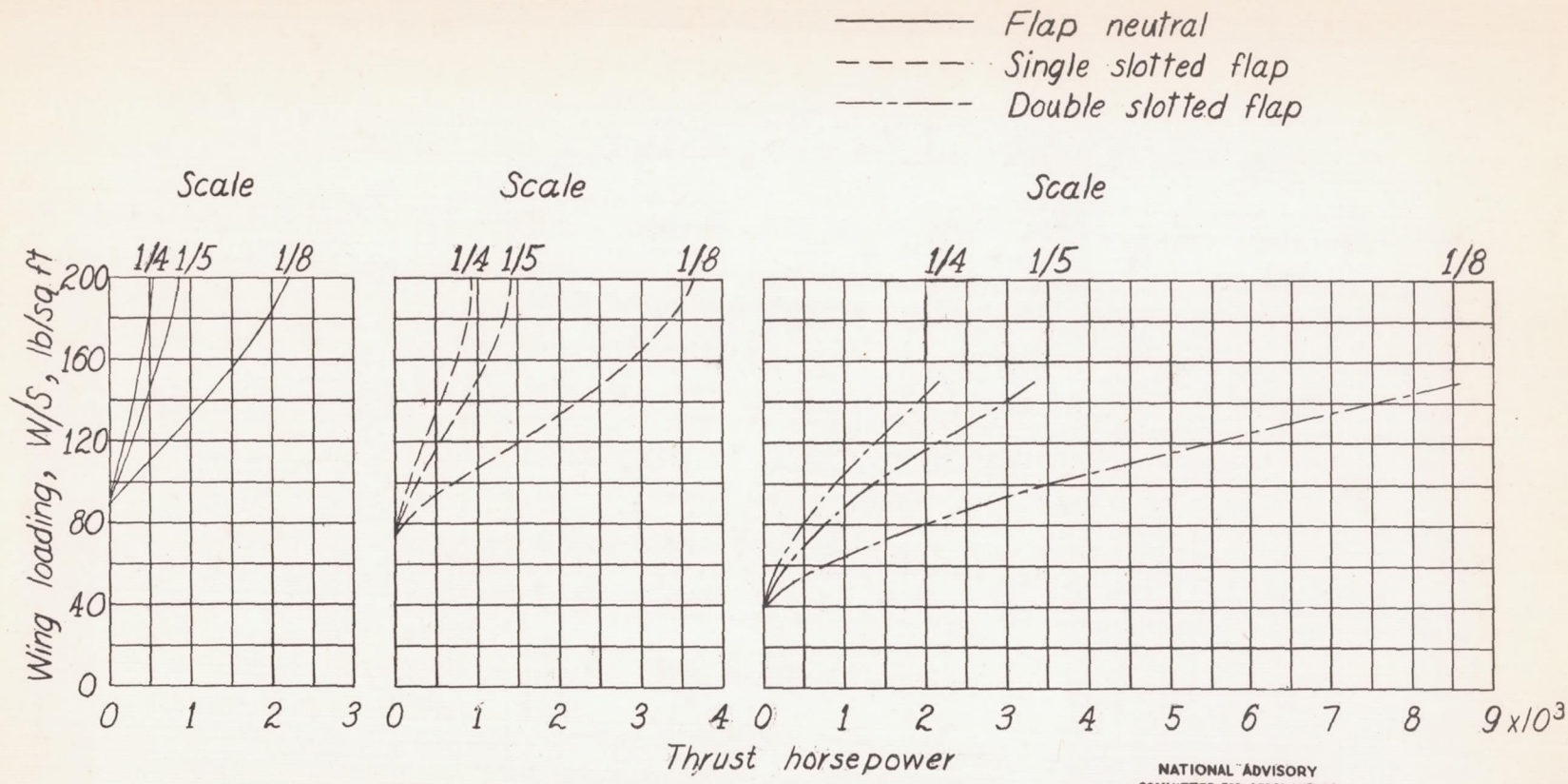


Figure 15.- Effect of scale and wing loading on the power required to maintain an indicated rate of descent of 25 feet per second at $0.85C_{L_{max}}$ for the model as a low-wing single-engine airplane.

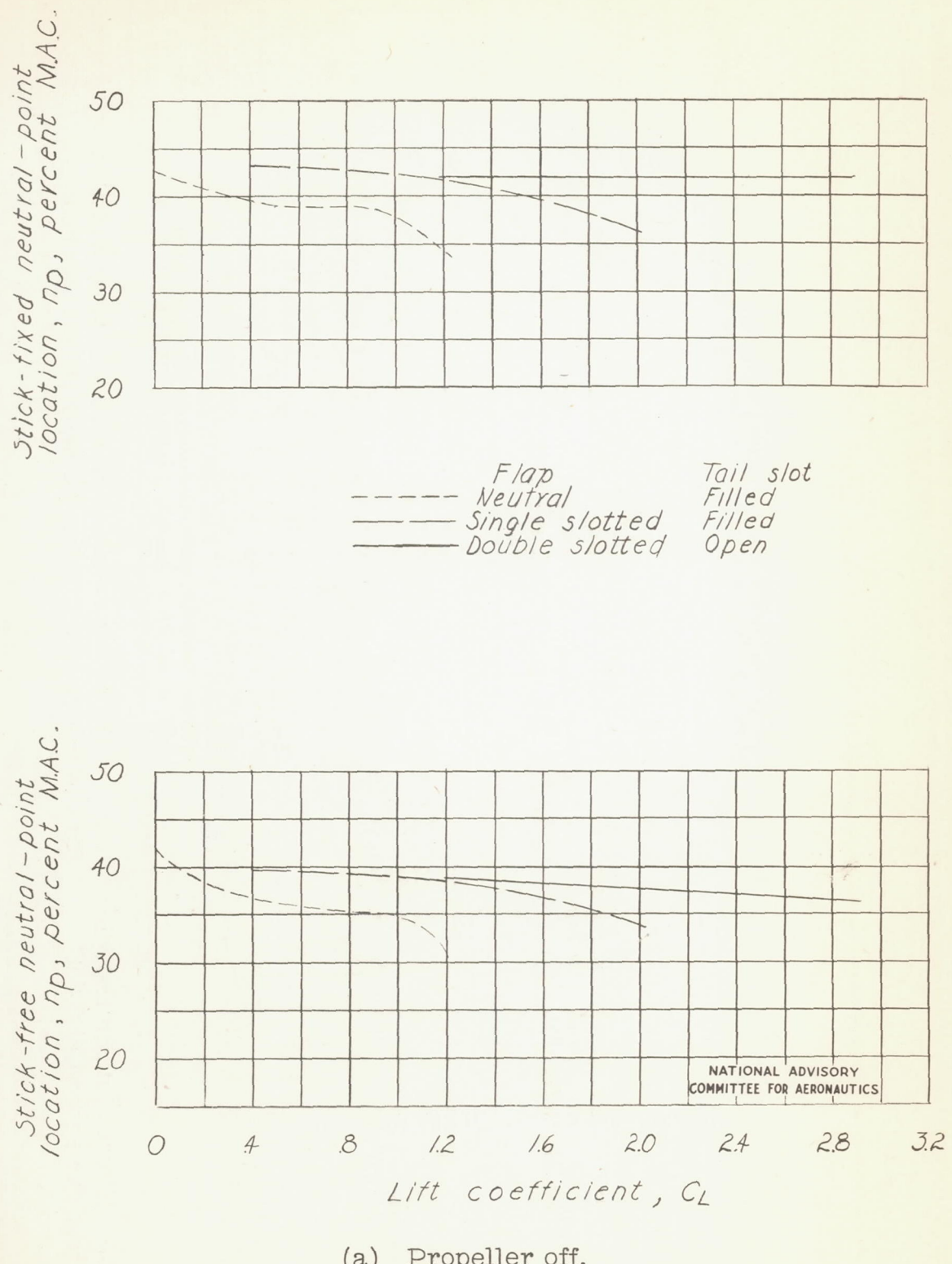
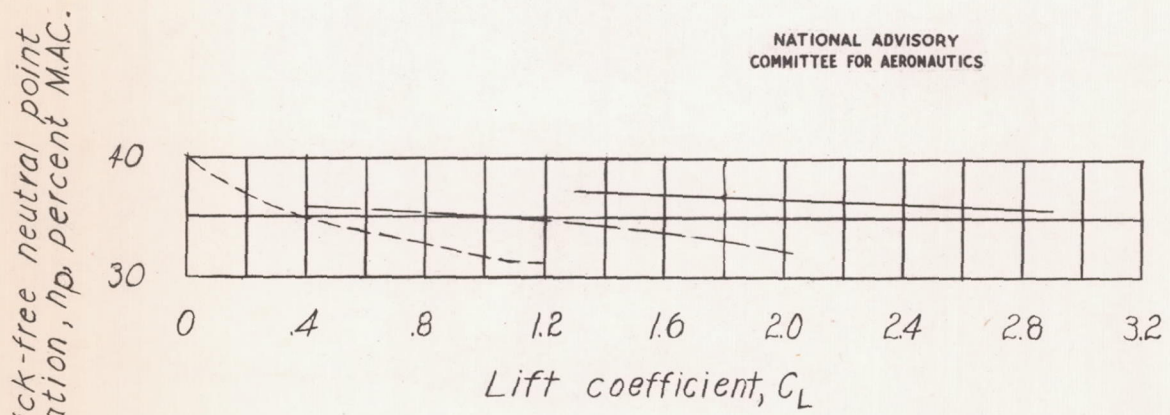
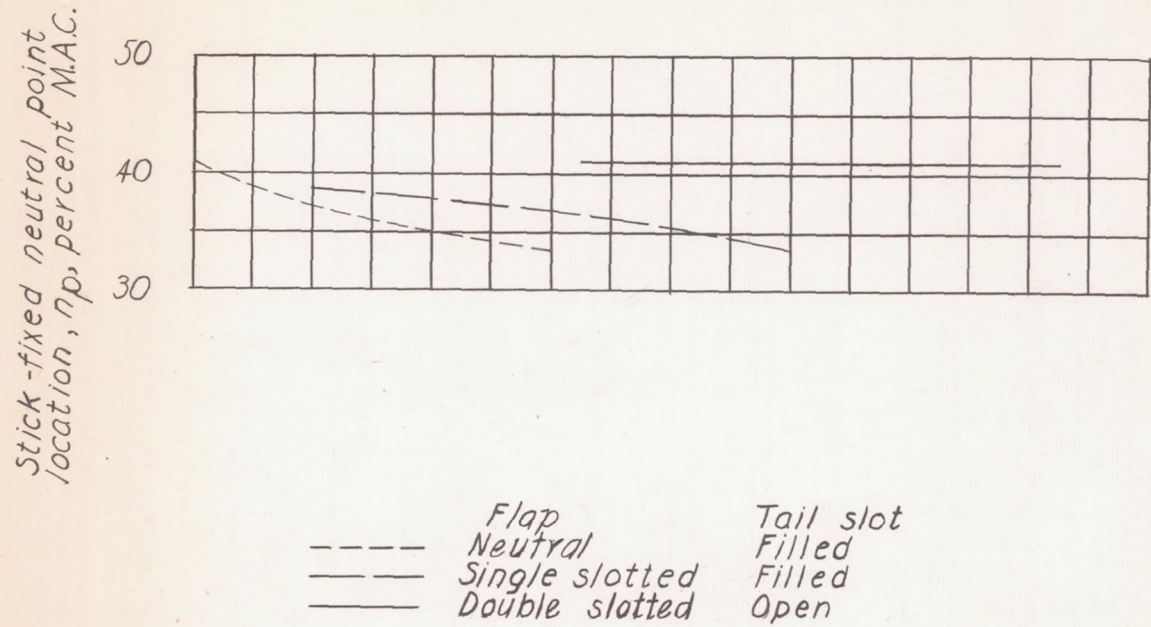
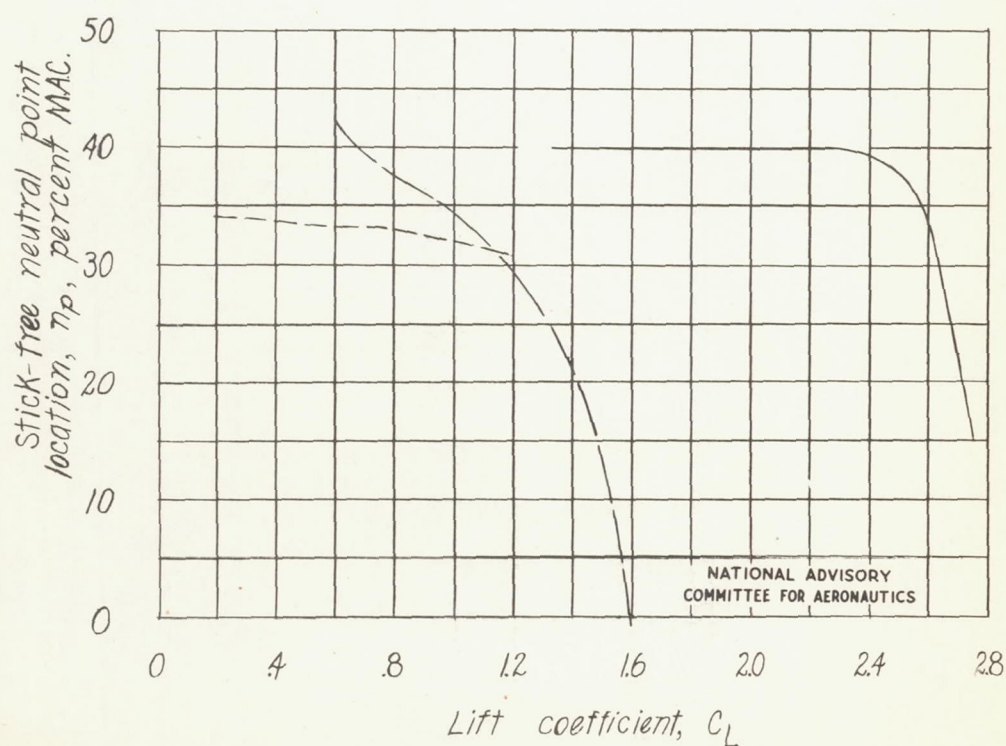
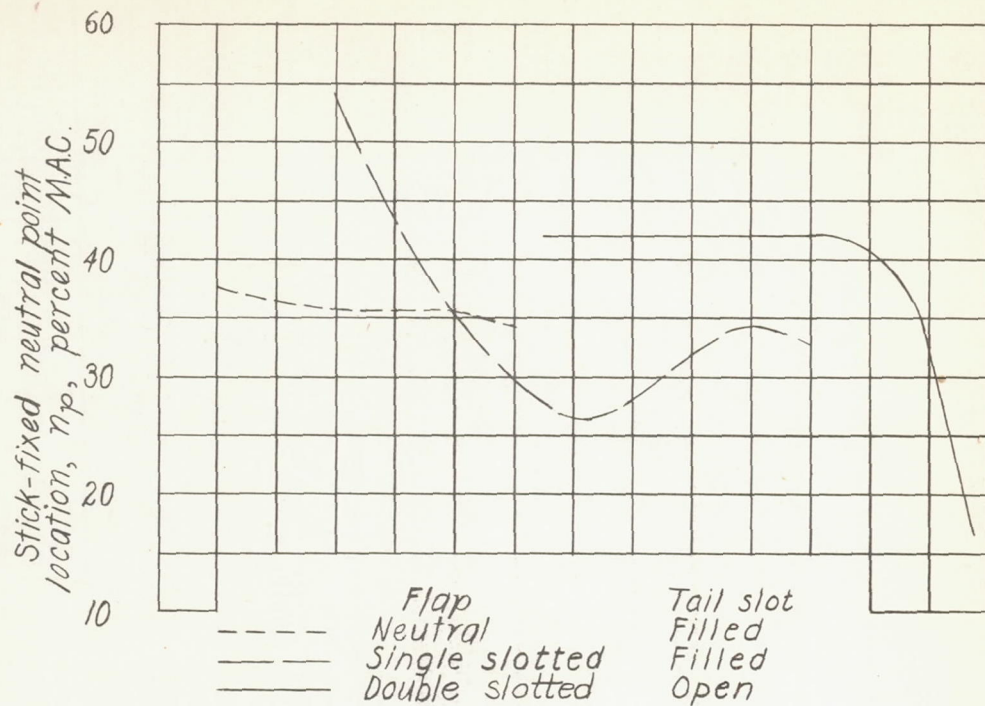


Figure 16.- Effect of flap deflection on the neutral-point location of the model as a low-wing airplane.



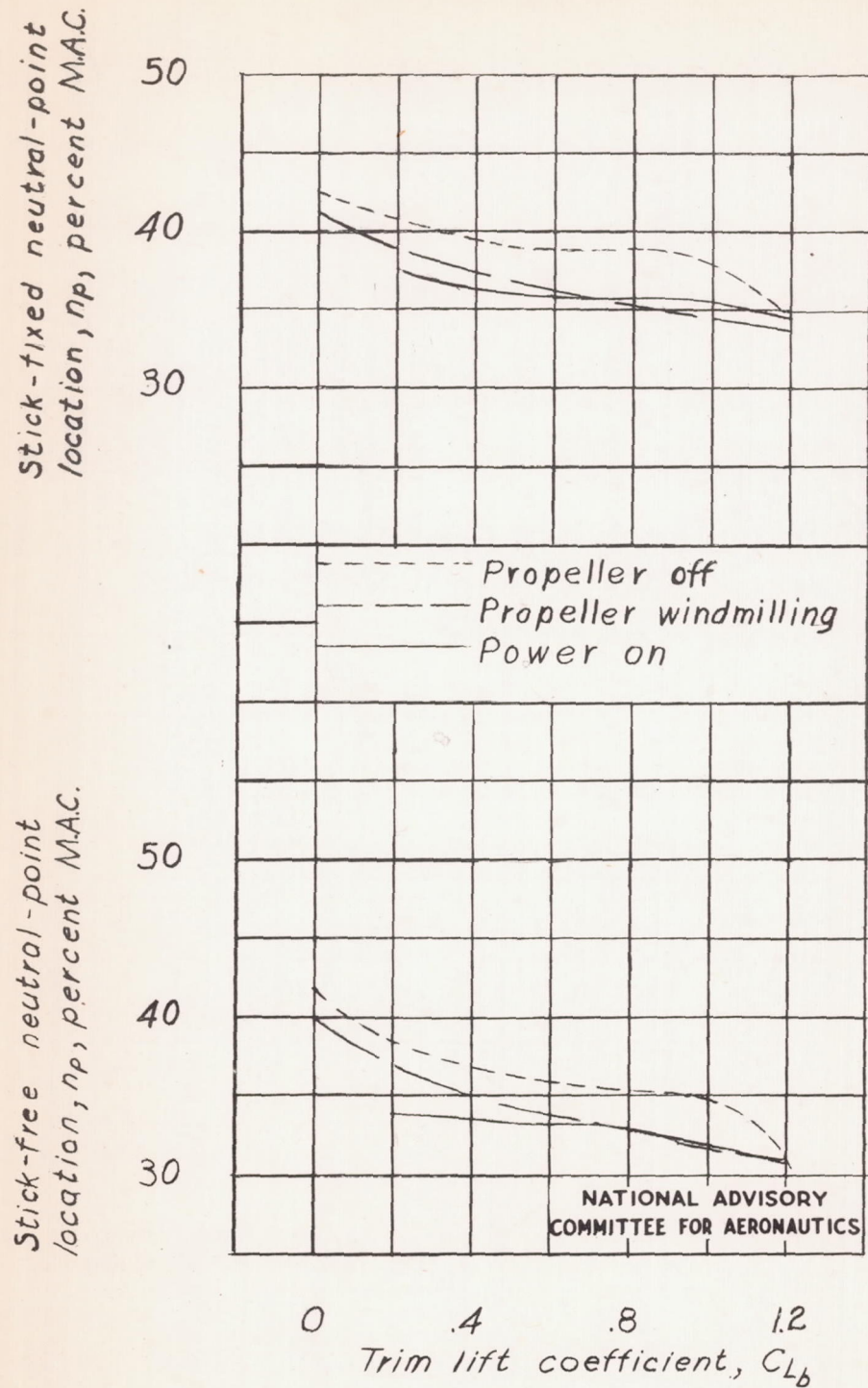
(b) Propeller windmilling.

Figure 16.- Continued.



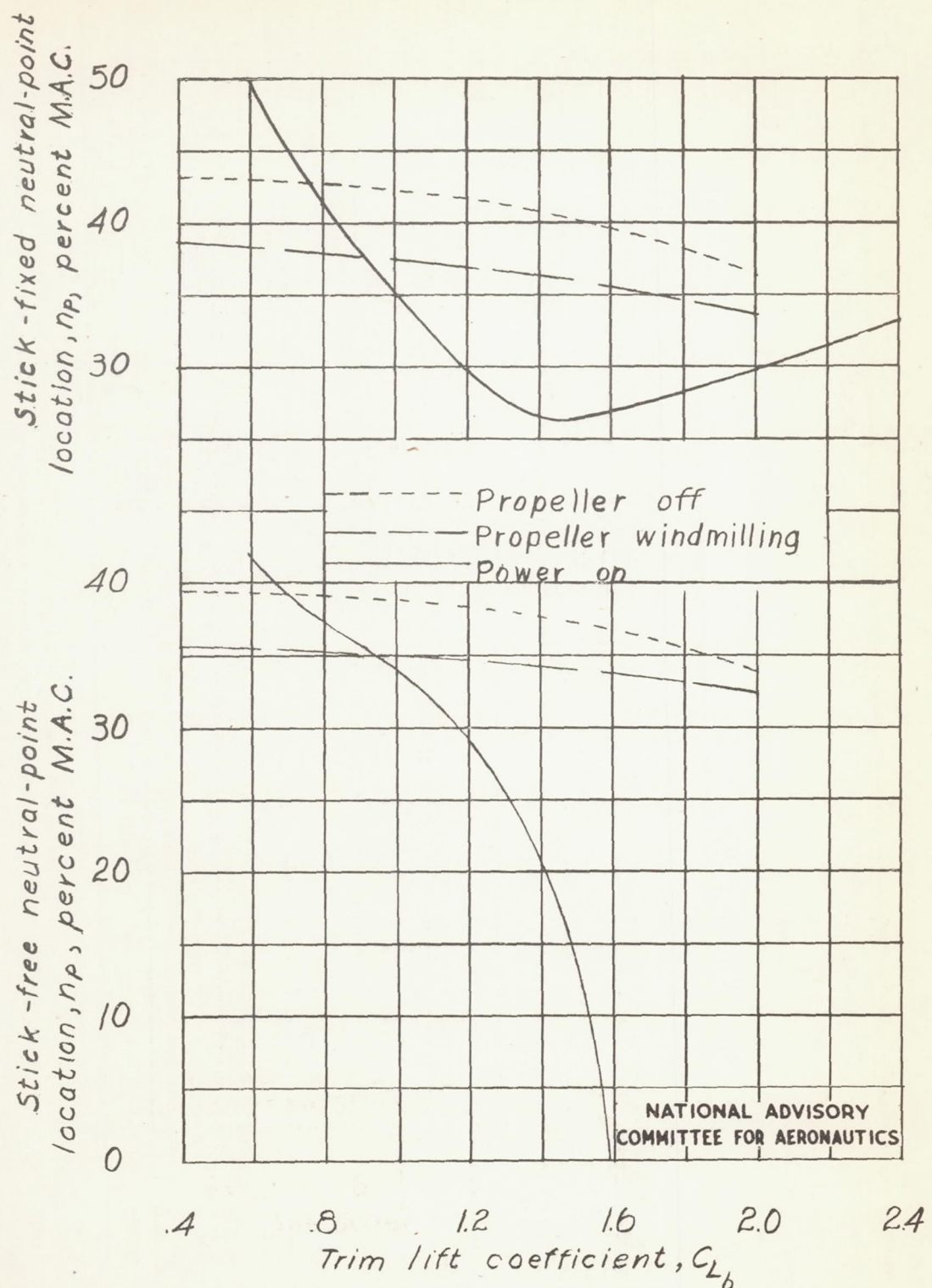
(c) Power on.

Figure 16.- Concluded.



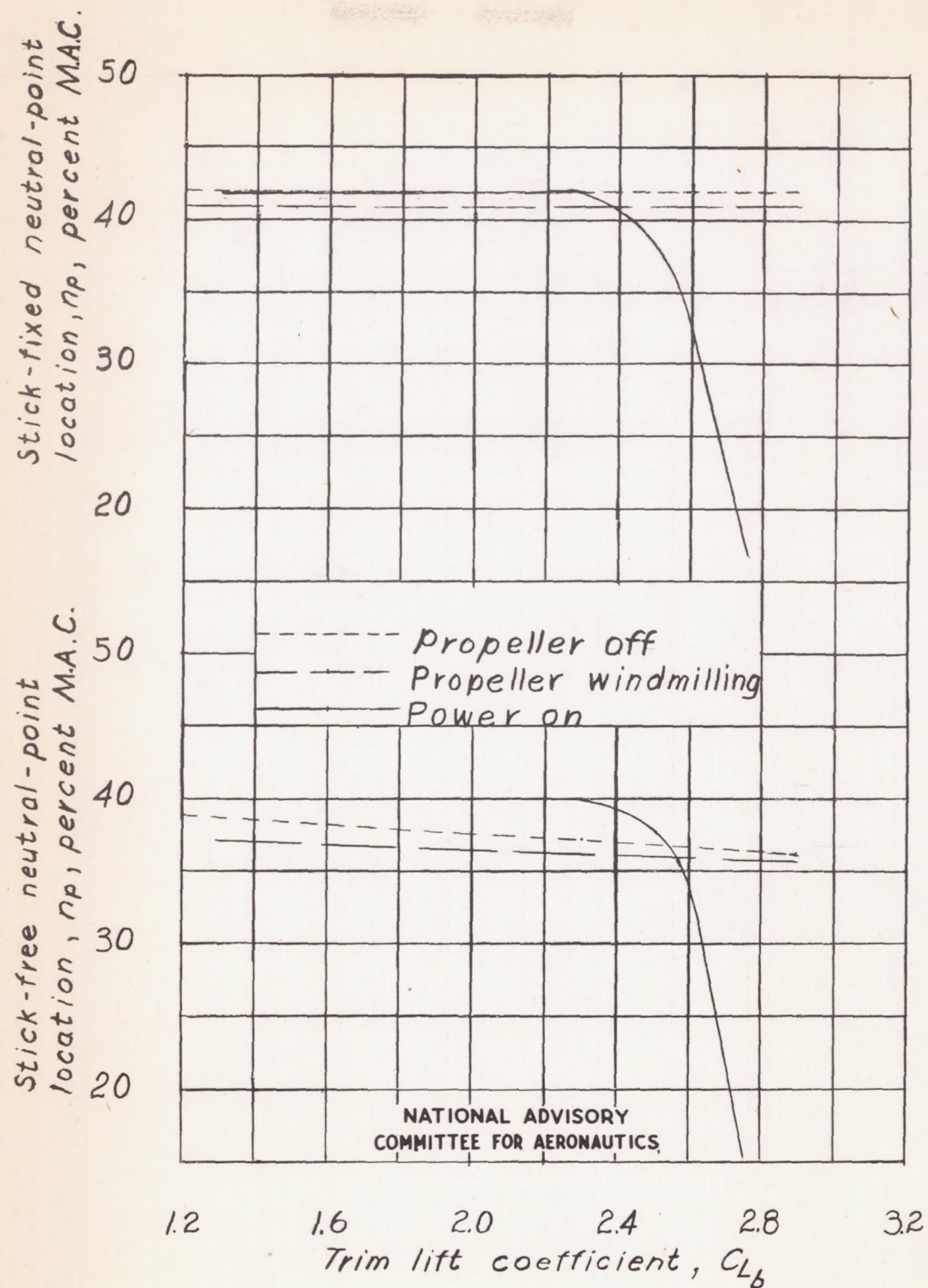
(a) Flap neutral.

Figure 17.- Effect of power on neutral-point location of the model as a low-wing airplane.



(b) Single slotted flap.

Figure 17.- Continued.



(c) Double slotted flap.

Figure 17.- Concluded.

Increment in neutral-point
location due to power, Δn_p

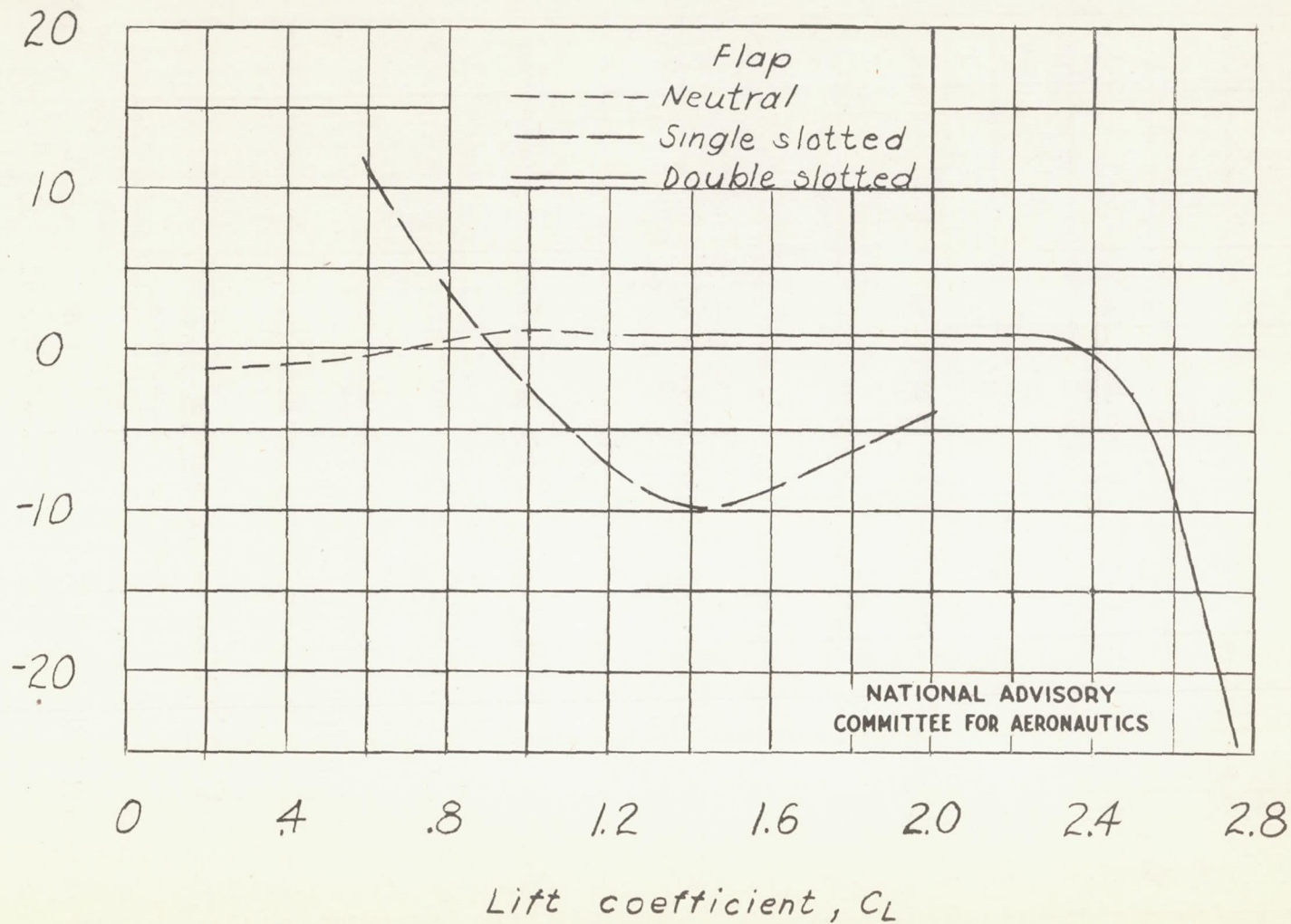


Figure 18.- Increments in neutral-point location due to power of the model as a low-wing airplane.

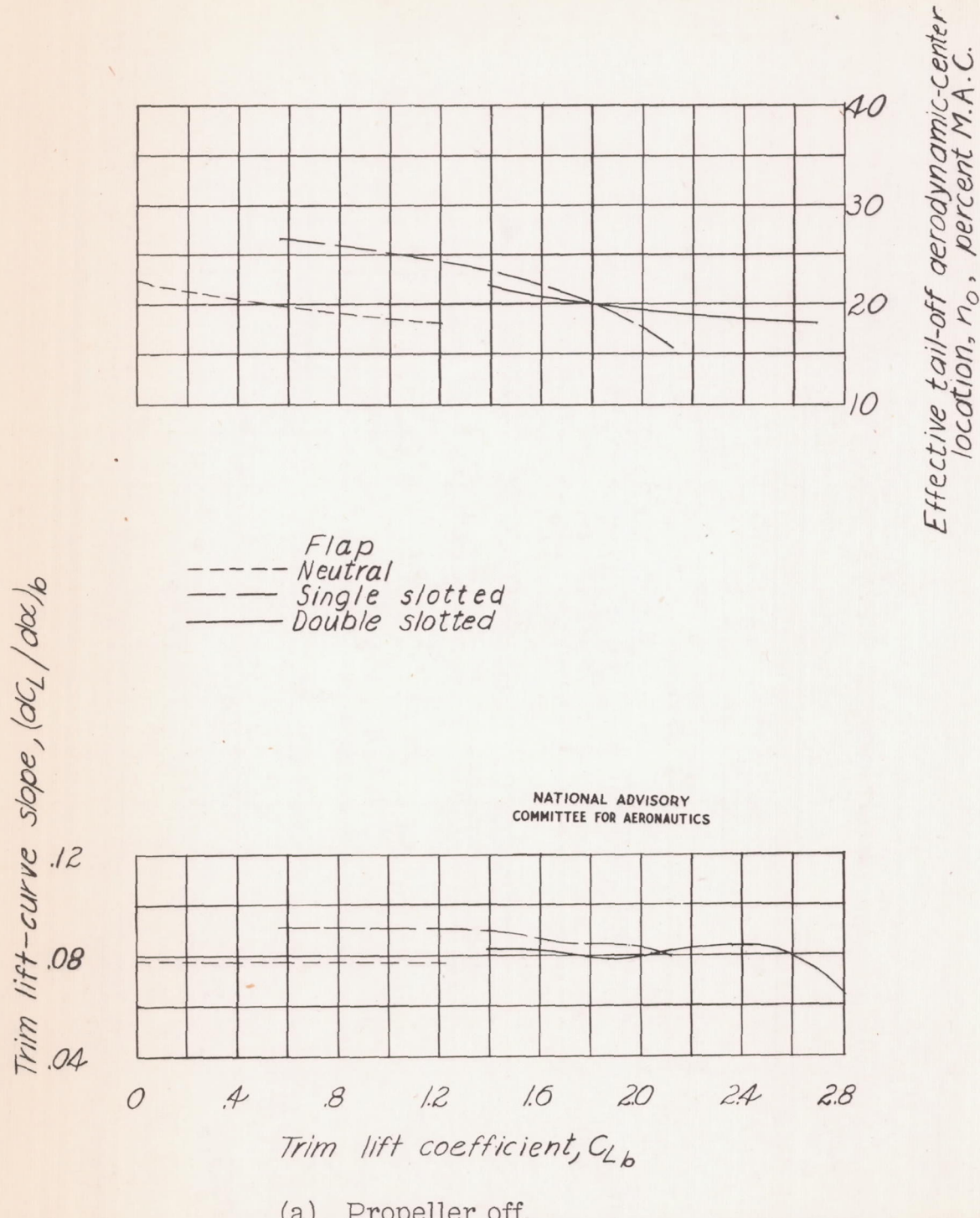
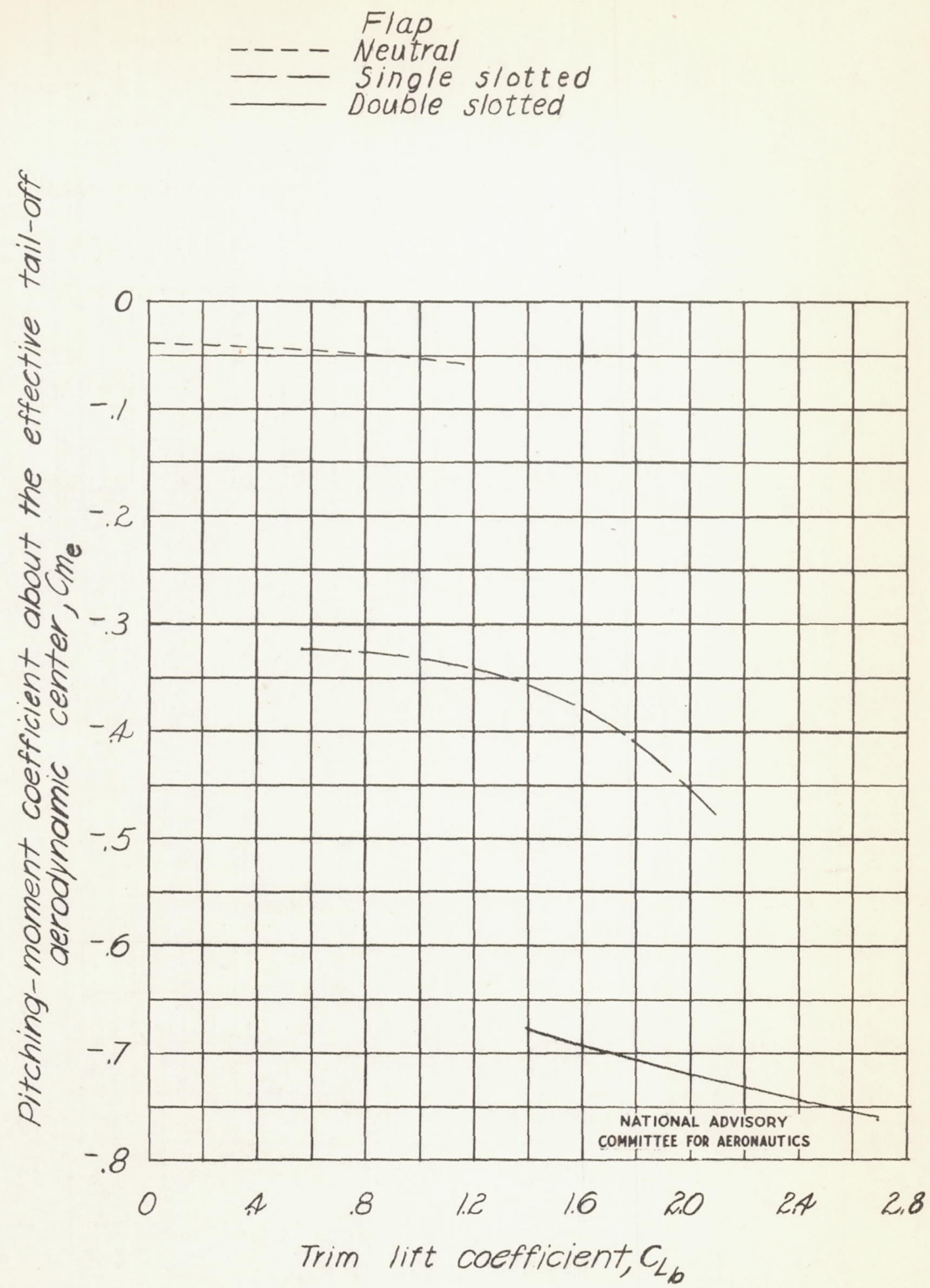
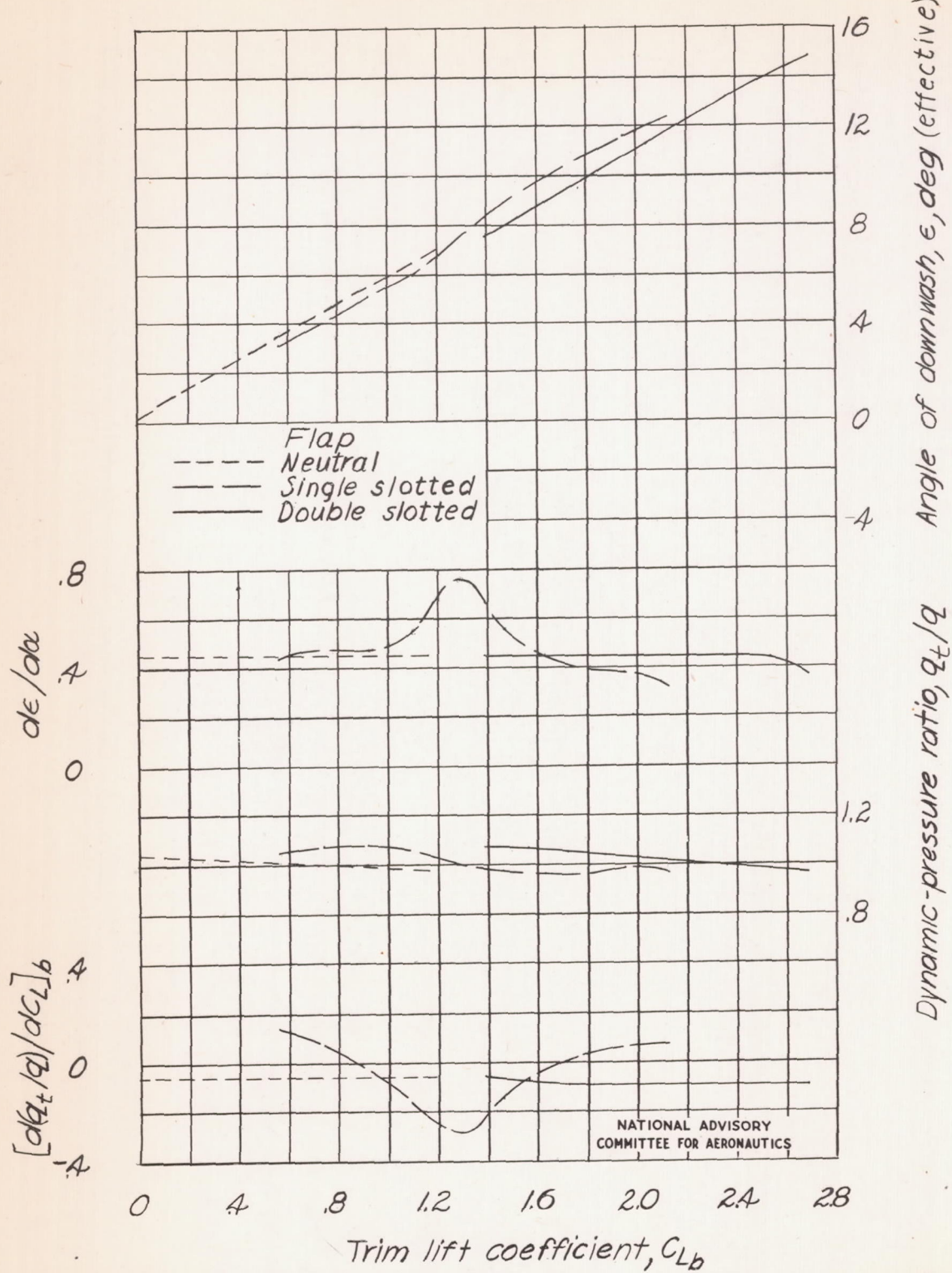


Figure 19.- Effect of flap on various longitudinal-stability parameters of the model as a low-wing airplane.



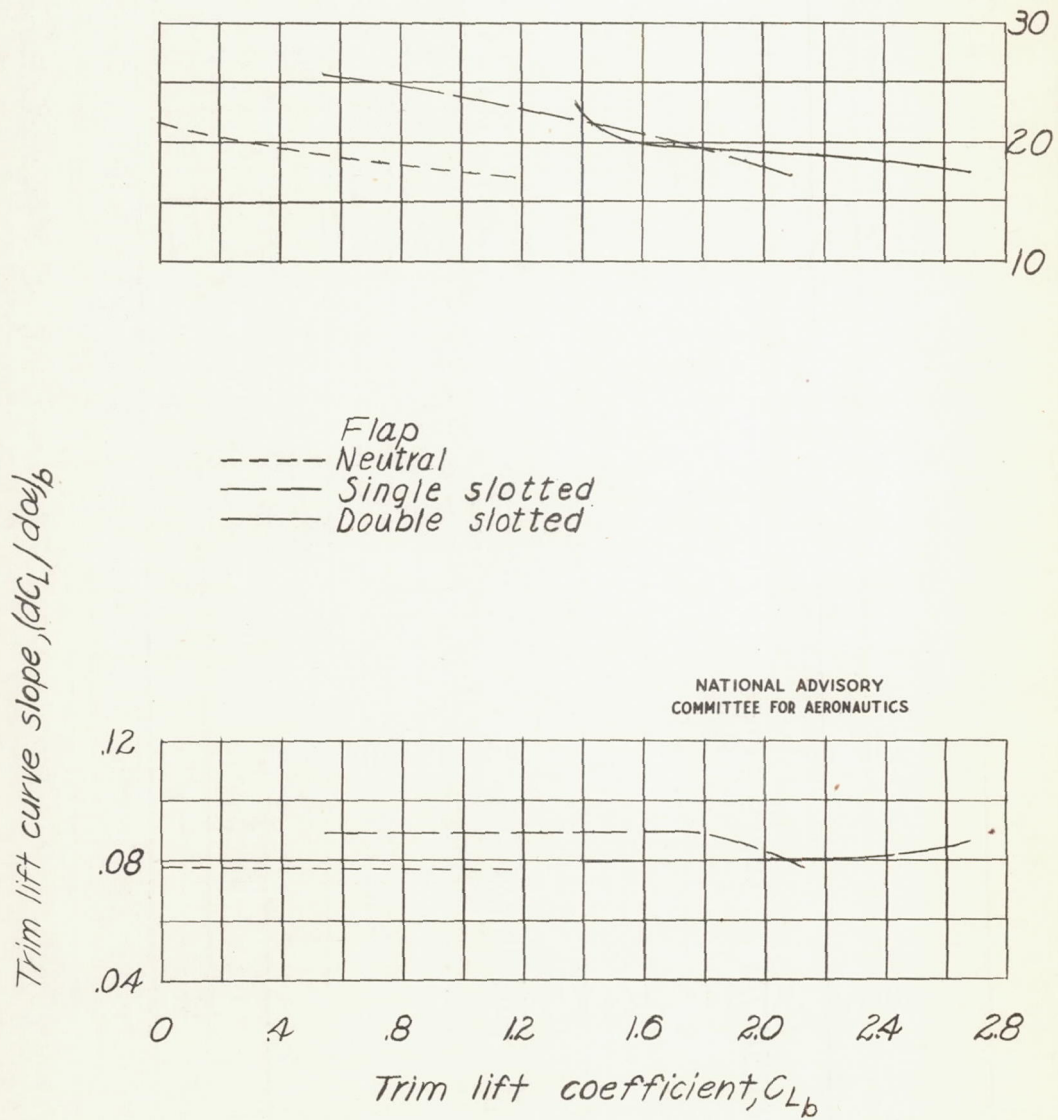
(a) Continued.

Figure 19.- Continued.



(a) Concluded.

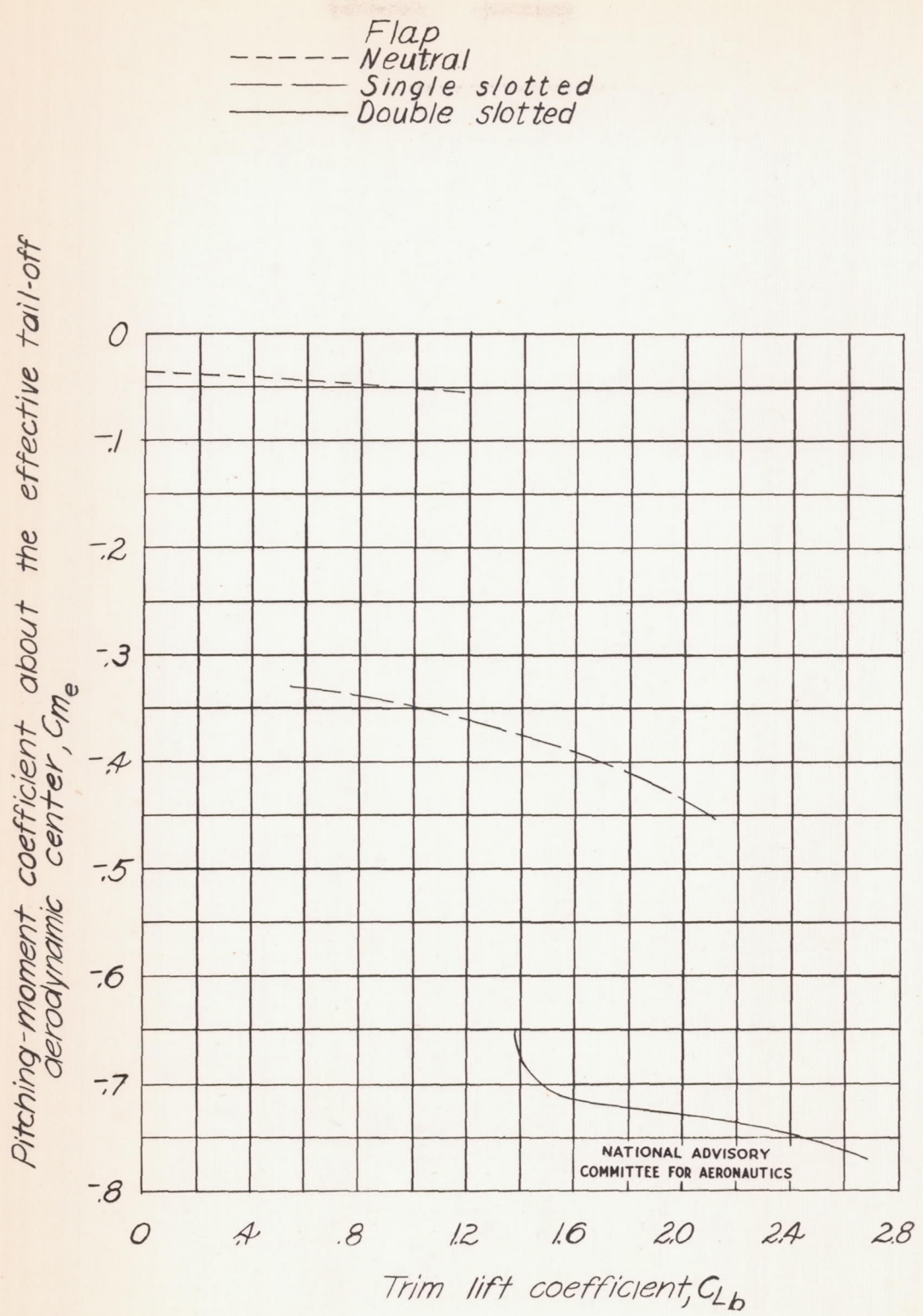
Figure 19.- Continued.



(b) Propeller windmilling.

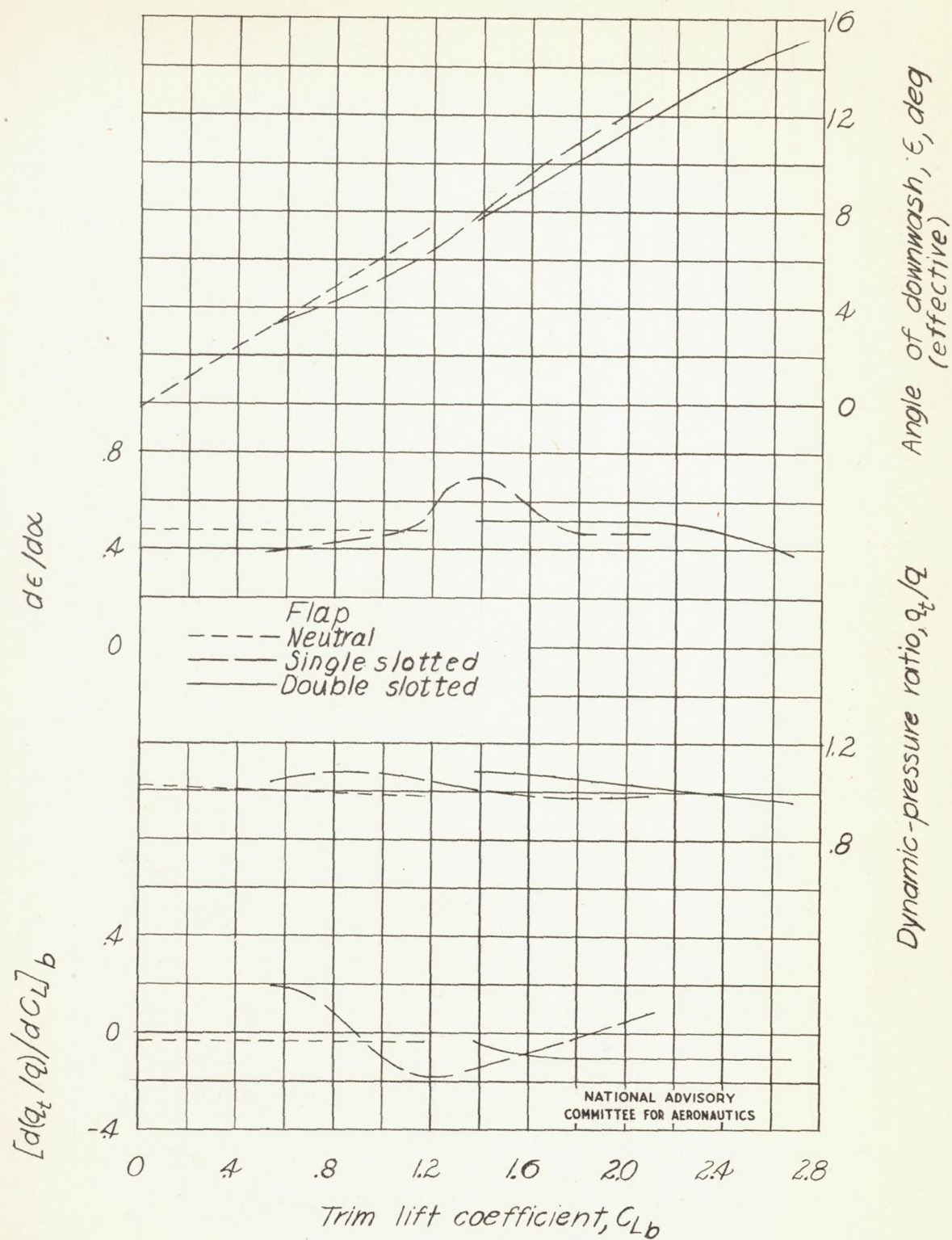
Figure 19.- Continued.

Effective tail-off aerodynamic-center
location, no, percent M.A.C.



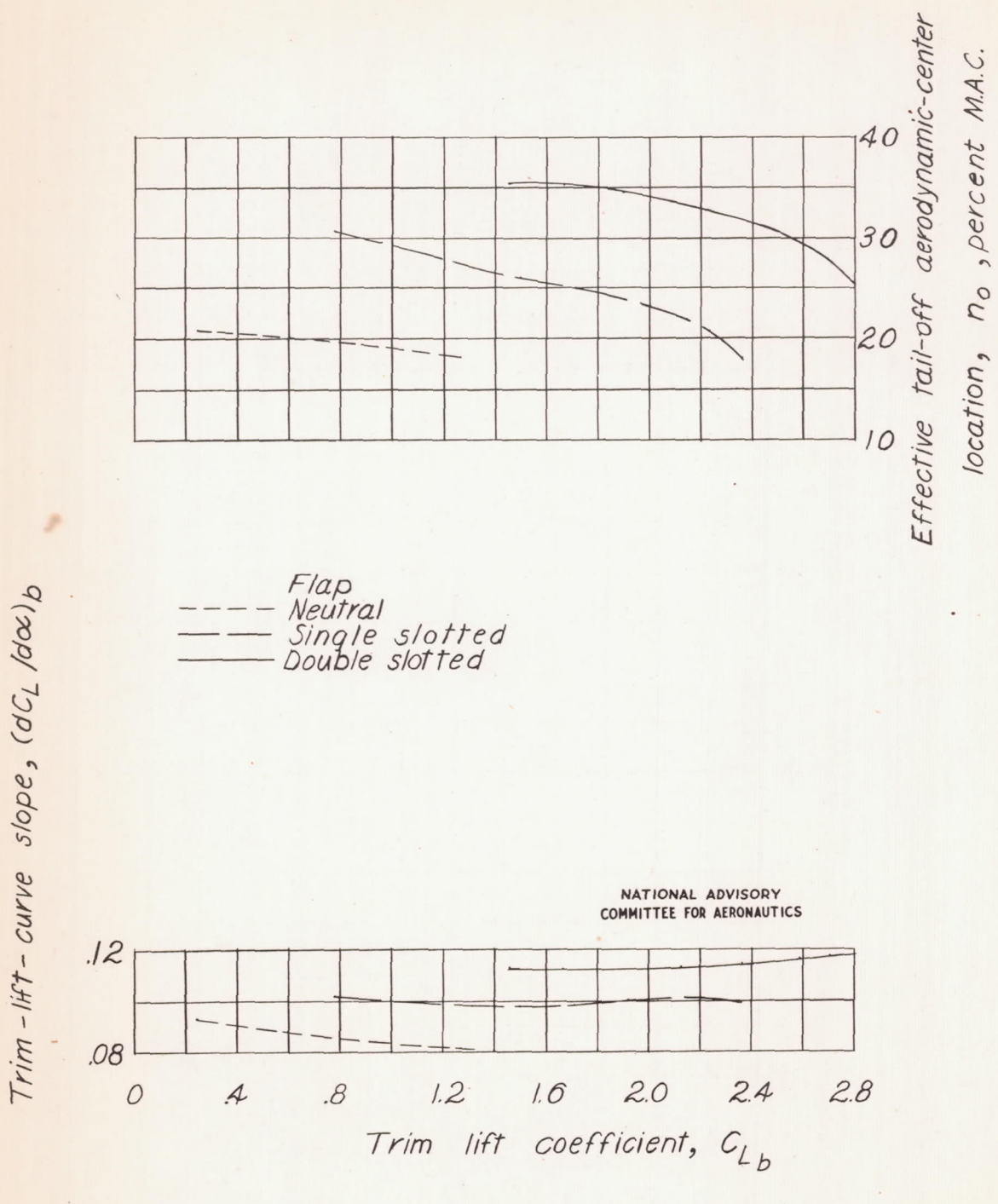
(b) Continued.

Figure 19.- Continued.



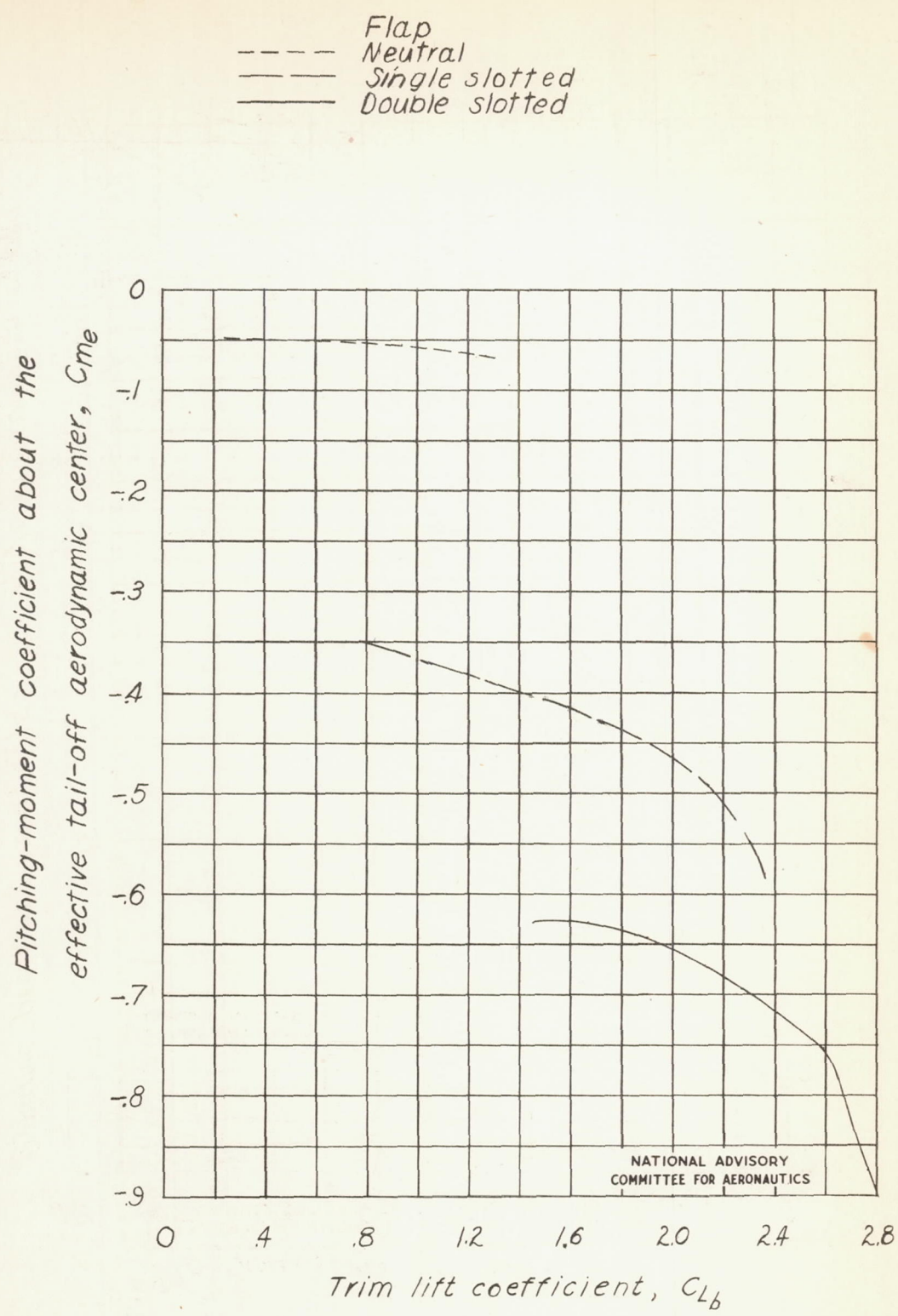
(b) Concluded.

Figure 19.- Continued.



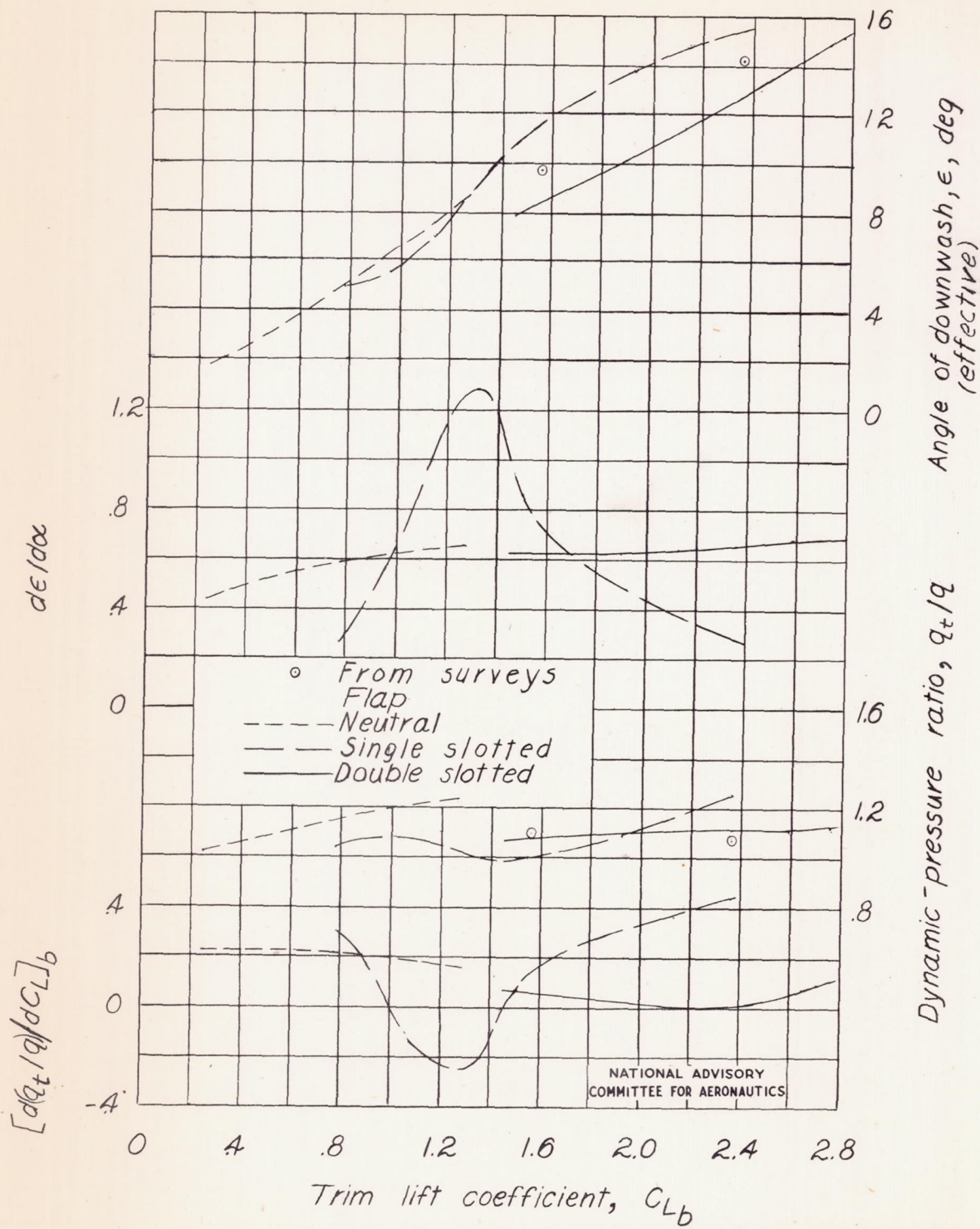
(c) Power on.

Figure 19.- Continued.



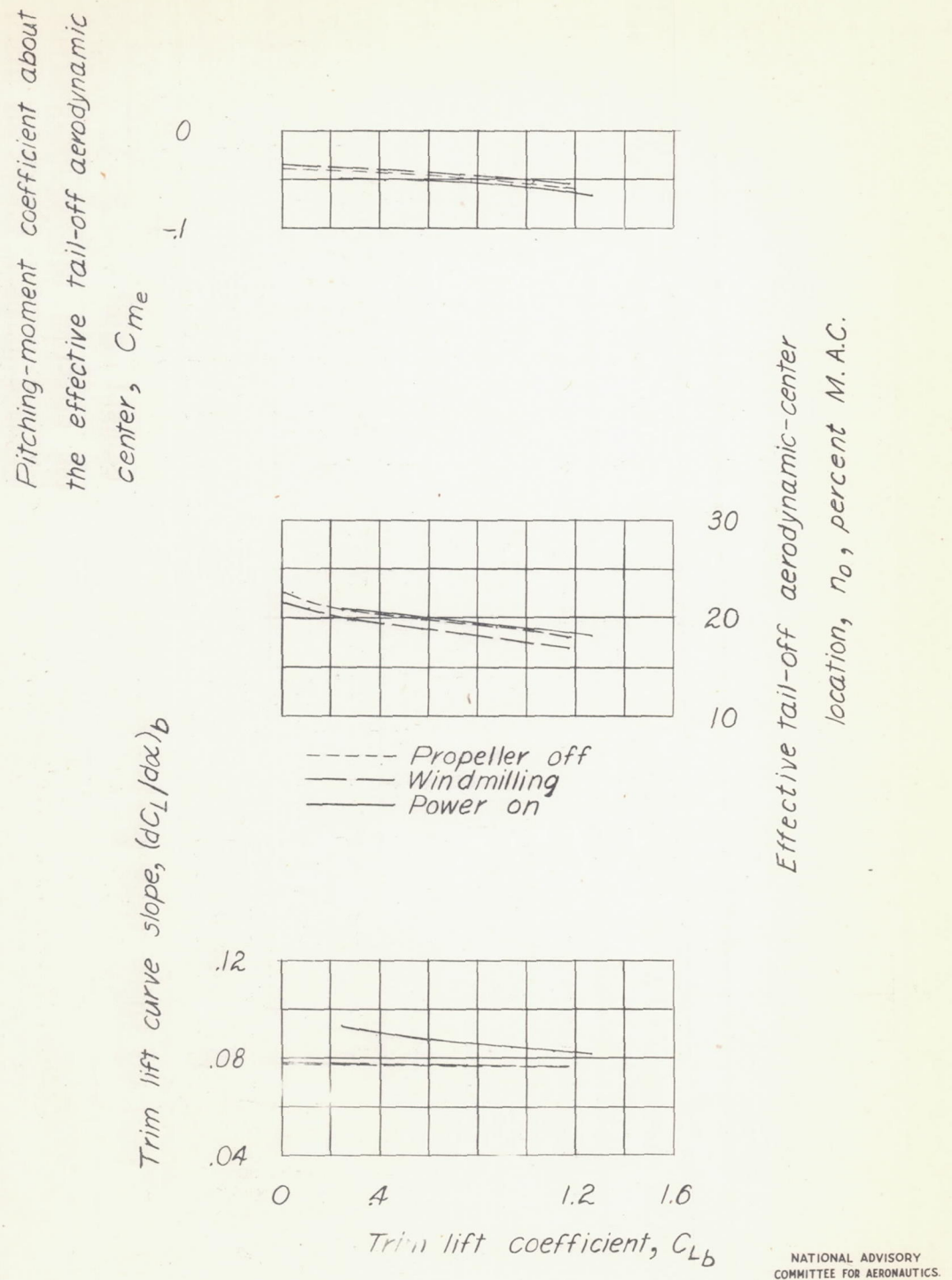
(c) Continued.

Figure 19c - Continued.



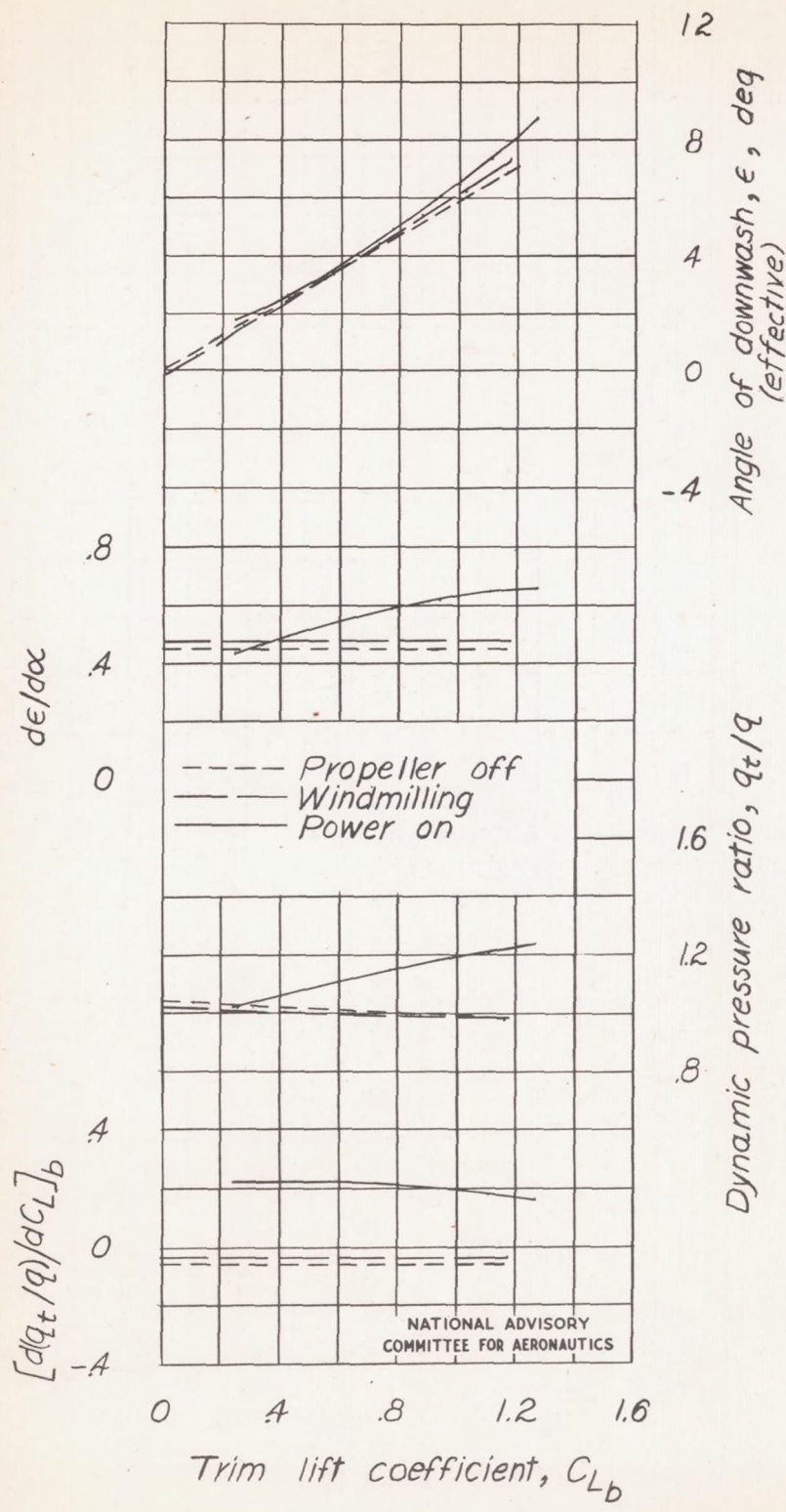
(c) Concluded.

Figure 19.- Concluded.



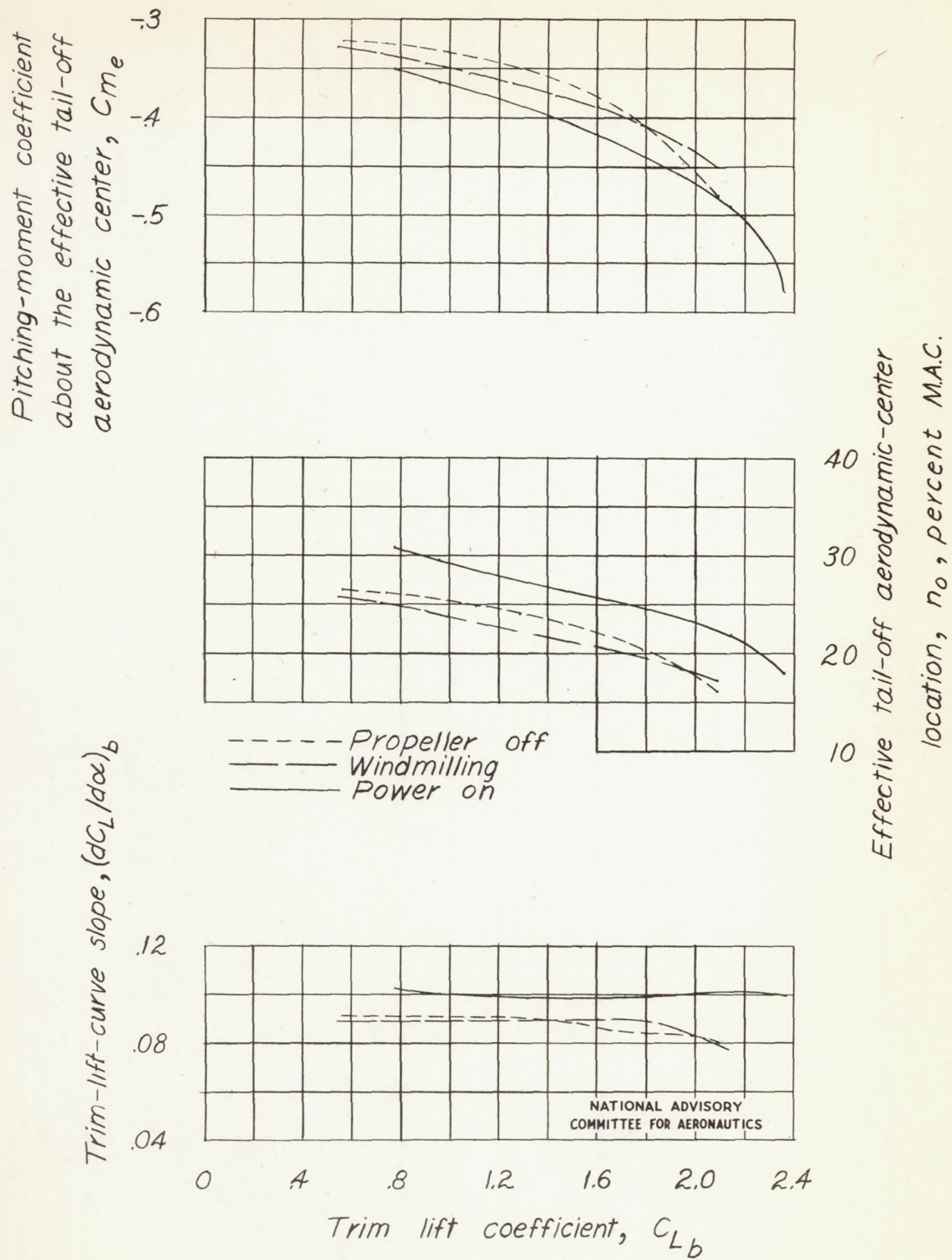
(a) Flap neutral; $\delta_{f1} = \delta_{f2} = 0^\circ$.

Figure 20.- Effect of power on various longitudinal-stability parameters of the model as a low-wing airplane.



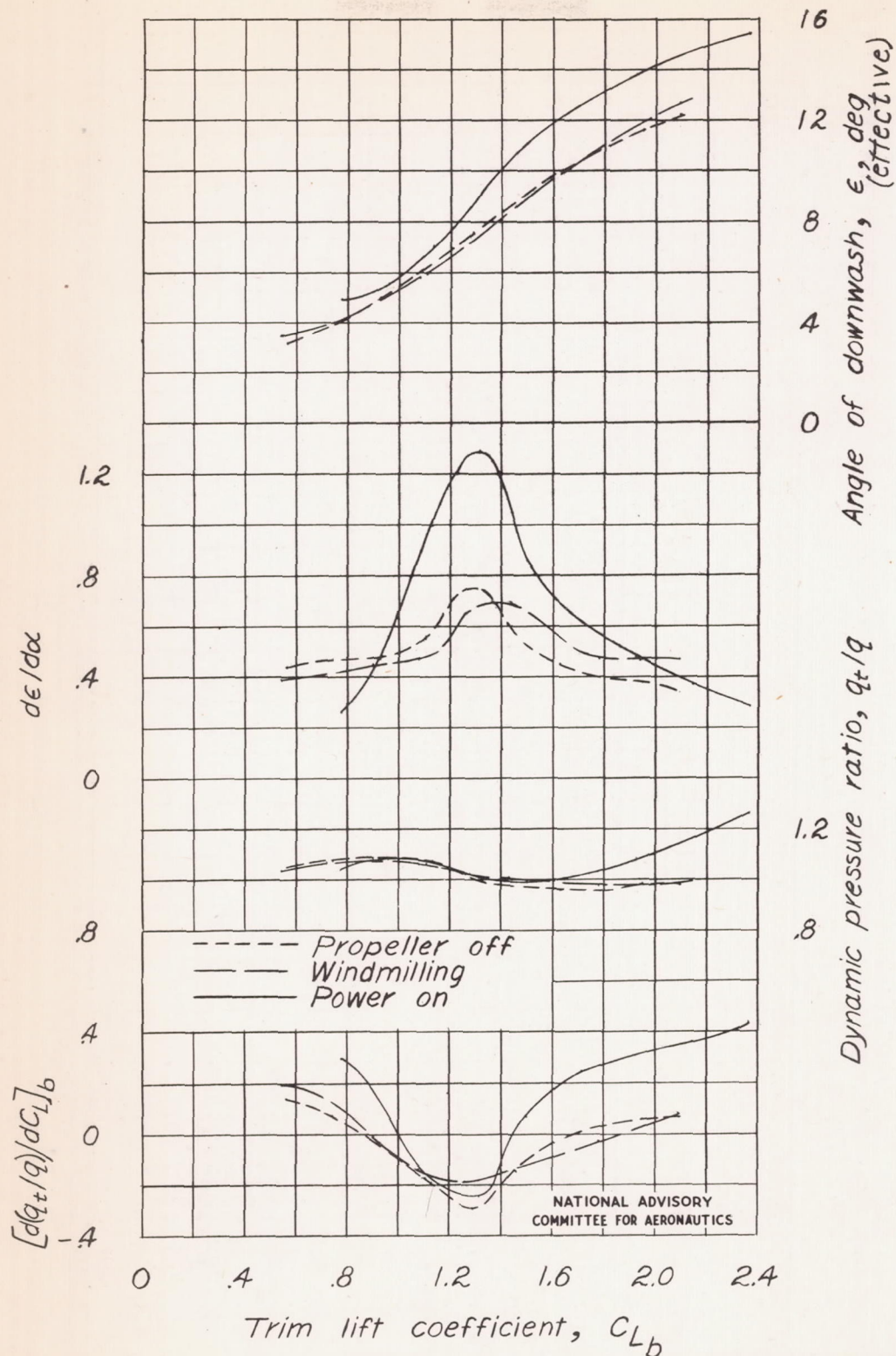
(a) Concluded.

Figure 20.- Continued.



(b) Slotted flap; $\delta_{f2} = 30^\circ$.

Figure 20.- Continued.



(b) Concluded.

Figure 20.- Continued.

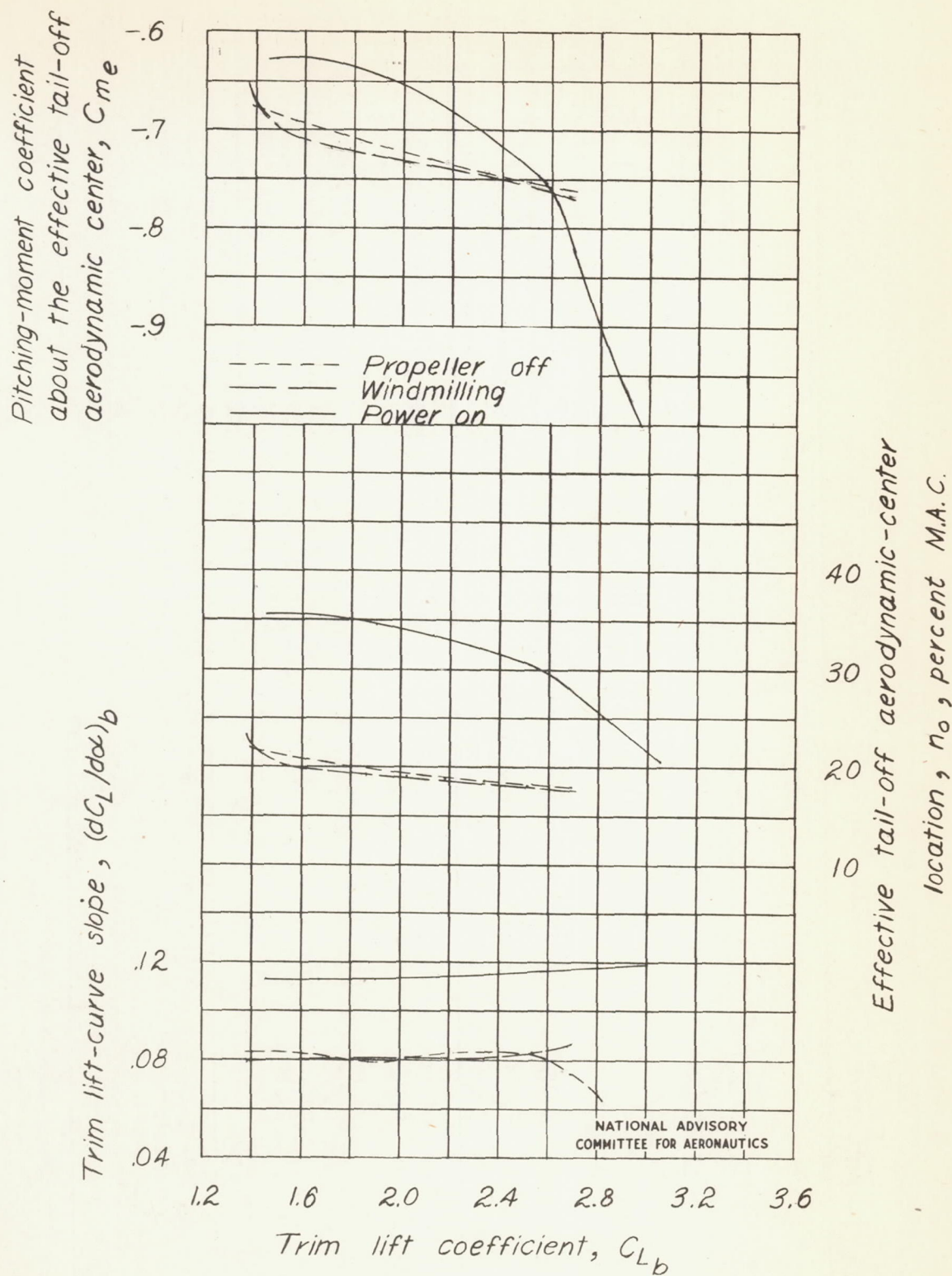
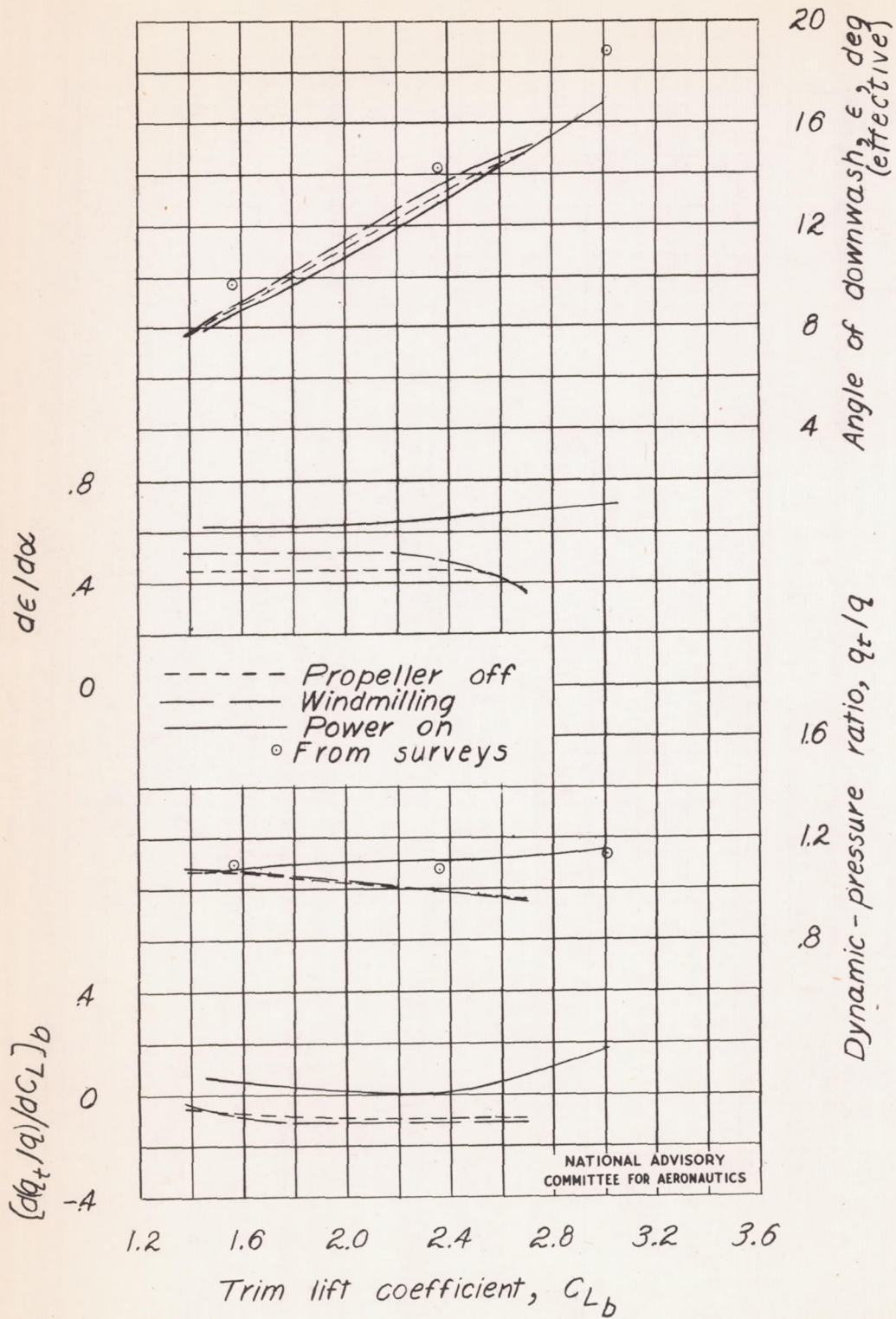
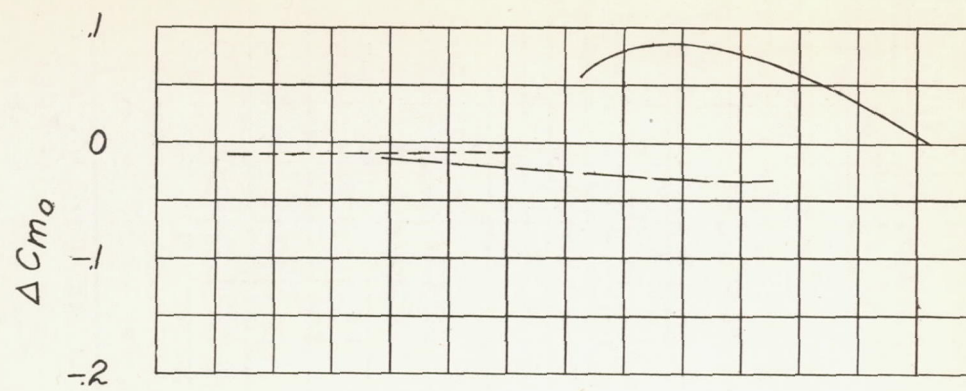


Figure 20.- Continued.



(c) Concluded.

Figure 20.- Concluded.



Legend:

- Flap Neutral
- Single slotted Filled
- Double slotted Open

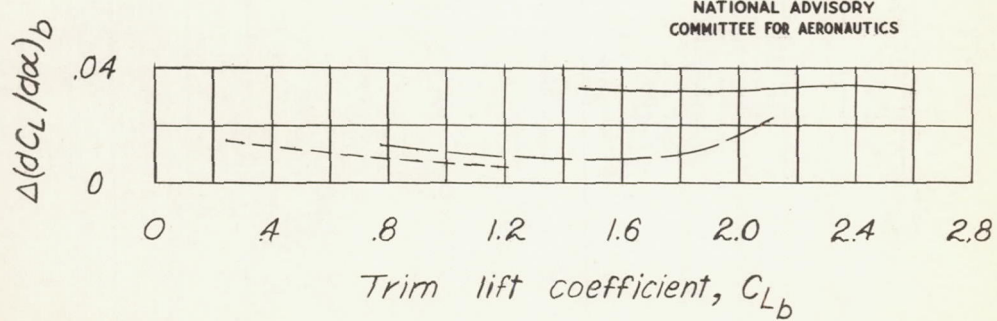
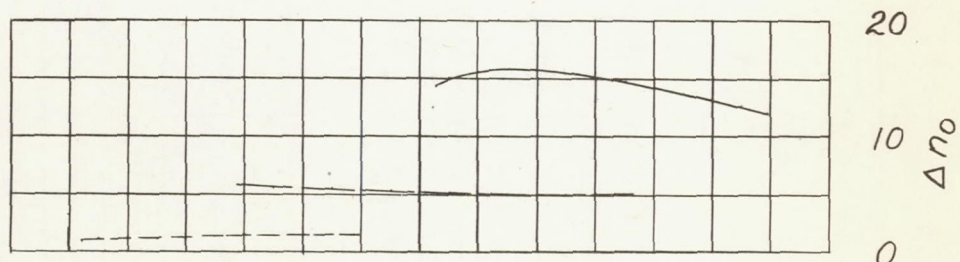


Figure 21.- Increments in longitudinal-stability parameters due to power of the model as a low-wing airplane.

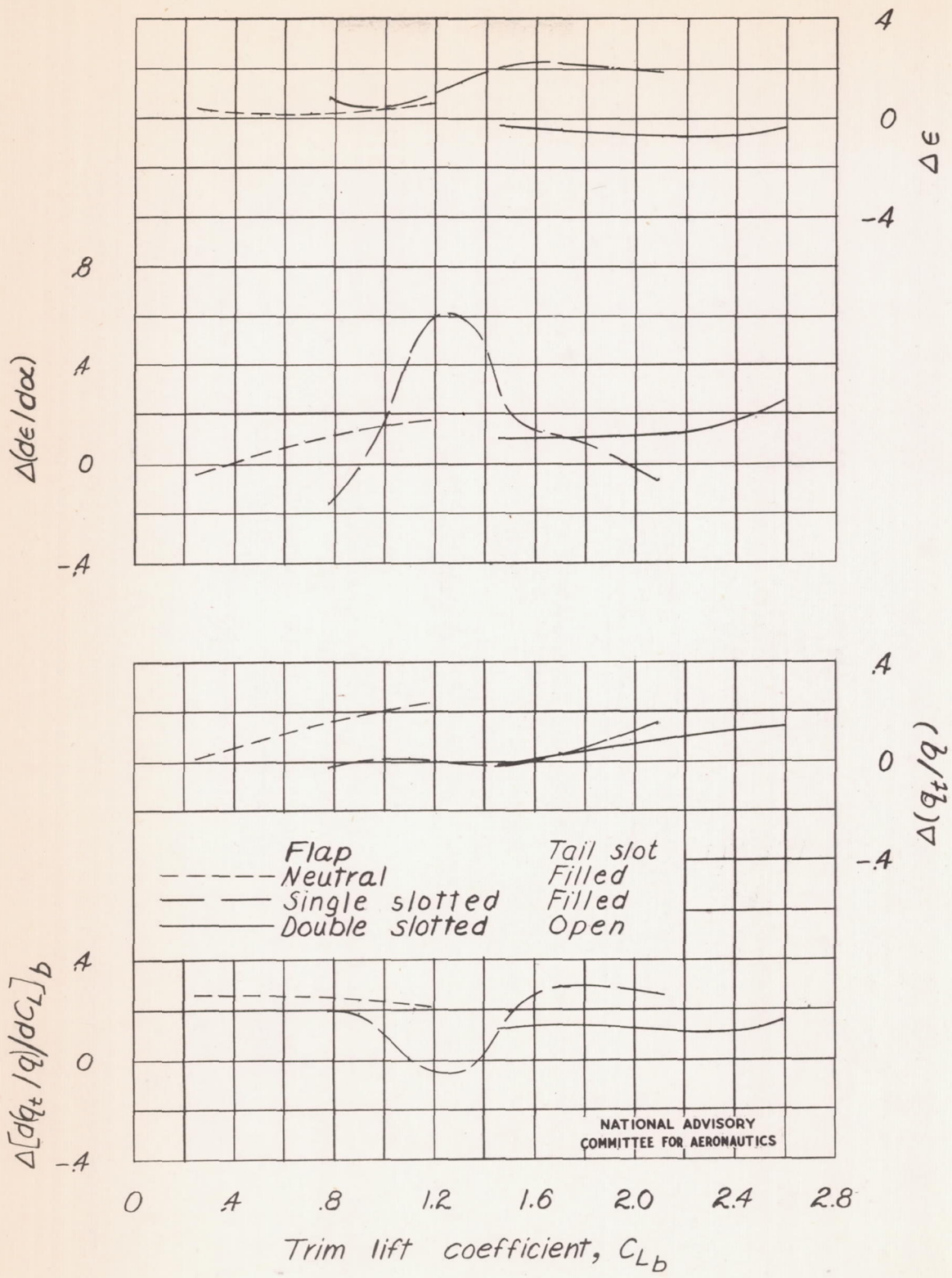
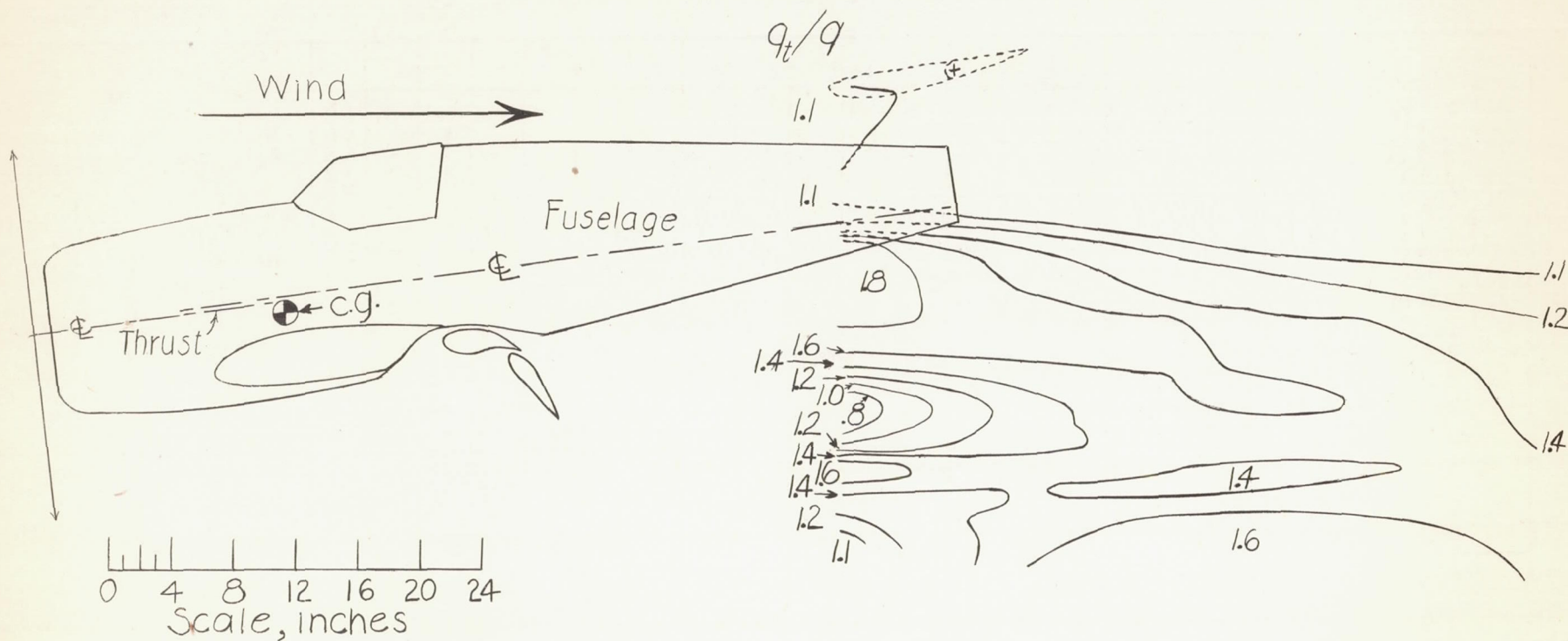


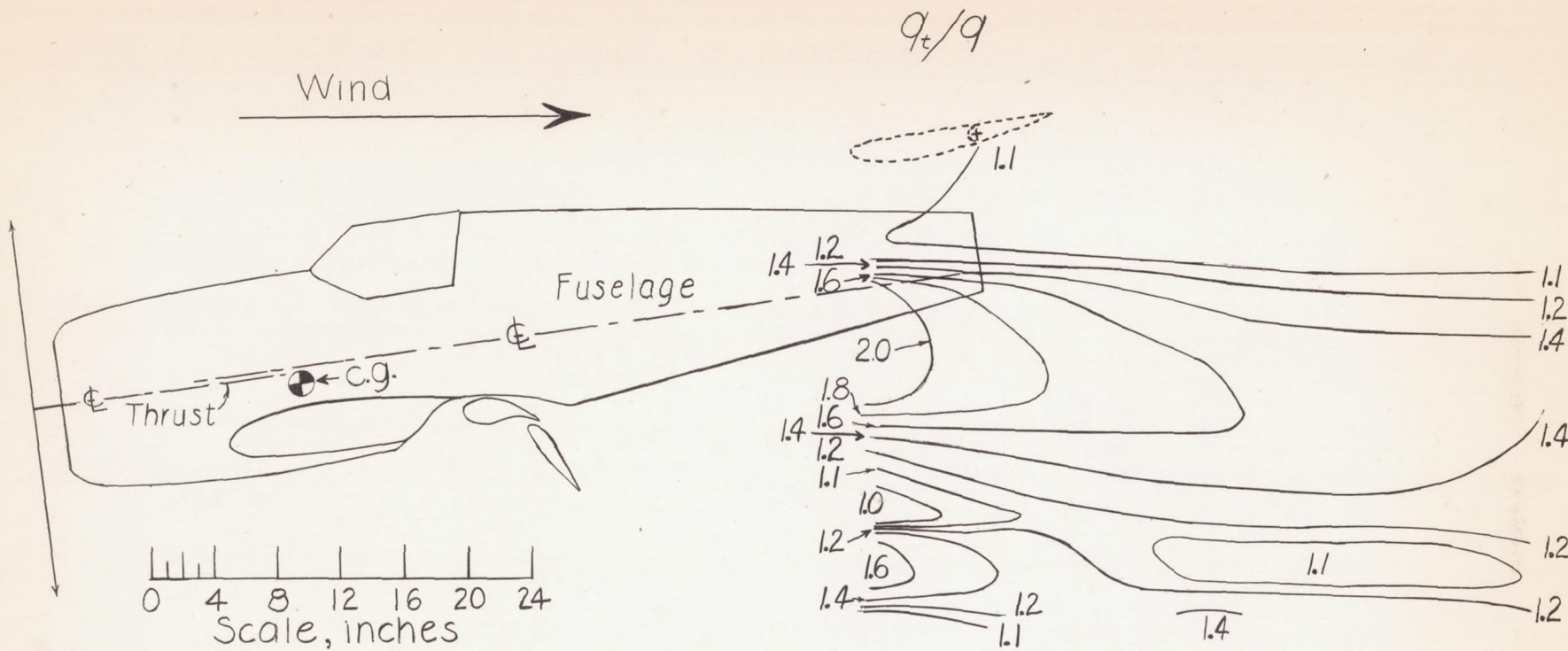
Figure 21.- Concluded.

Fig. 22a



(a) $\alpha = -8.9^\circ$; $C_L = 1.56$; 6 inches right of center line; $T_C' = 0.26$.

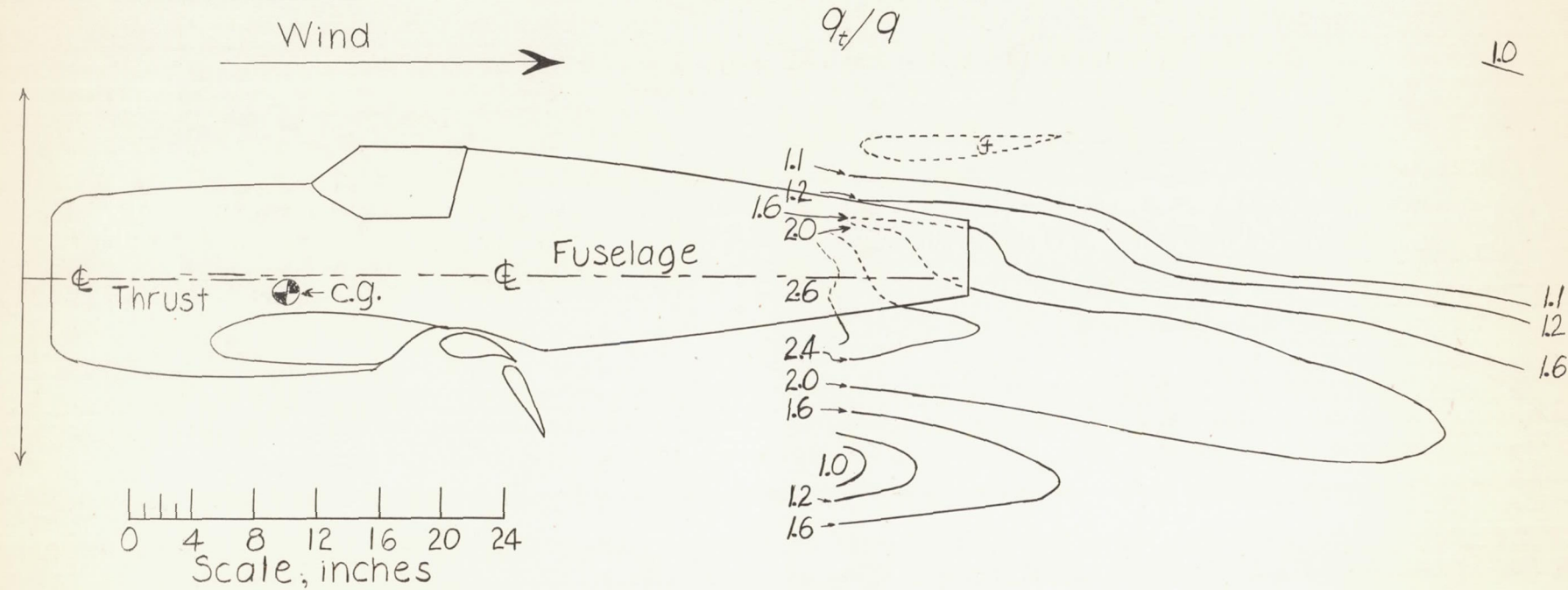
Figure 22.- Contours of dynamic-pressure ratios behind model as a low-wing airplane with full-span double slotted flap. $\delta_{f1} = \delta_{f2} = 30^\circ$; tail off; power on.



NATIONAL ADVISORY
COMMITTEE FOR AERONAUTICS

(b) $\alpha = -8.9^\circ$; $C_L = 1.56$; 6 inches left of center line; $T_C' = 0.26$.

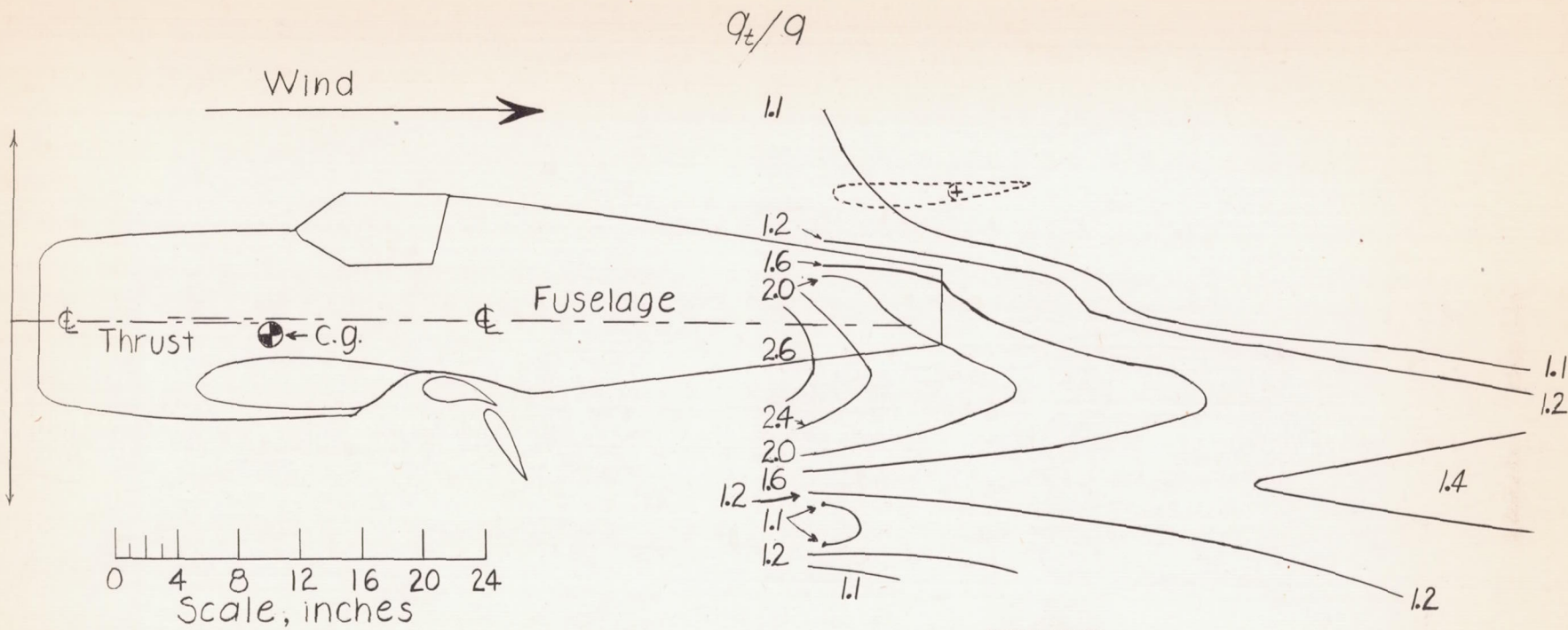
Figure 22.- Continued.



NATIONAL ADVISORY
COMMITTEE FOR AERONAUTICS

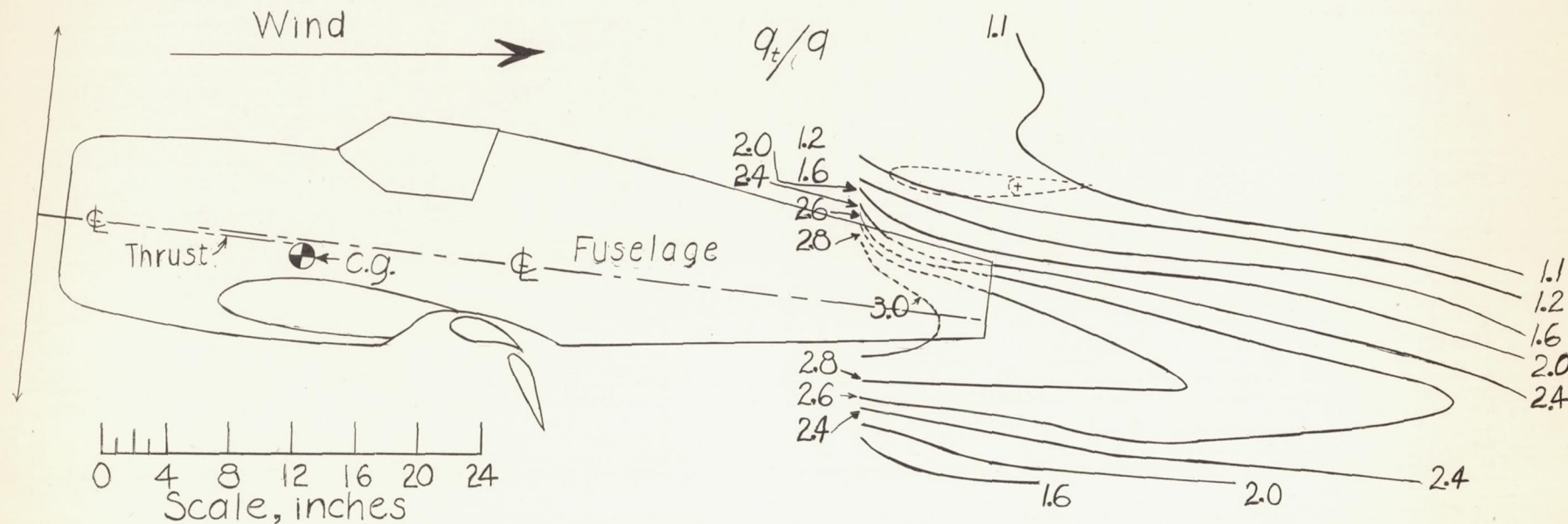
(c) $\alpha = -1.6^\circ$; $C_L = 2.36$; 6 inches right of center line; $T_C' = 0.38$.

Figure 22.- Continued.



(d) $\alpha = -1.6^\circ$; $C_L = 2.36$; 6 inches left of center line; $T_C' = 0.38$.

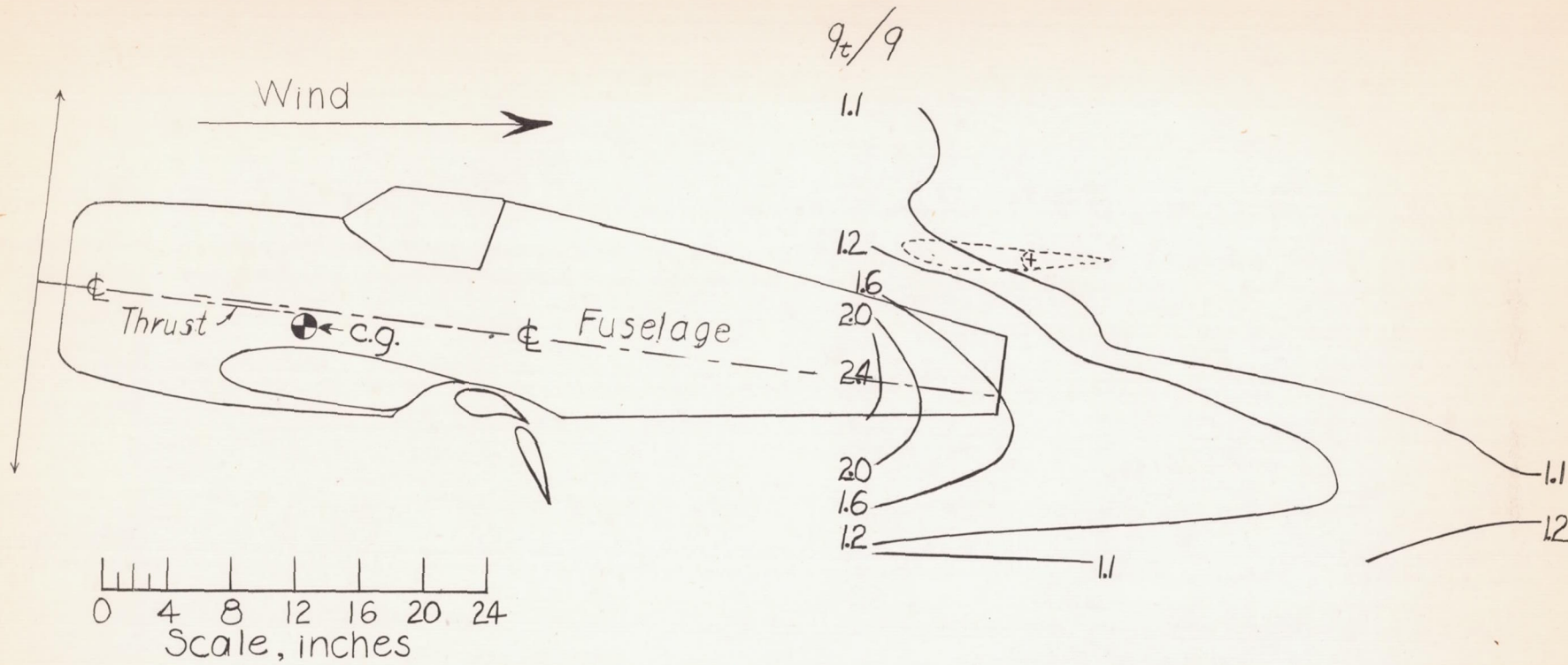
Figure 22.- Continued.



NATIONAL ADVISORY
COMMITTEE FOR AERONAUTICS

(e) $\alpha = 4.3^\circ$; $C_L = 3.01$; 6 inches right of center line; $T_C' = 0.49$.

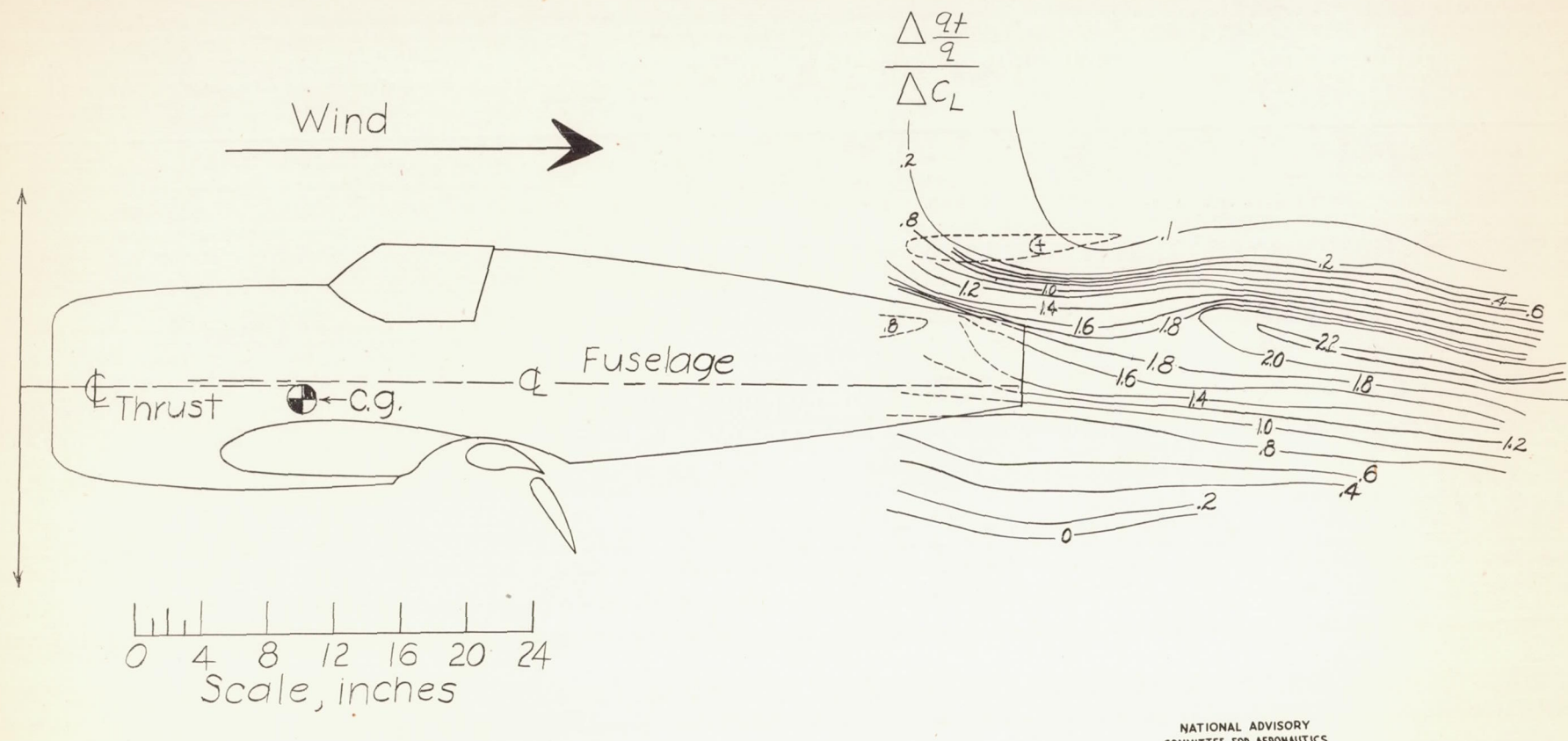
Figure 22.- Continued.



NATIONAL ADVISORY
COMMITTEE FOR AERONAUTICS

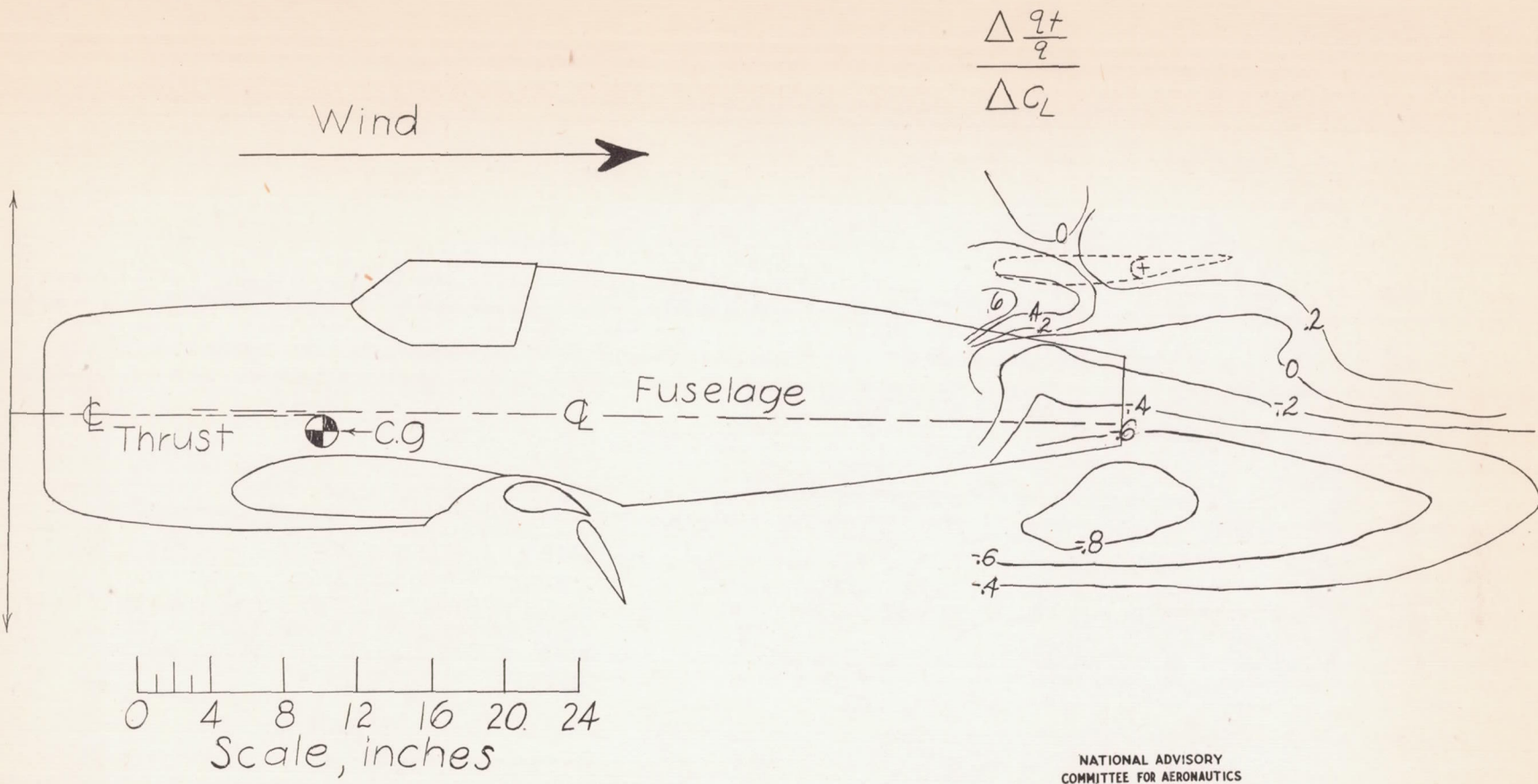
(f) $\alpha = 4.3^\circ$; $C_L = 3.01$; 6 inches left of center line; $T_C' = 0.49$.

Figure 22.- Concluded.



(a) $\alpha = 1.35^\circ$; $C_L = 2.69$; 6 inches right of center line; $T_c' = 0.44$.

Figure 23.- Contours of $\frac{\Delta q_t}{q} / \Delta C_L$ behind model as a low-wing airplane with full-span double slotted flap. $\delta_{f1} = \delta_{f2} = 30^\circ$; tail off; power on.

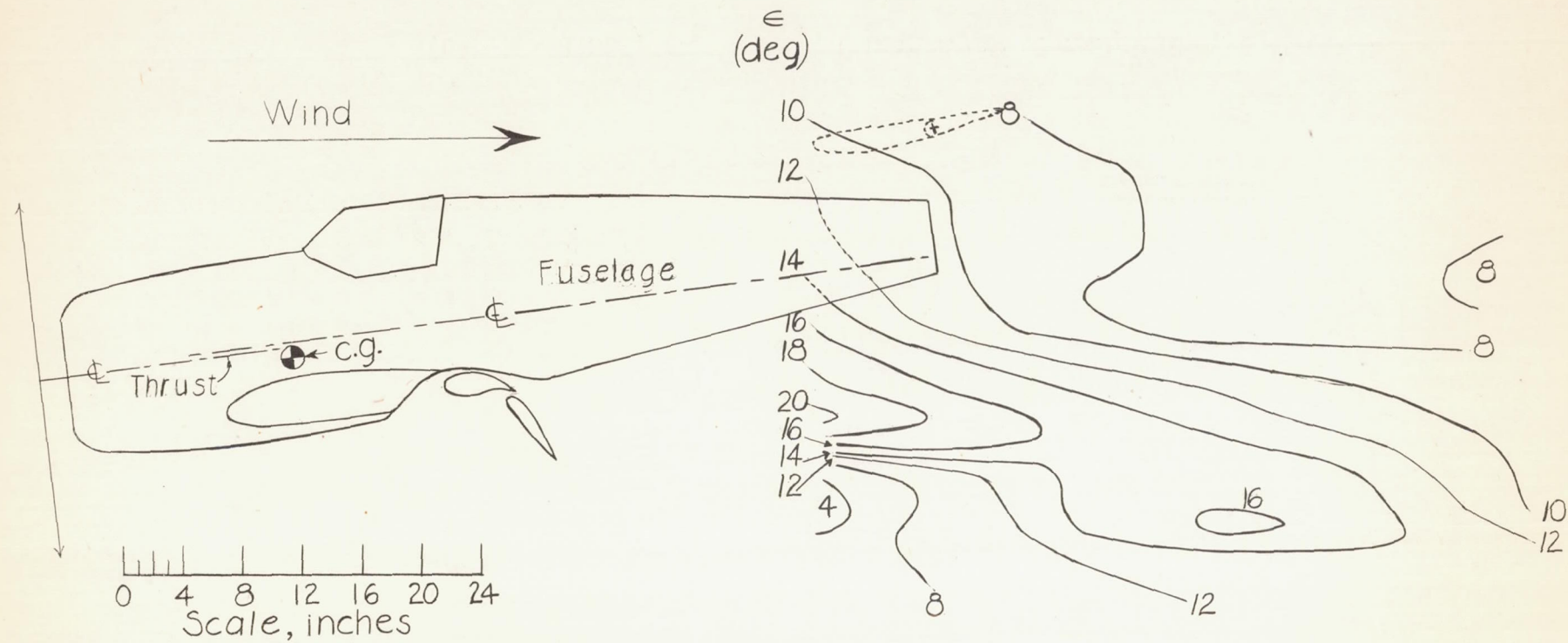


NATIONAL ADVISORY
COMMITTEE FOR AERONAUTICS

(b) $\alpha = 1.35^\circ$; $C_L = 2.69$; 6 inches left of center line; $T_C' = 0.44$.

Figure 23.- Concluded.

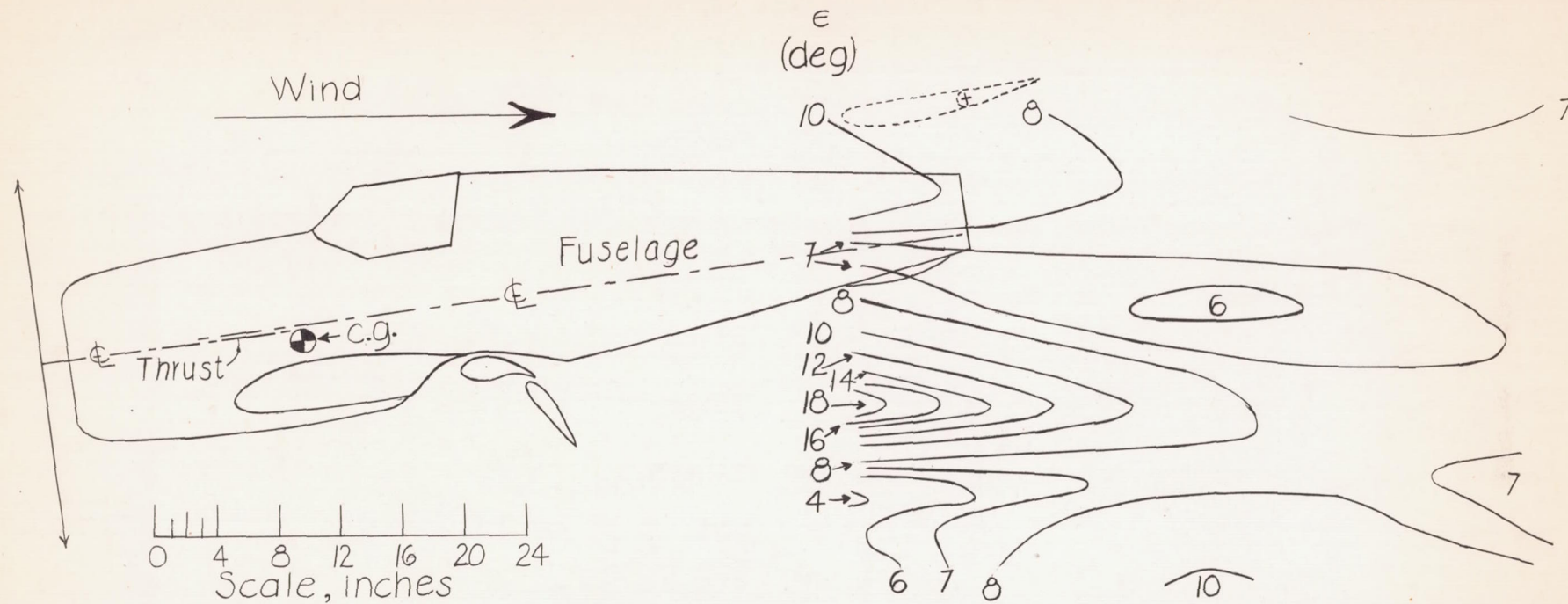
Fig. 24a



NATIONAL ADVISORY
COMMITTEE FOR AERONAUTICS

$$(a) \quad \alpha = -8.9^\circ; \quad C_L = 1.56; \quad \text{6 inches right of center line}; \quad T_C' = 0.26.$$

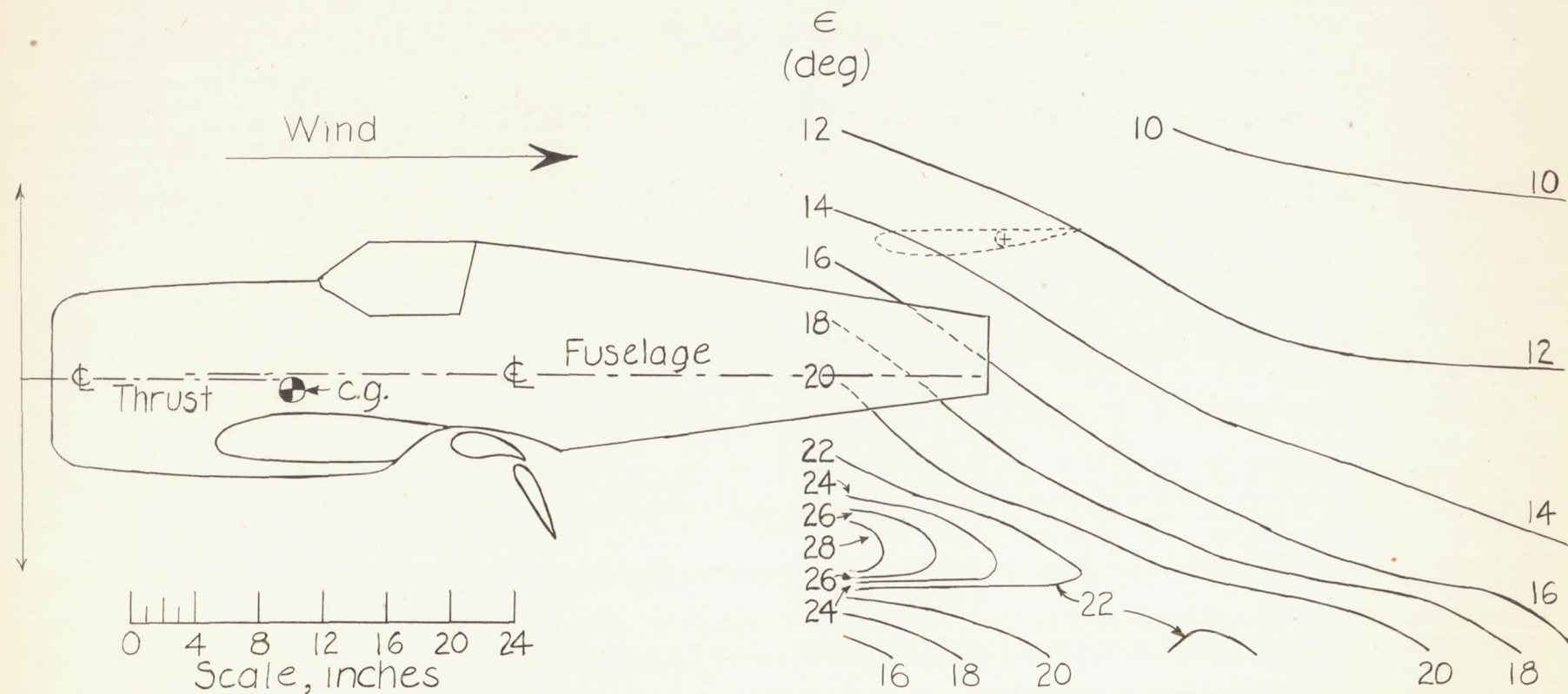
Figure 24.- Contours of downwash angles behind model as a low-wing airplane with full-span double slotted flap. $\delta_{f1} = \delta_{f2} = 30^\circ$; tail off; power on.



NATIONAL ADVISORY
COMMITTEE FOR AERONAUTICS

(b) $\alpha = -8.9^\circ$; $C_L = 1.56$; 6 inches left of center line; $T_C' = 0.26$.

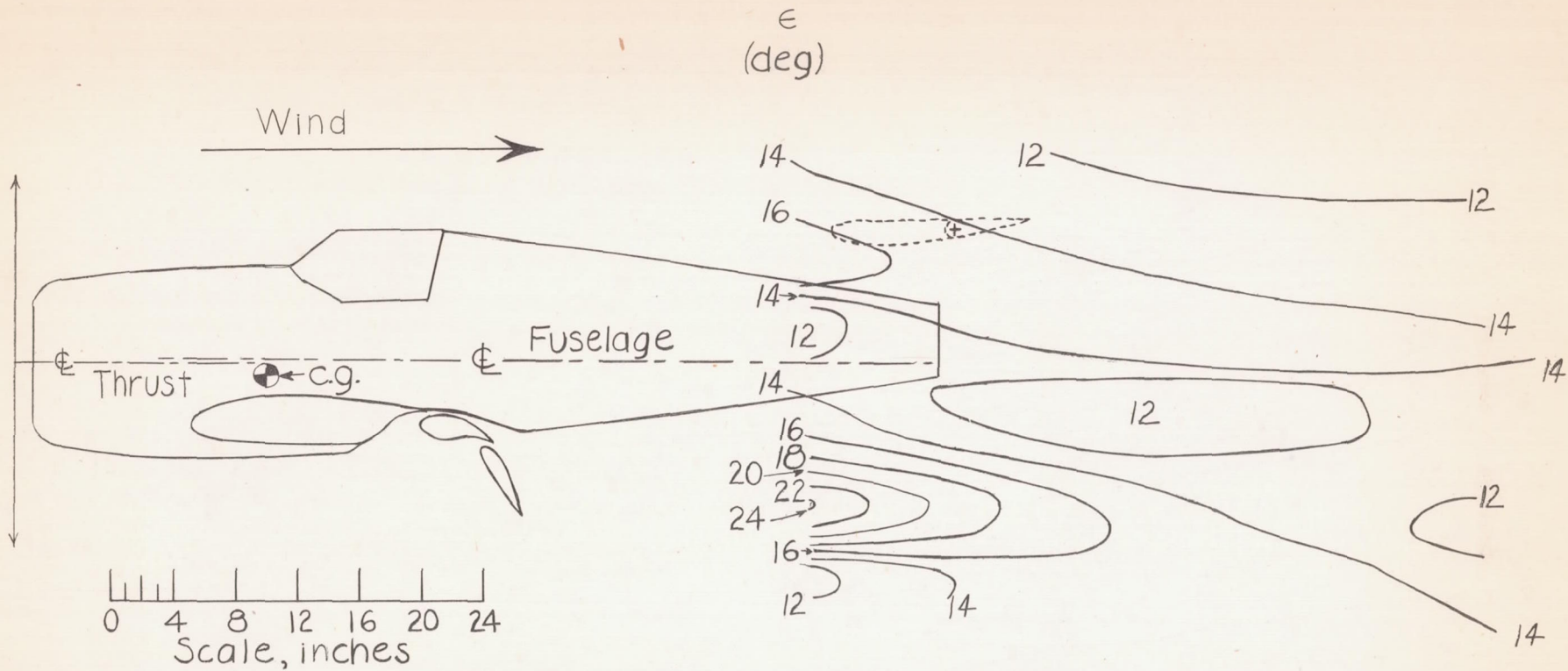
Figure 24.- Continued.



NATIONAL ADVISORY
COMMITTEE FOR AERONAUTICS

(c) $\alpha = -1.6^\circ$; $C_L = 2.36$; 6 inches right of center line; $T_C' = 0.38$.

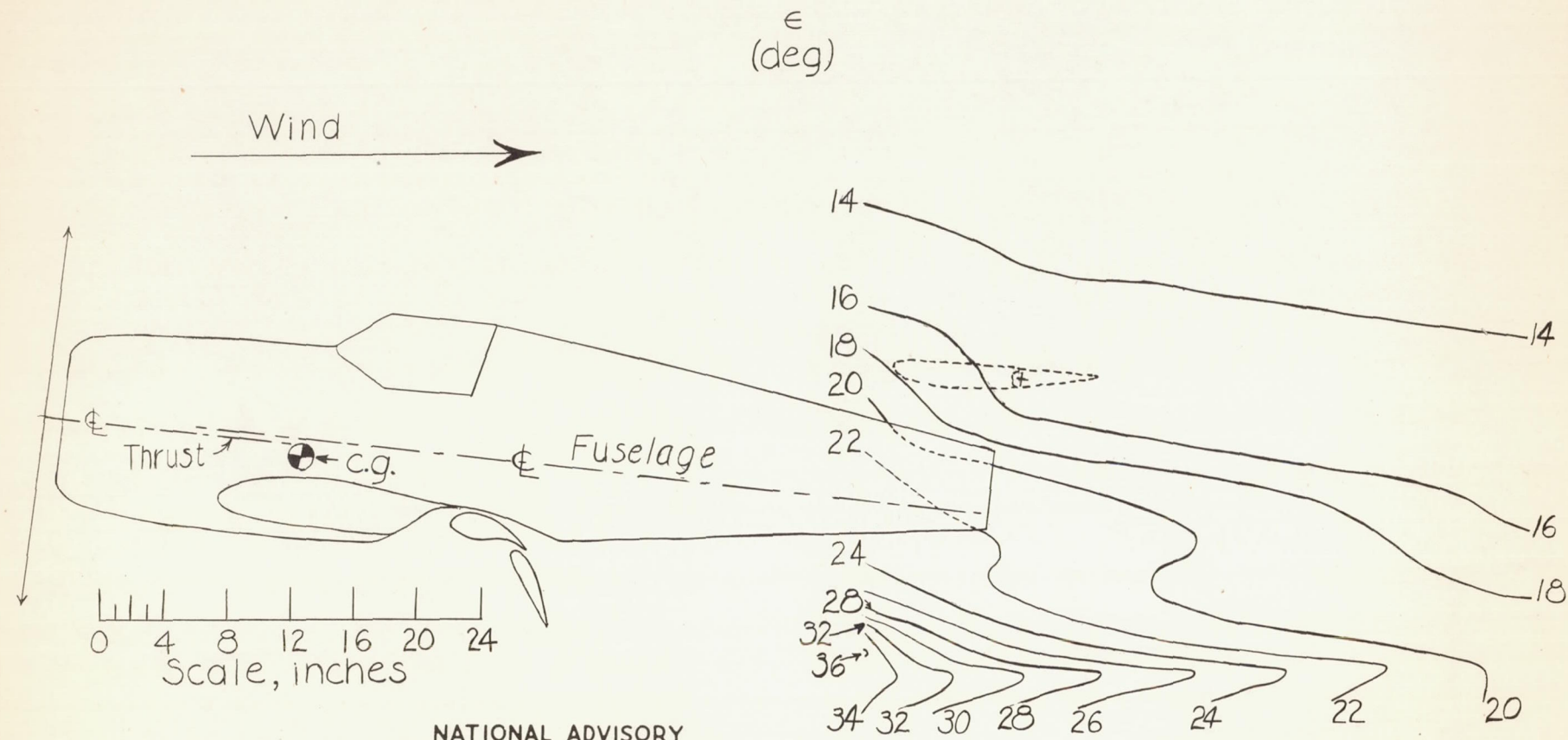
Figure 24.- Continued.



NATIONAL ADVISORY
COMMITTEE FOR AERONAUTICS

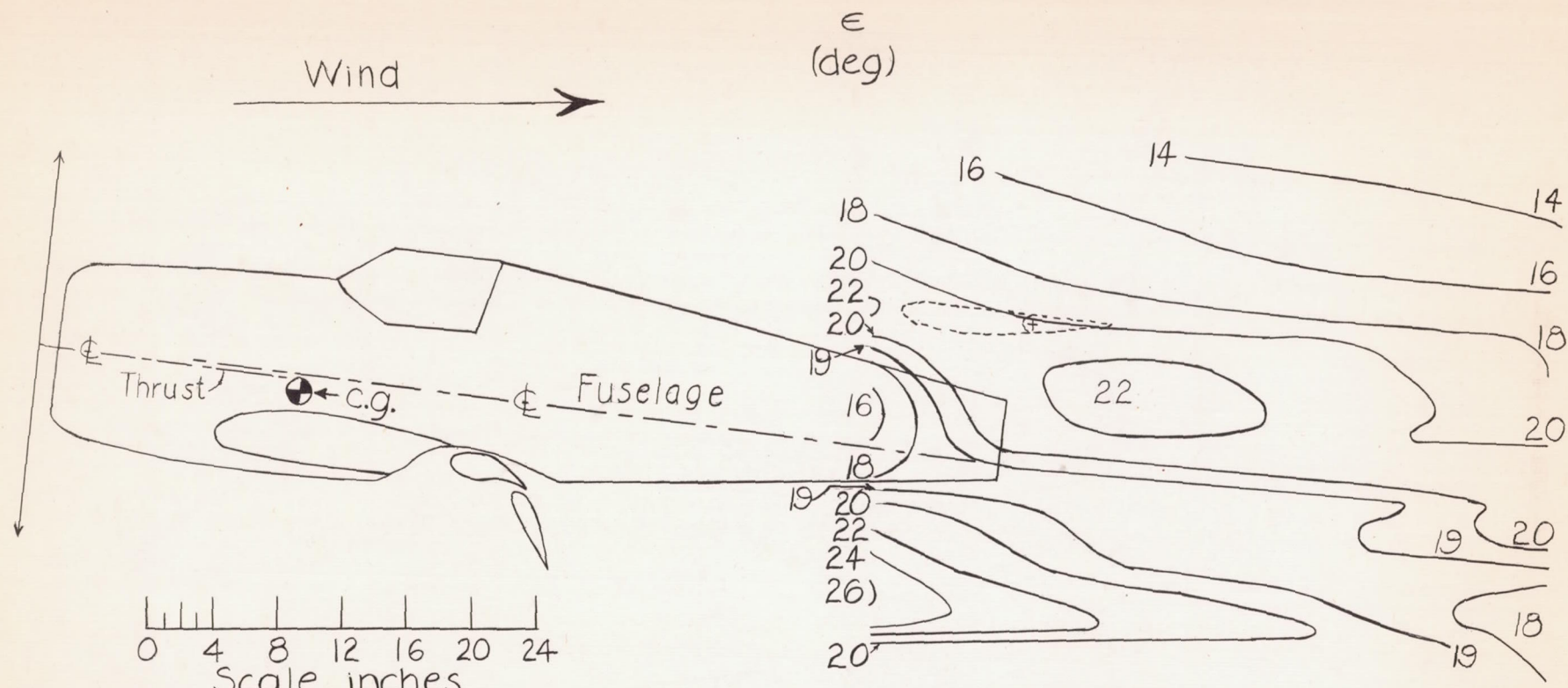
(d) $\alpha = -1.6^\circ$; $C_L = 2.36$; 6 inches left of center line; $T_C' = 0.38$.

Figure 24.- Continued.



(e) $\alpha = 4.3^\circ$; $C_L = 3.01$; 6 inches right of center line; $T_C' = 0.49$.

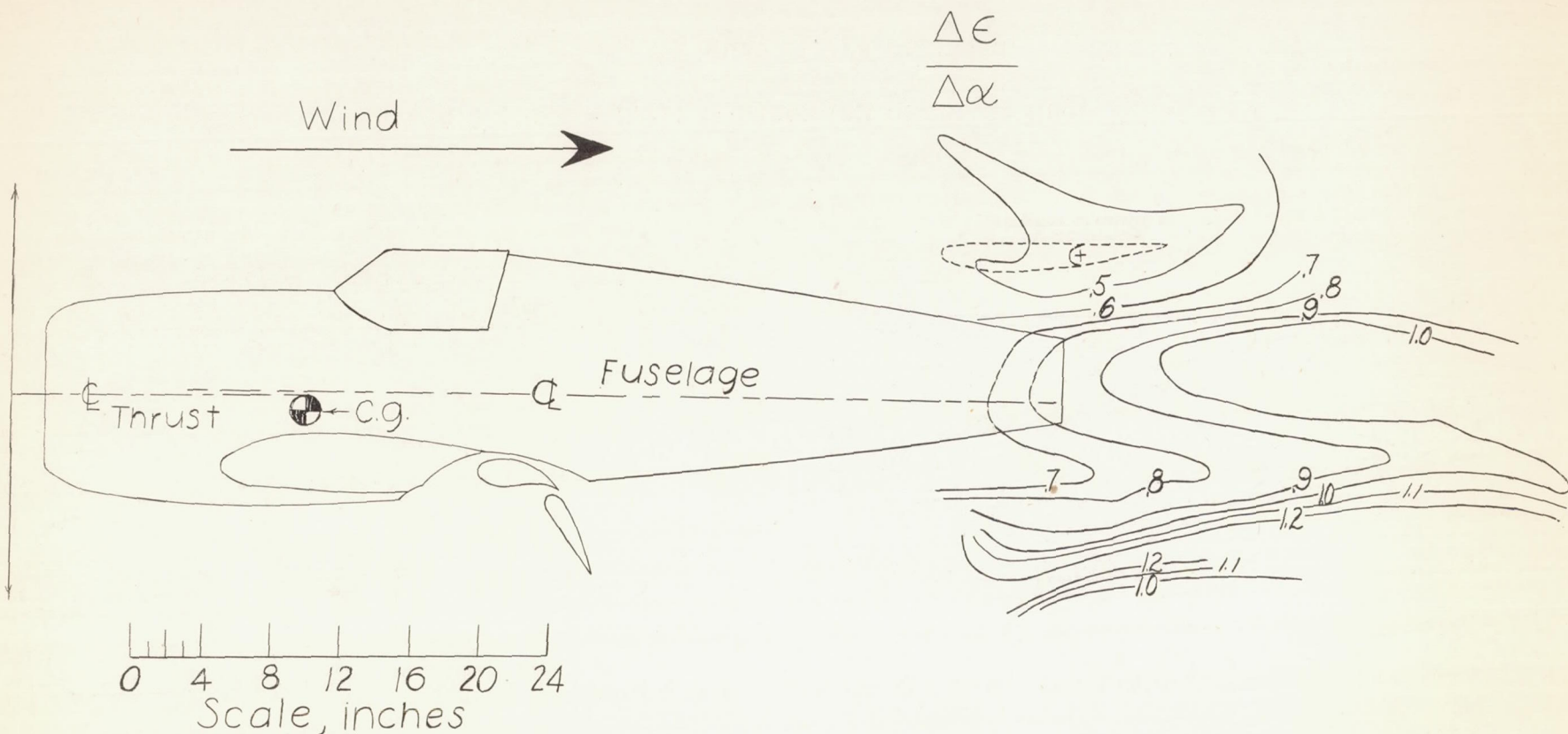
Figure 24.- Continued.



(f) $\alpha = 4.3^\circ$; $C_L = 3.01$; 6 inches left of center line; $T_c' = 0.49$.

Figure 24.- Concluded.

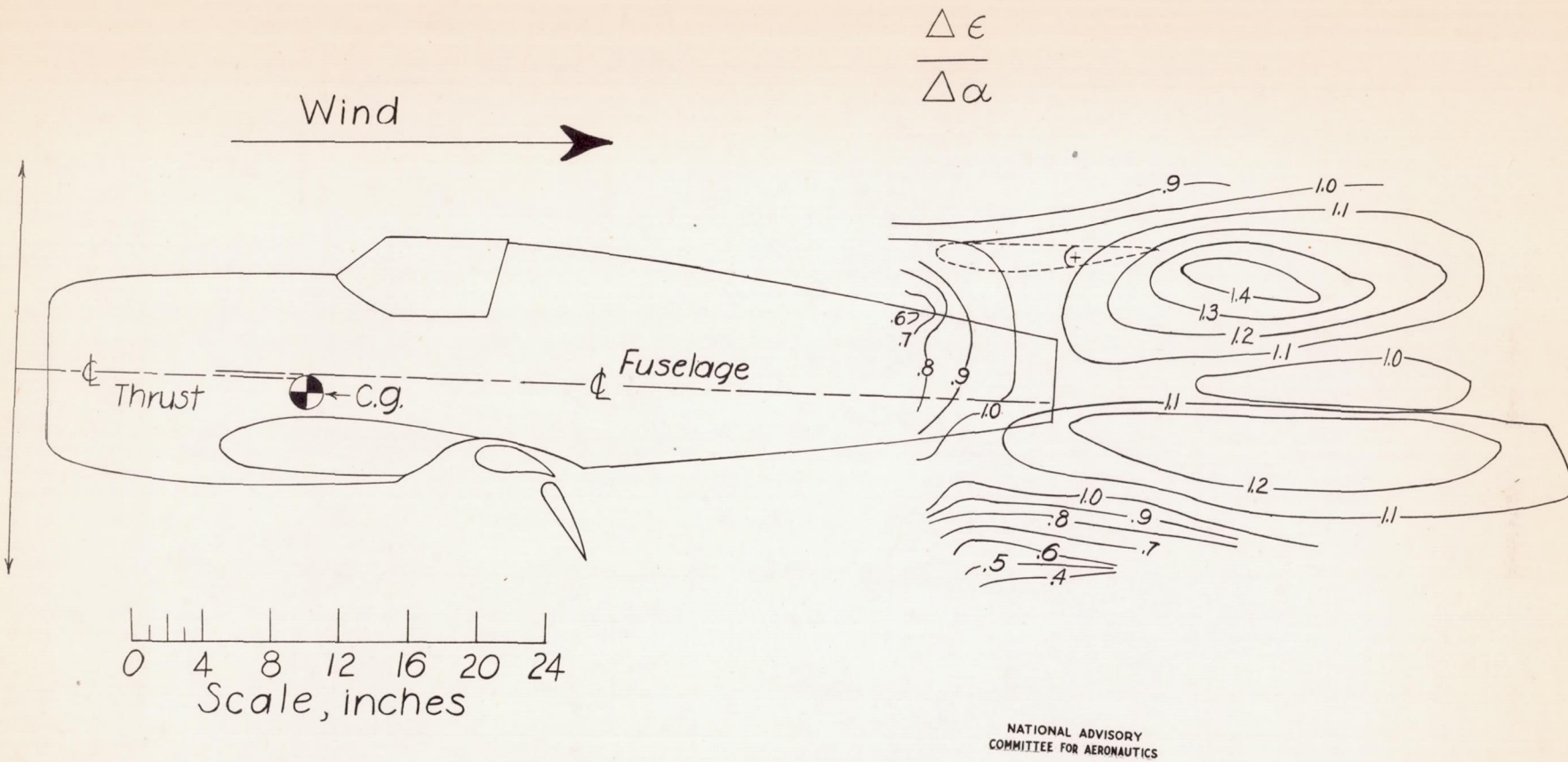
Fig. 25a



NATIONAL ADVISORY
COMMITTEE FOR AERONAUTICS

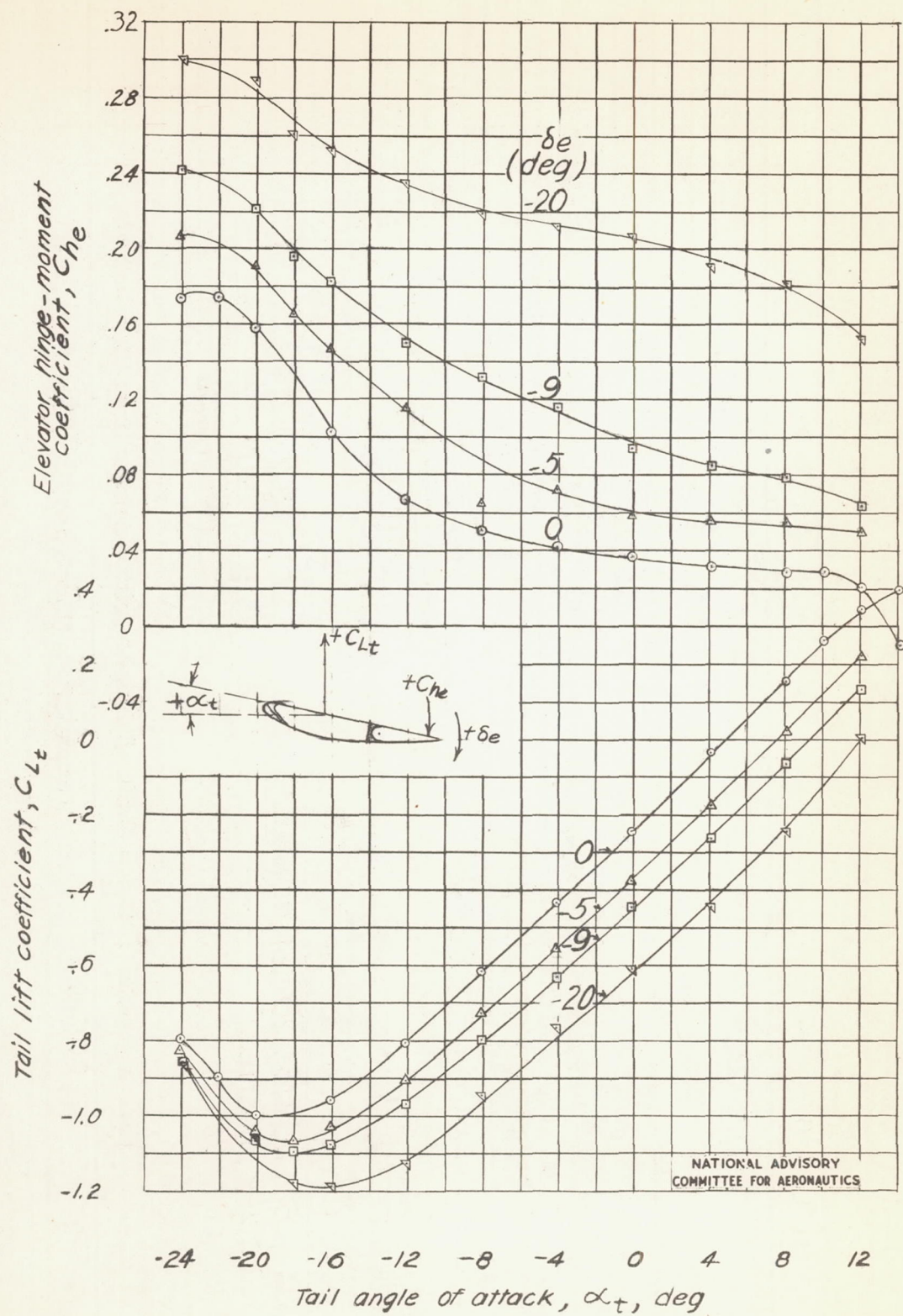
(a) $\alpha = 1.35^\circ$; $C_L = 2.69$; 6 inches right of center line; $T_C' = 0.44$.

Figure 25.- Contours of $\Delta\epsilon/\Delta\alpha$ behind model as a low-wing airplane with full-span double slotted flap.
 $\delta_{f1} = \delta_{f2} = 30^\circ$; tail off; power on.



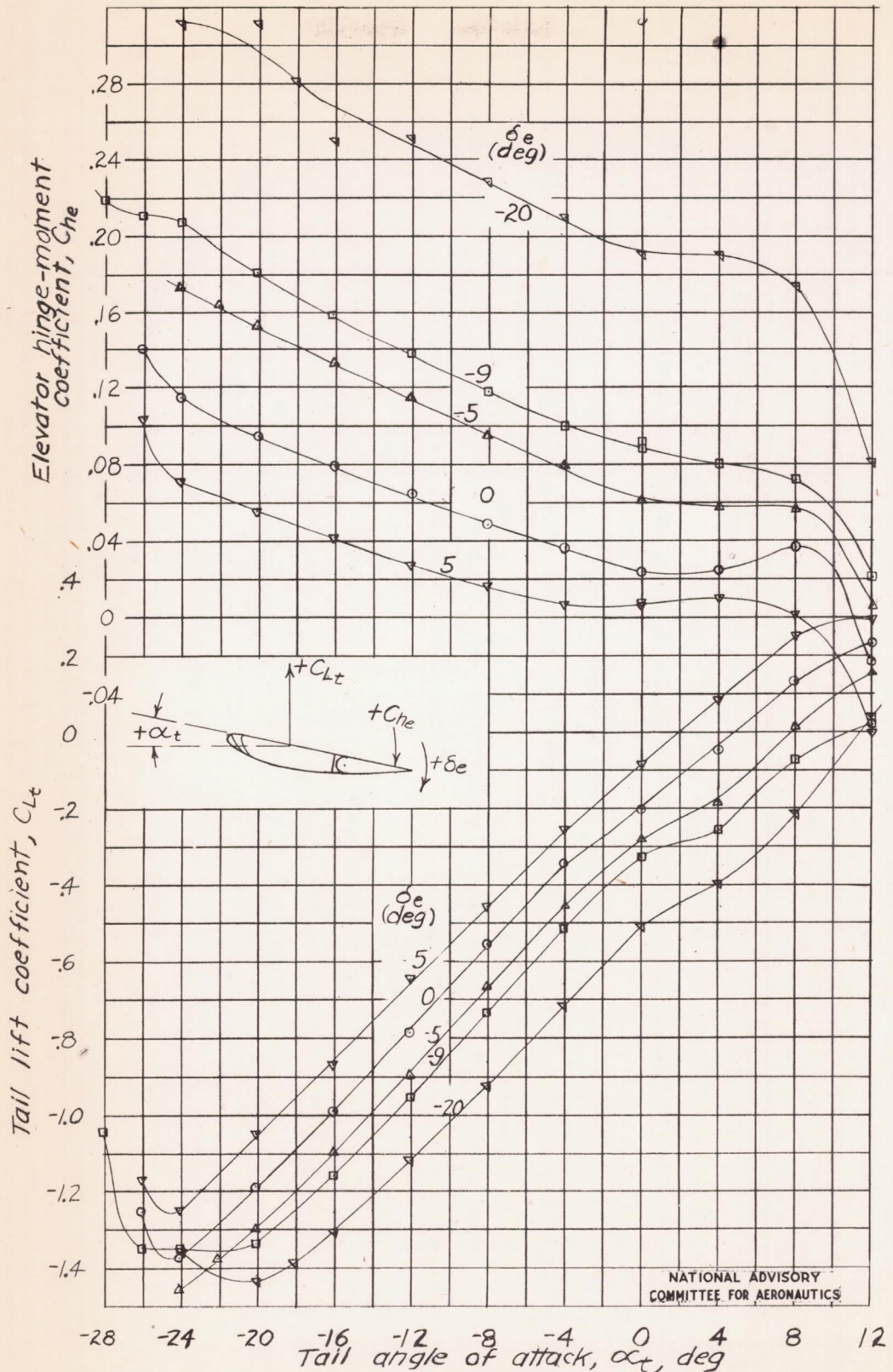
(b) $\alpha = 1.35^\circ$; $C_L = 2.69$; 6 inches left of center line; $T_C' = 0.44$.

Figure 25.- Concluded.

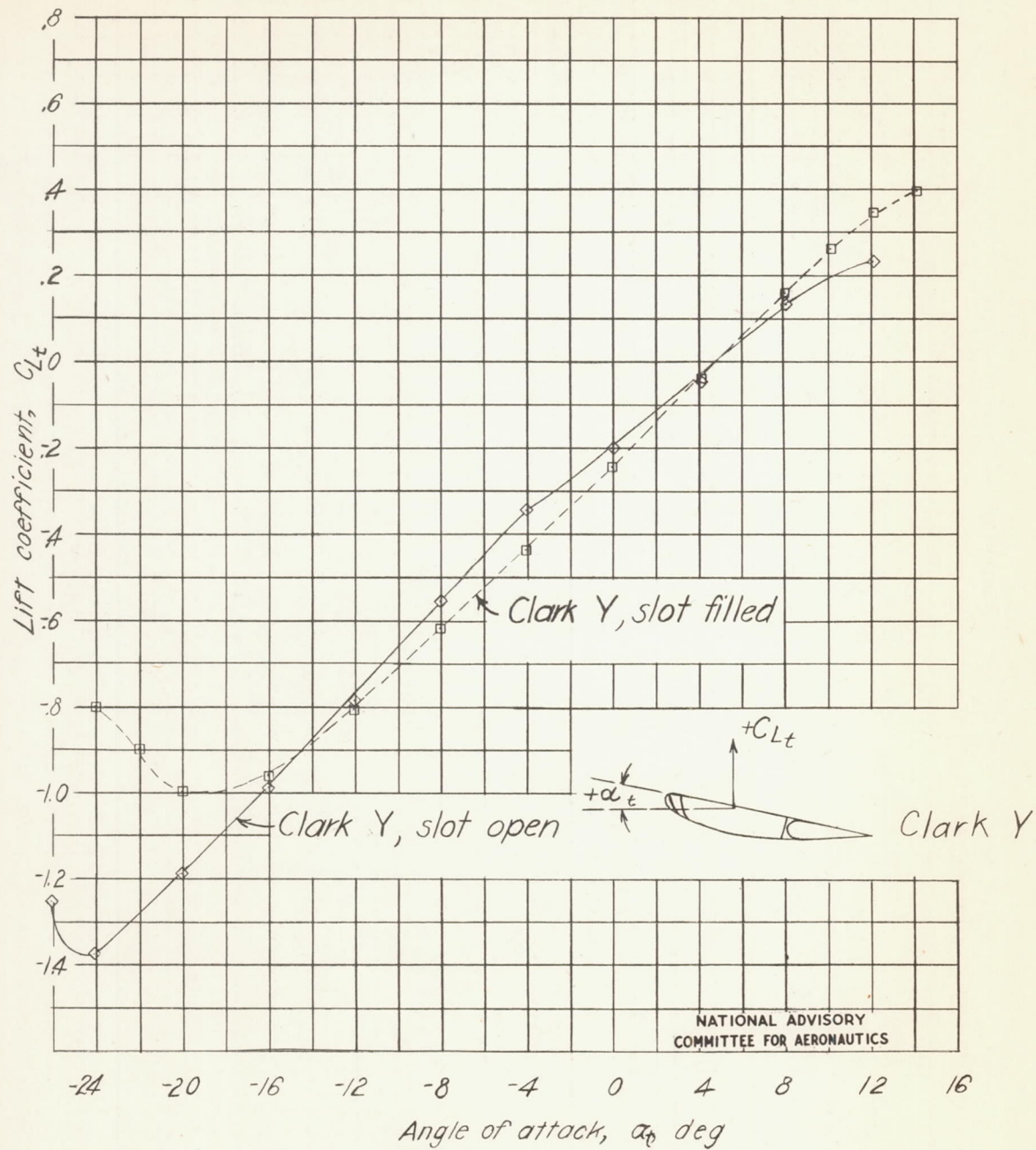


(a) Slot filled.

Figure 26.- Aerodynamic characteristics of the isolated horizontal tail.

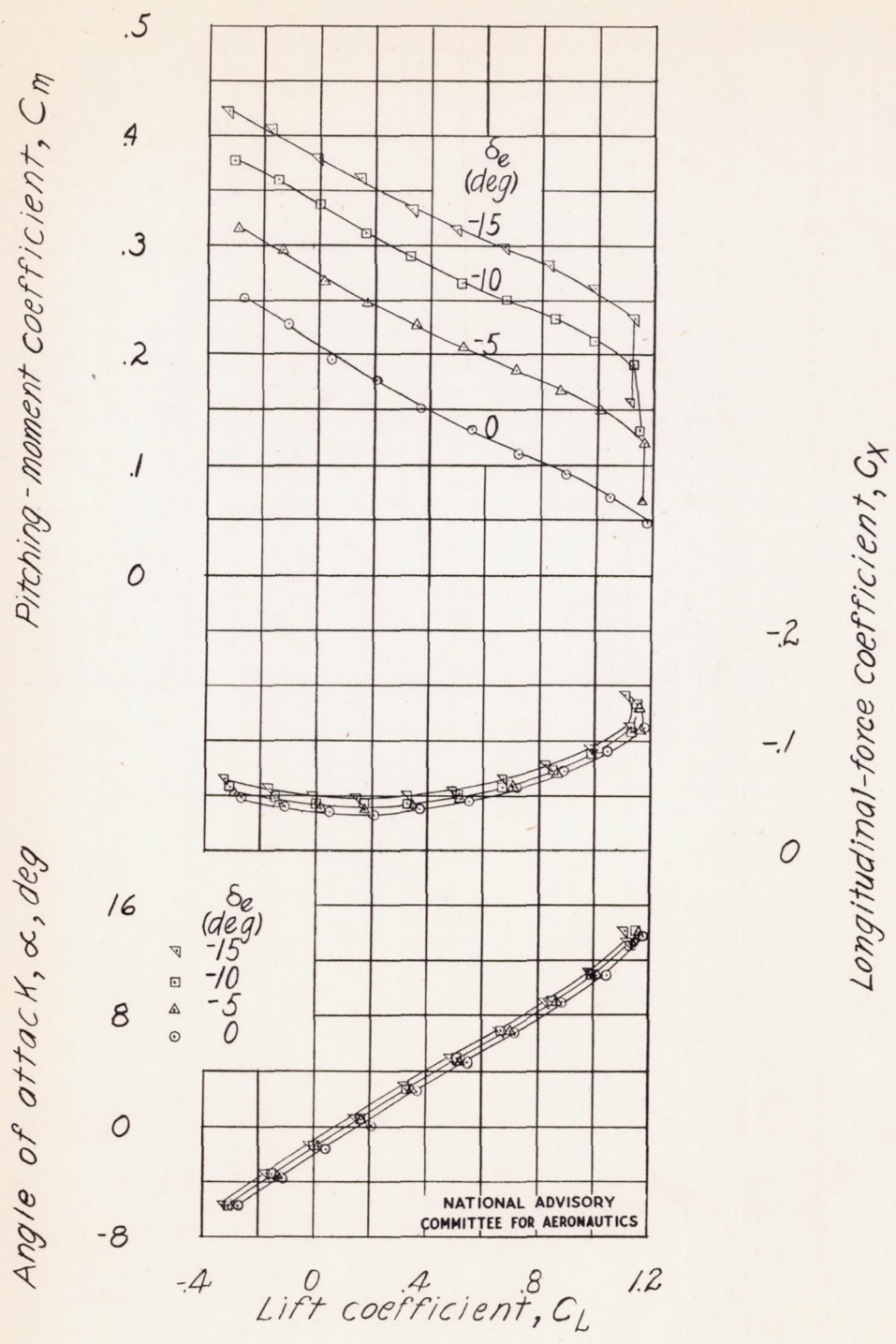


(b) Slot open.



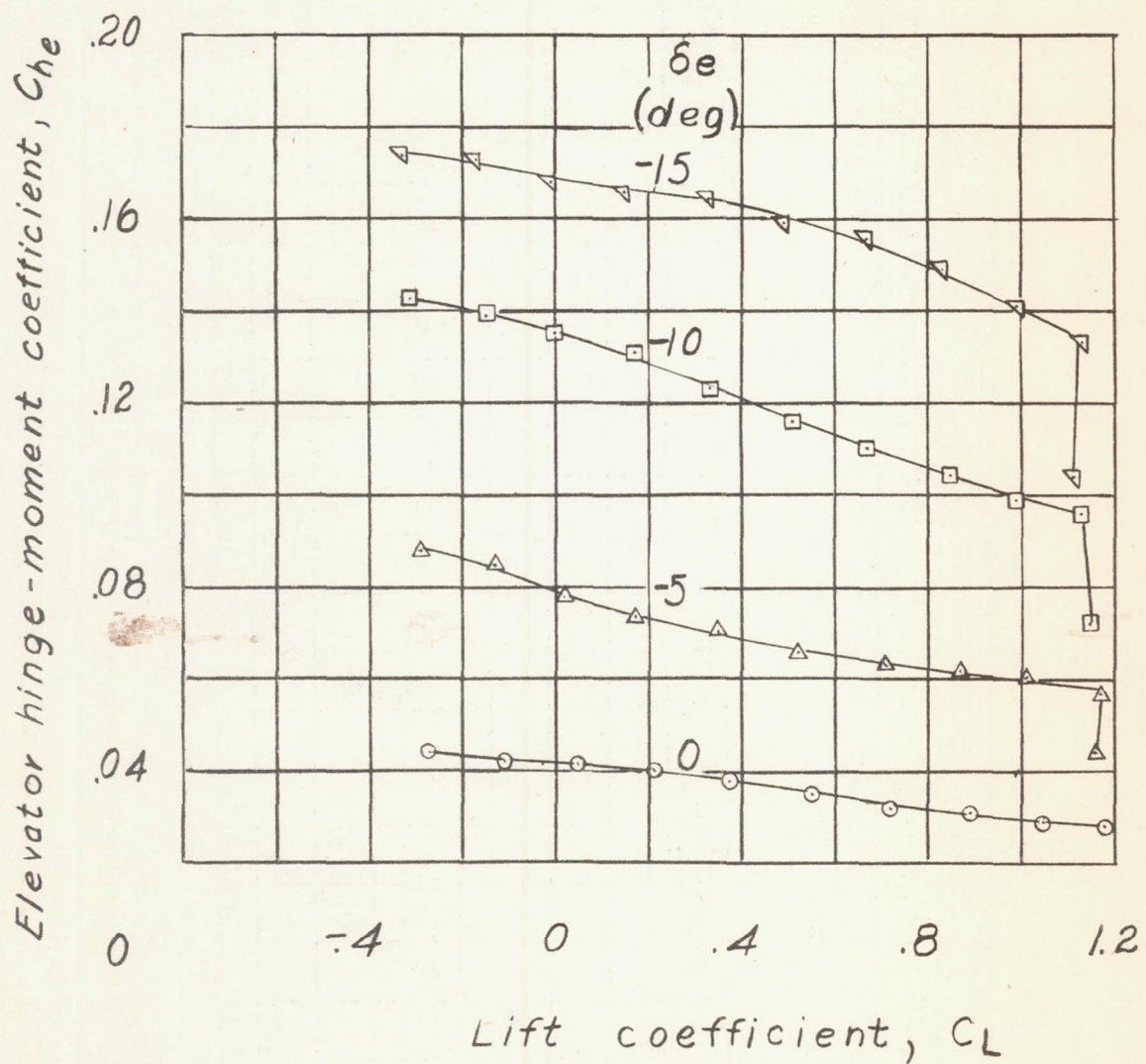
(c) Comparison of the lift curves.

Figure 26.- Concluded.



(a) Propeller off.

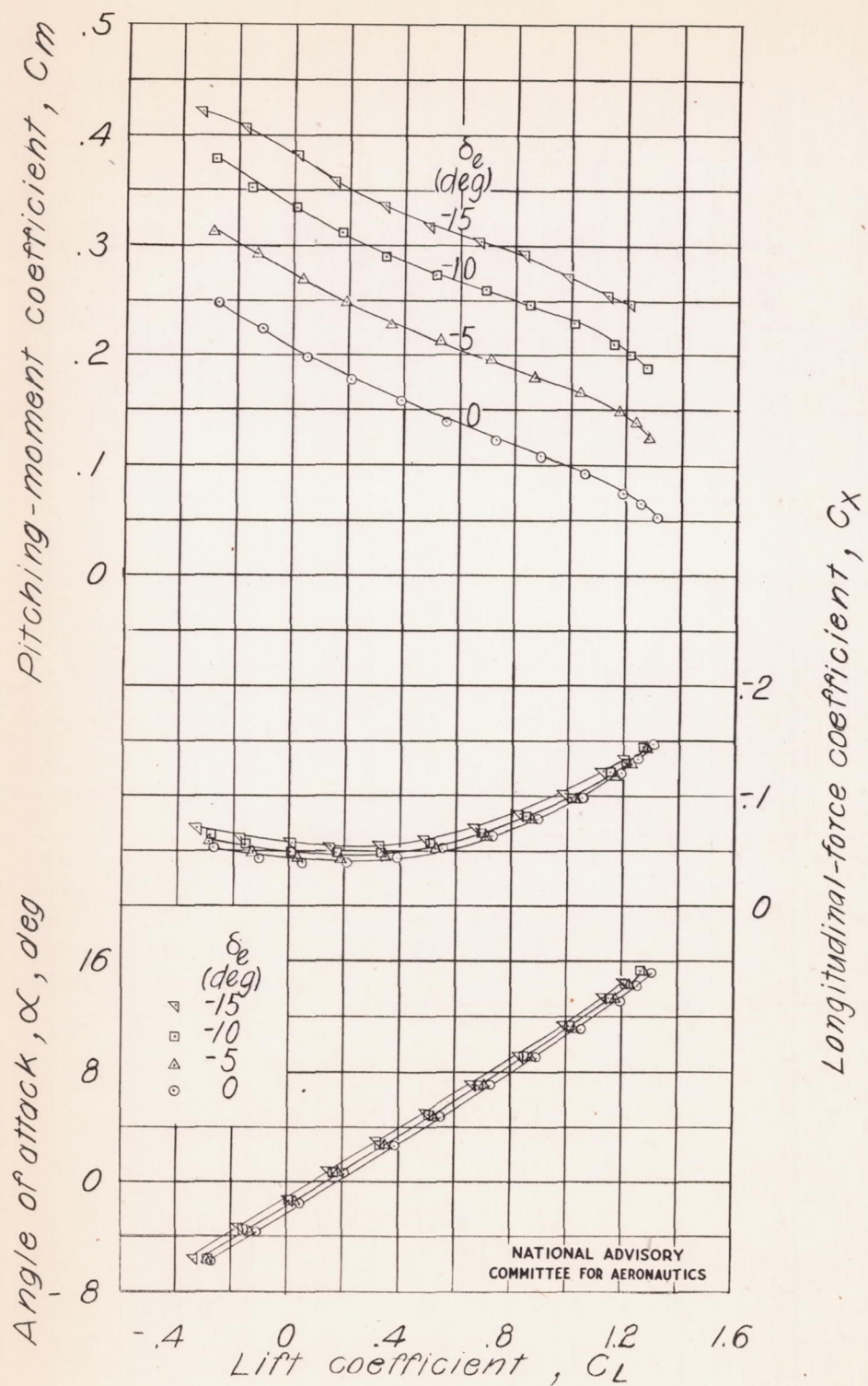
Figure 27.- Effect of elevator deflection on the aerodynamic characteristics of the model as a low-wing airplane with flap neutral.
 $i_t = -1.3^\circ$; tail slot filled.



NATIONAL ADVISORY
COMMITTEE FOR AERONAUTICS.

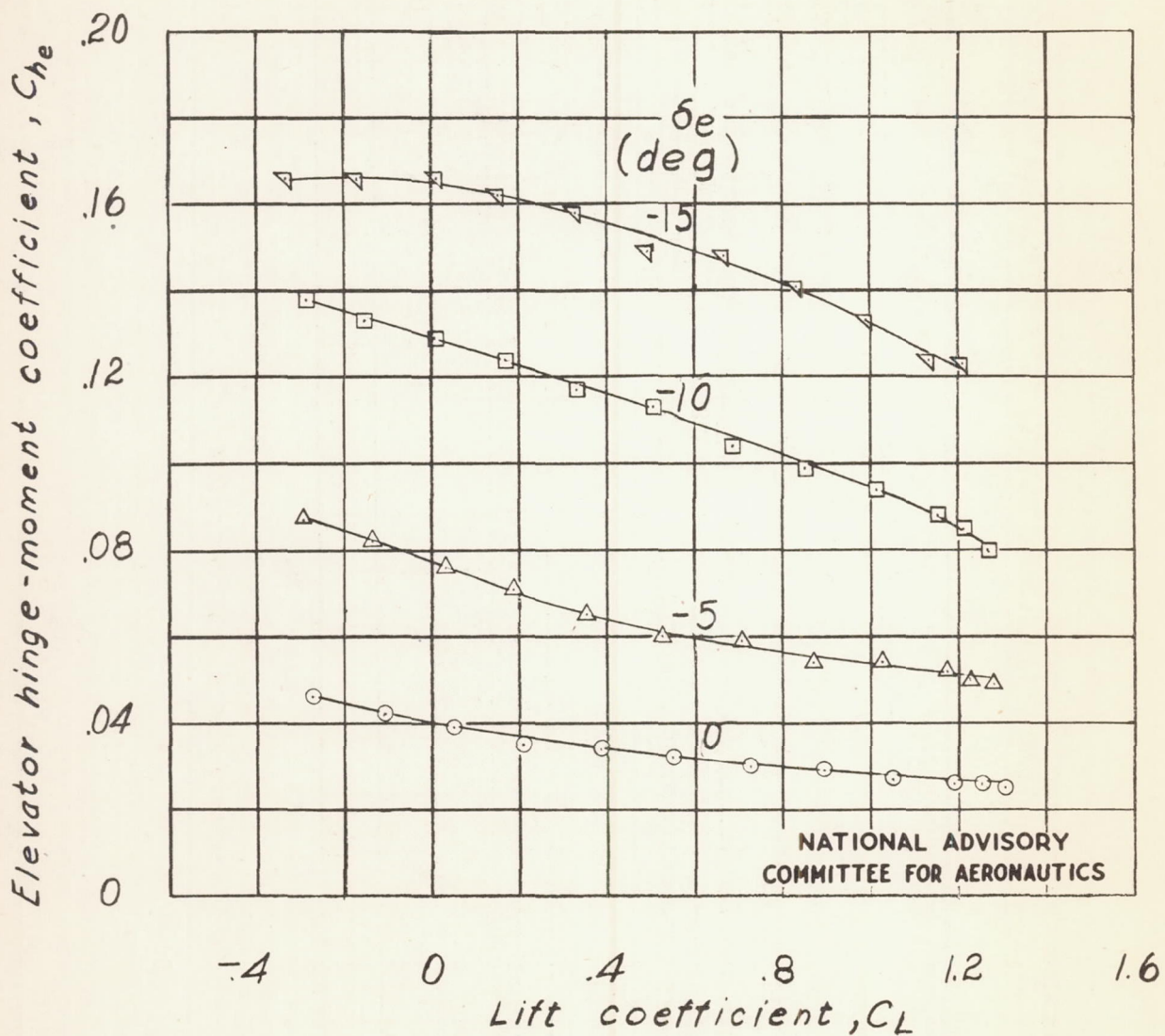
(a) Concluded.

Figure 27.- Continued.



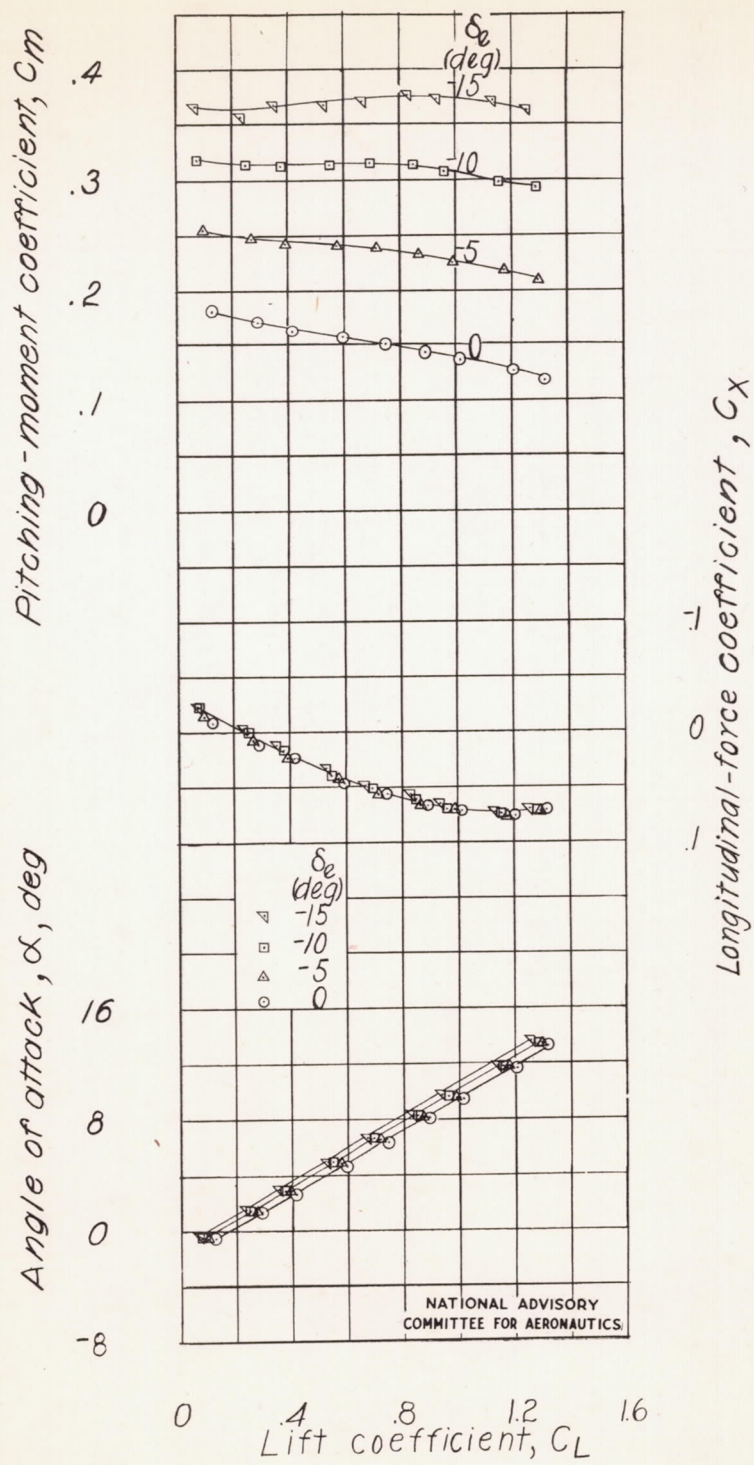
(b) Propeller windmilling.

Figure 27.- Continued.



(b) Concluded.

Figure 27.- Continued.

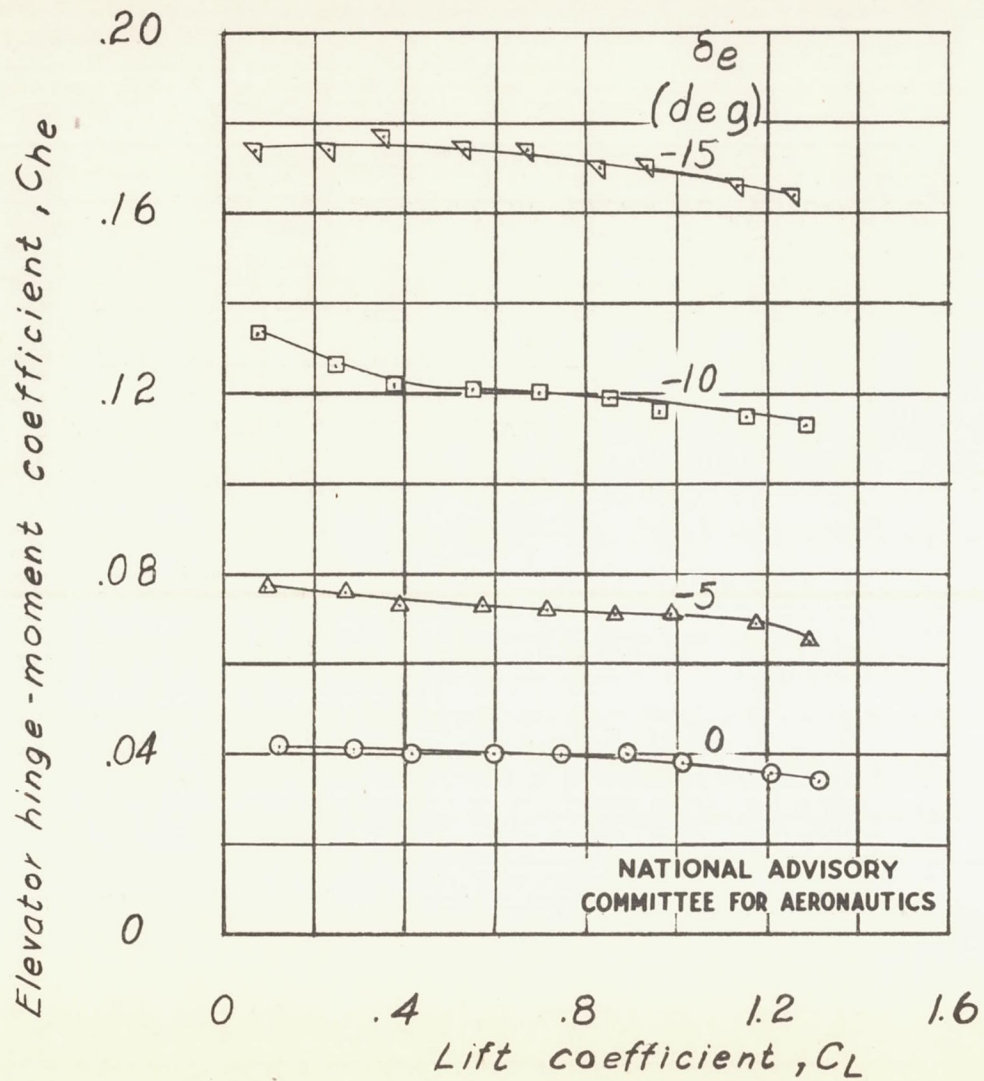


(c) Power on.

Figure 27.- Continued.

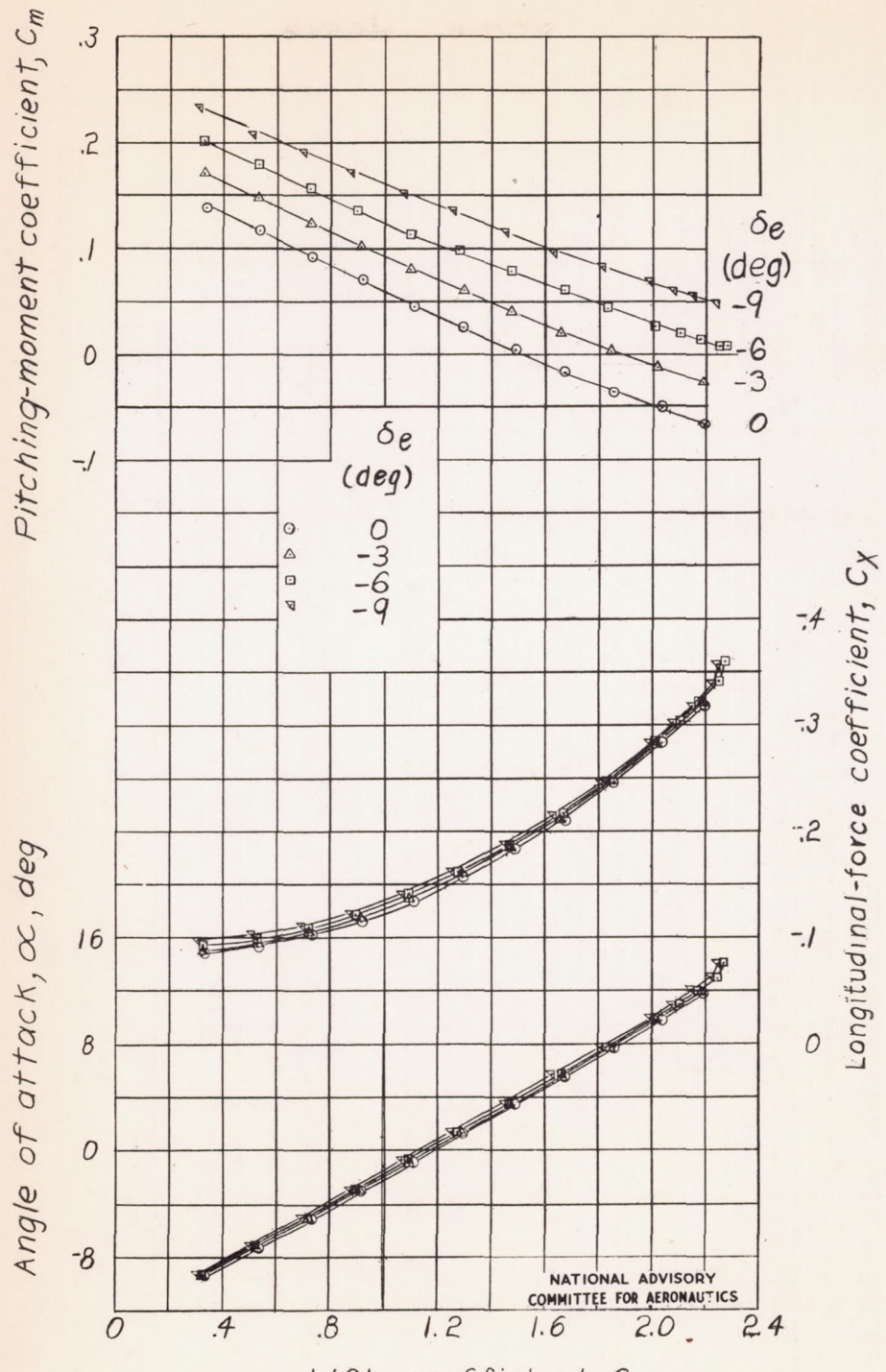
Fig. 27c conc.

NACA TN No. 1239



(c) Concluded.

Figure 27.- Concluded.

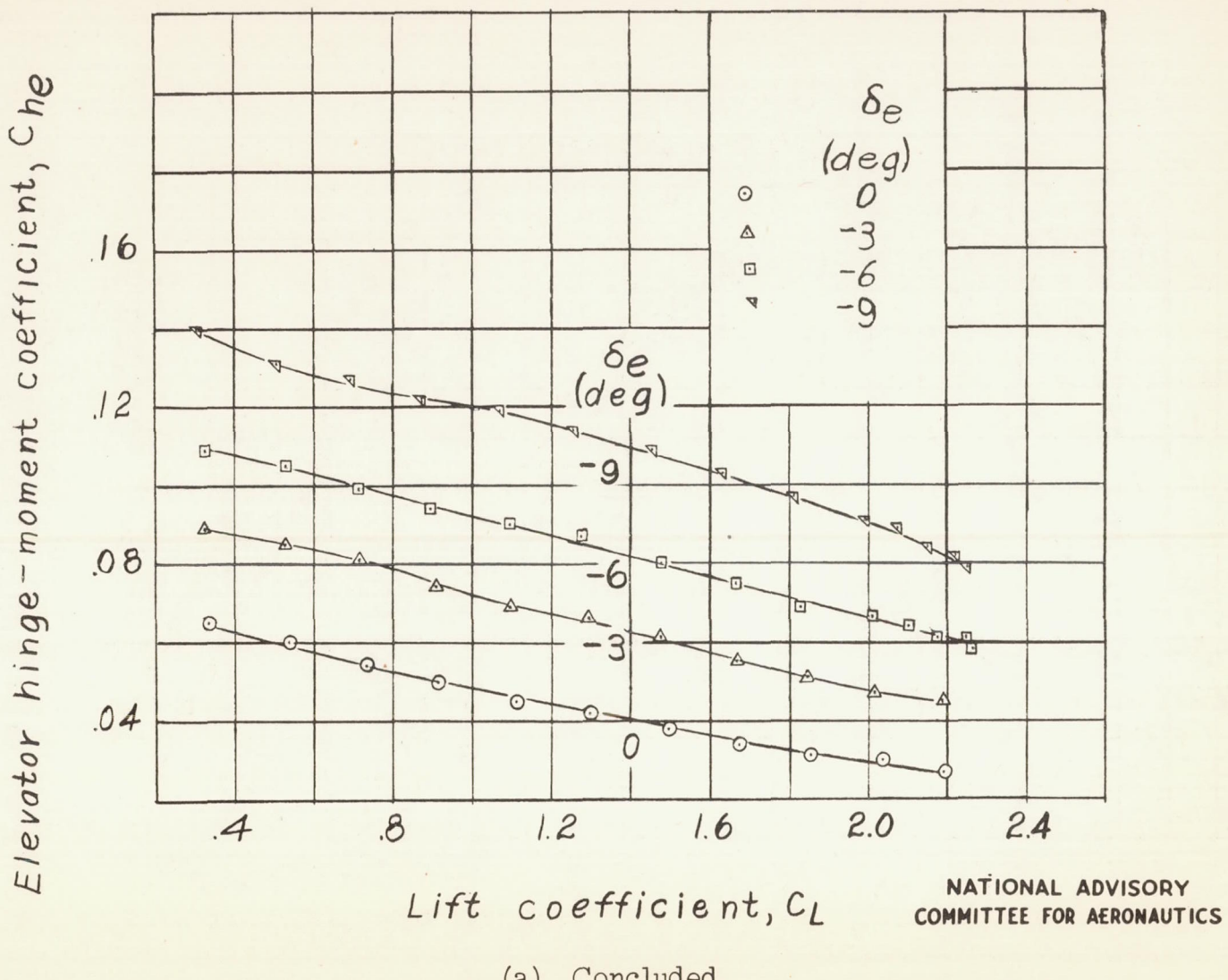


(a) Propeller off.

Figure 28.- Effect of elevator deflection on the aerodynamic characteristics of the model as a low-wing airplane with a full-span slotted flap. $\delta_{f2} = 30^\circ$; $i_t = -1.3^\circ$; tail slot filled.

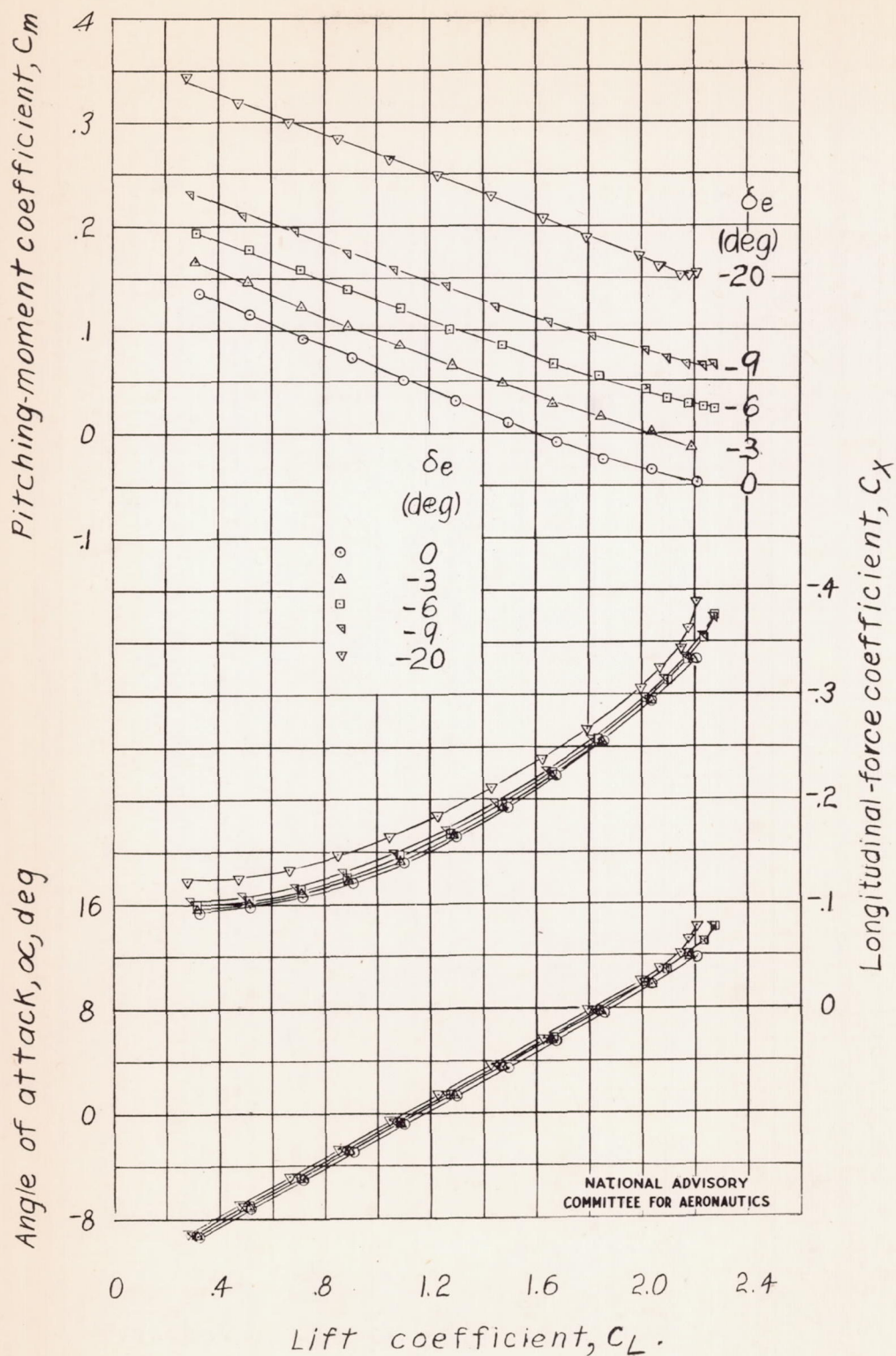
Fig. 28a conc.

NACA TN No. 1239



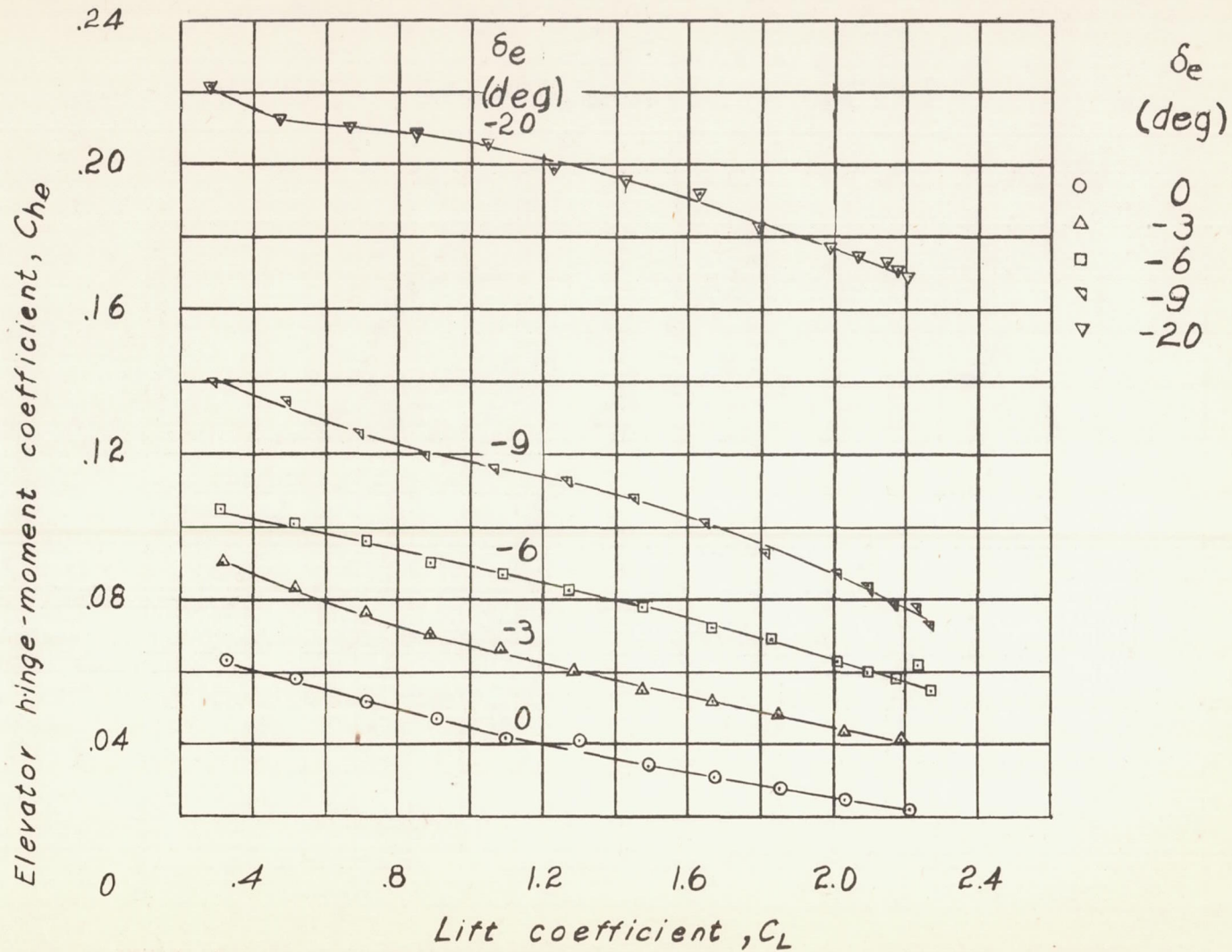
(a) Concluded.

Figure 28.- Continued.



(b) Propeller windmilling.

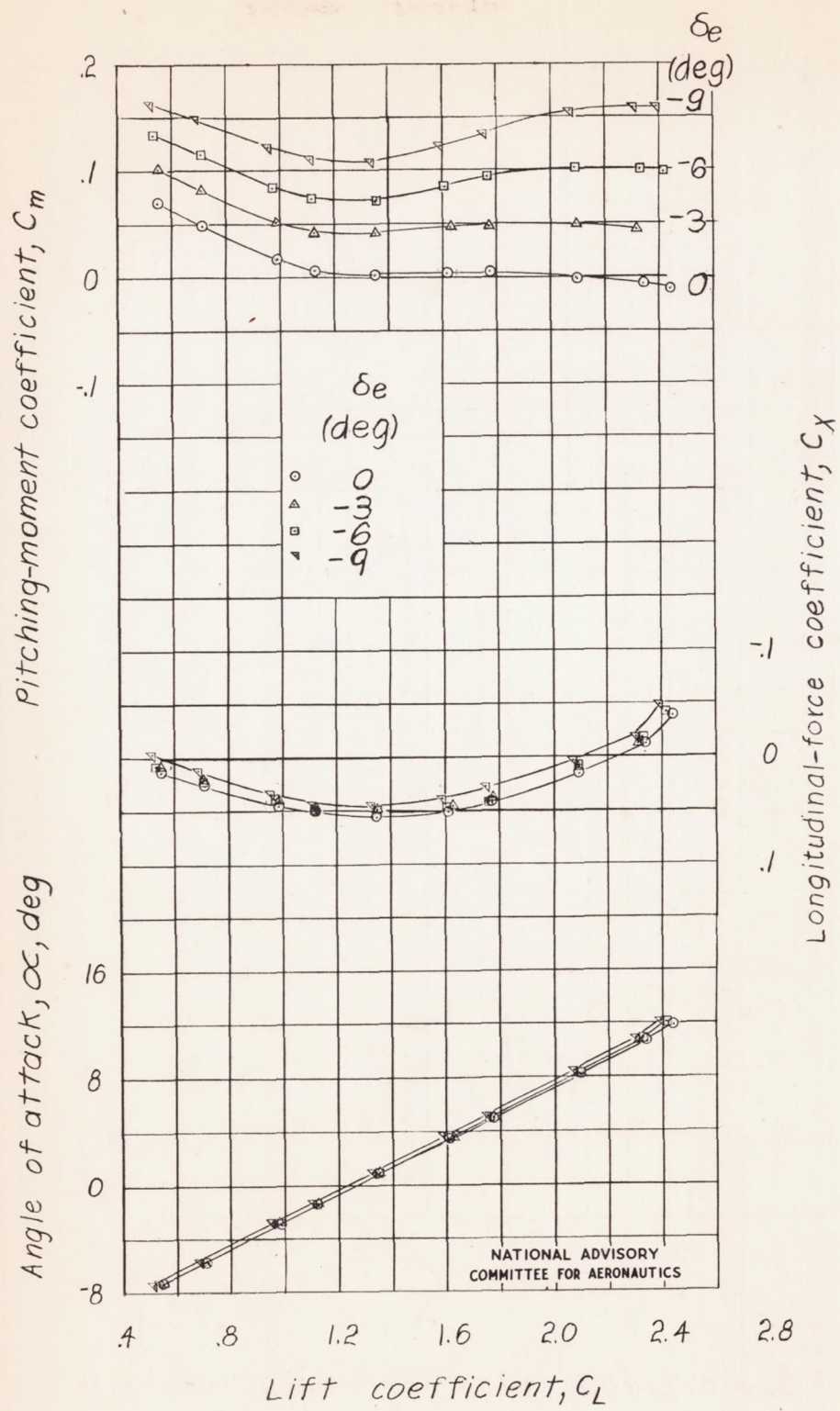
Figure 28.- Continued.



(b) Concluded.

NATIONAL ADVISORY
COMMITTEE FOR AERONAUTICS.

Figure 28.- Continued.

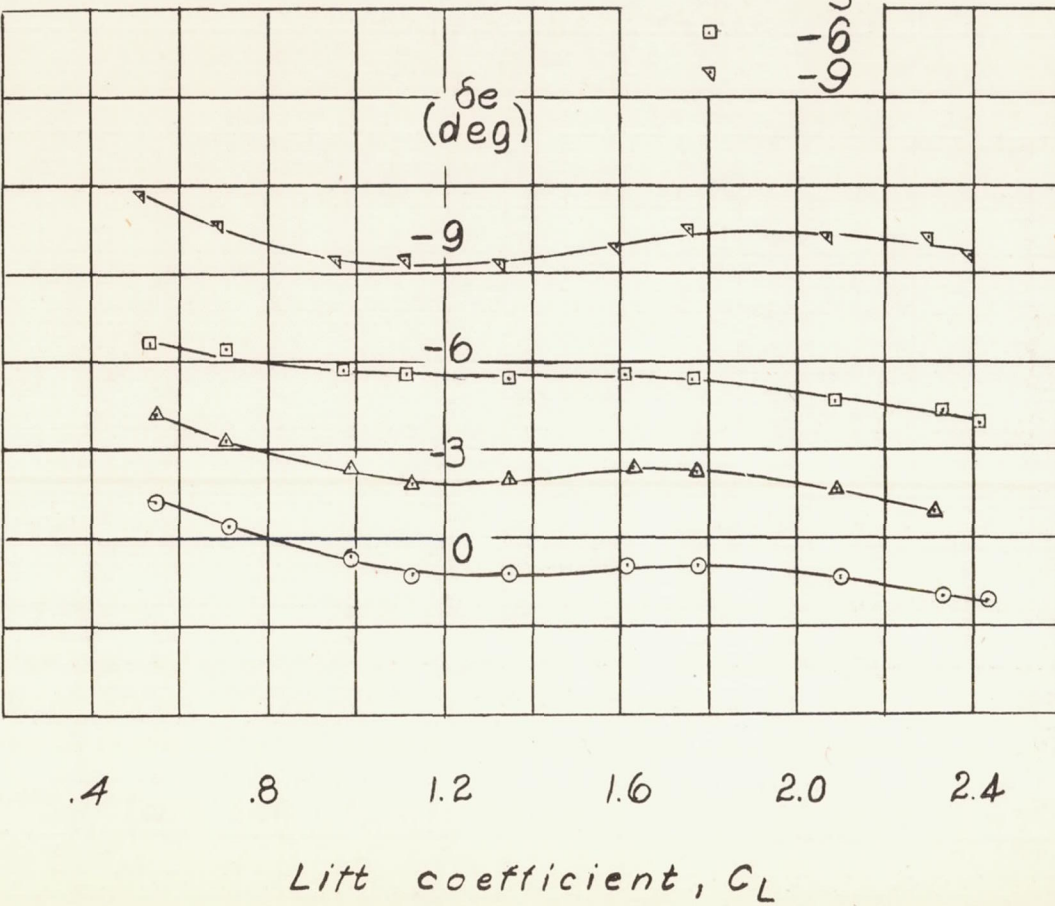


(c) Power on.

Figure 28.- Continued.

Elevator hinge-moment coefficient, C_{he}

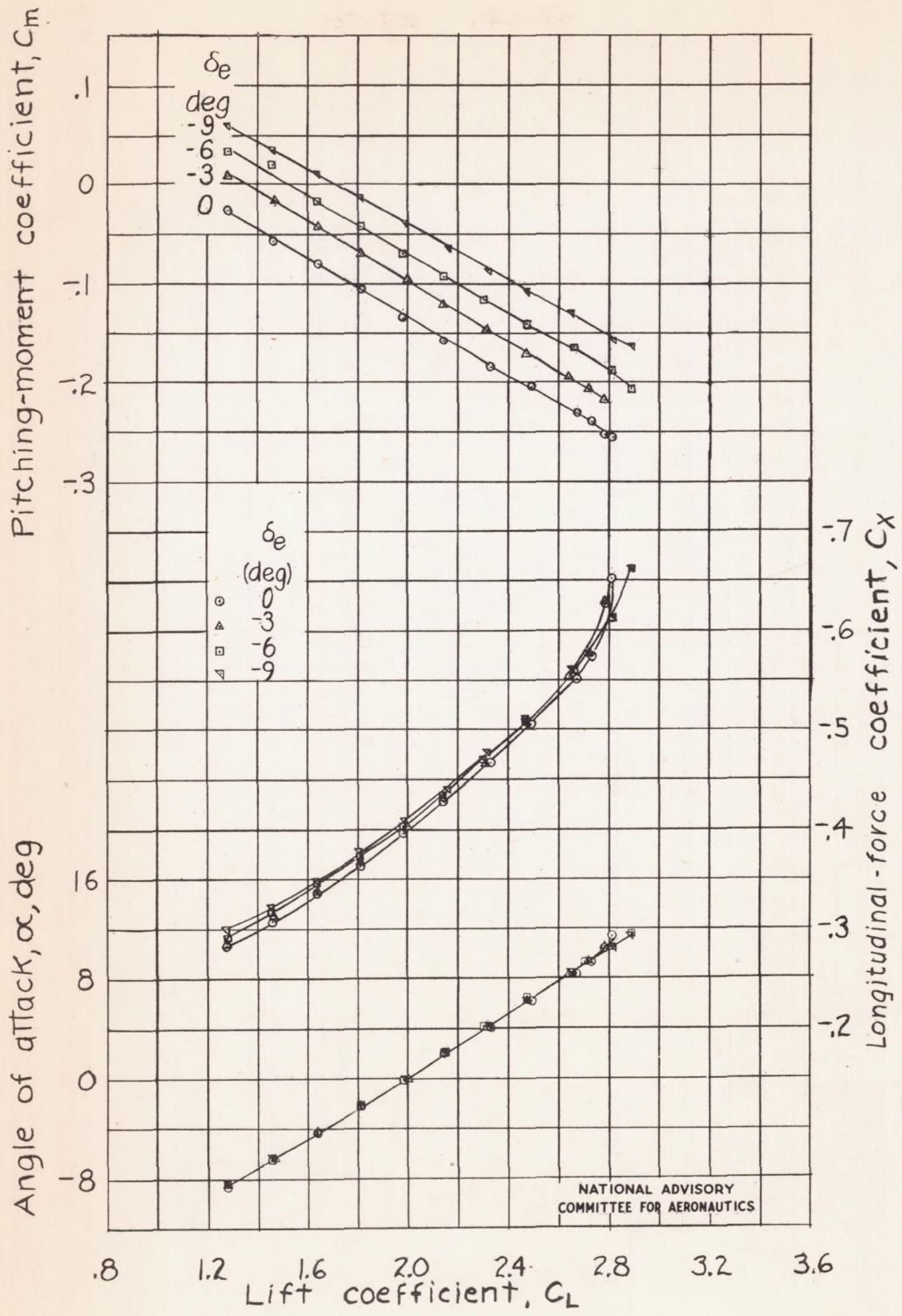
.16
.12
.08
.04



(c) Concluded.

NATIONAL ADVISORY
COMMITTEE FOR AERONAUTICS.

Figure 28.- Concluded.

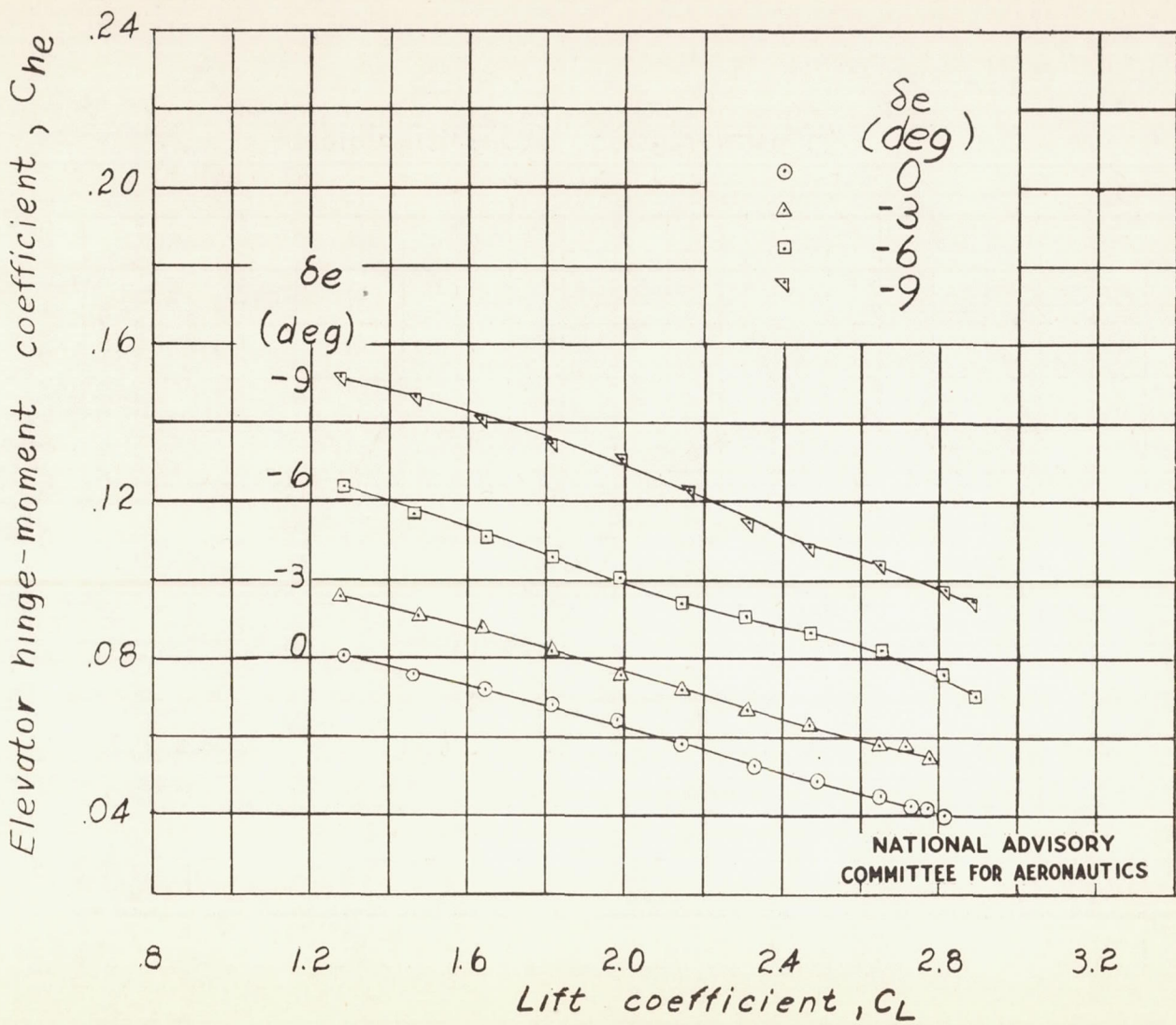


(a) Propeller off.

Figure 29.- Effect of elevator deflection on the aerodynamic characteristics of the model as a low-wing airplane with full-span double slotted flap. $\delta_{f1} = \delta_{f2} = 30^\circ$; $i_t = -1.3^\circ$; tail slot open.

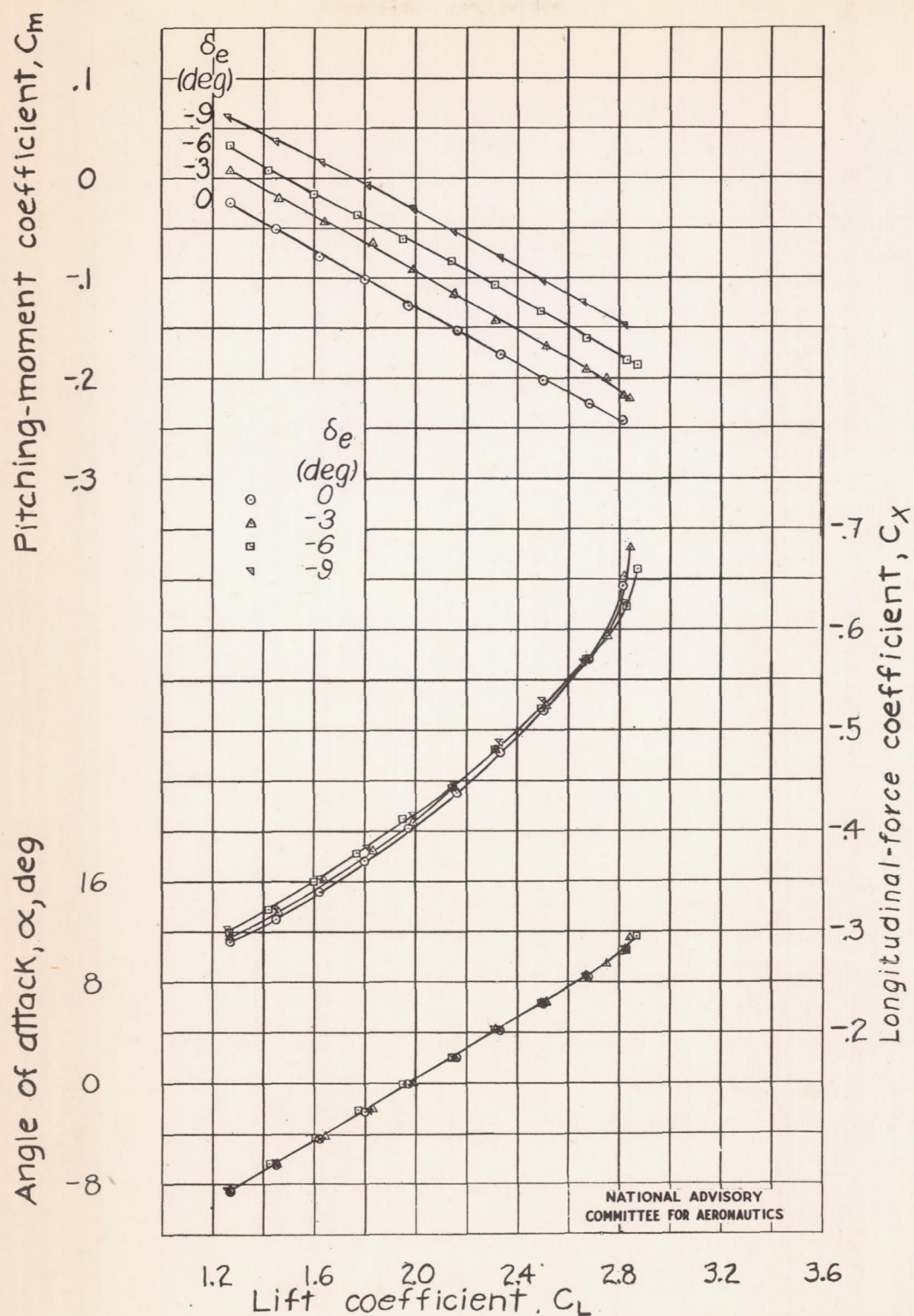
Fig. 29a conc.

NACA TN No. 1239



(a) Concluded.

Figure 29.- Continued.

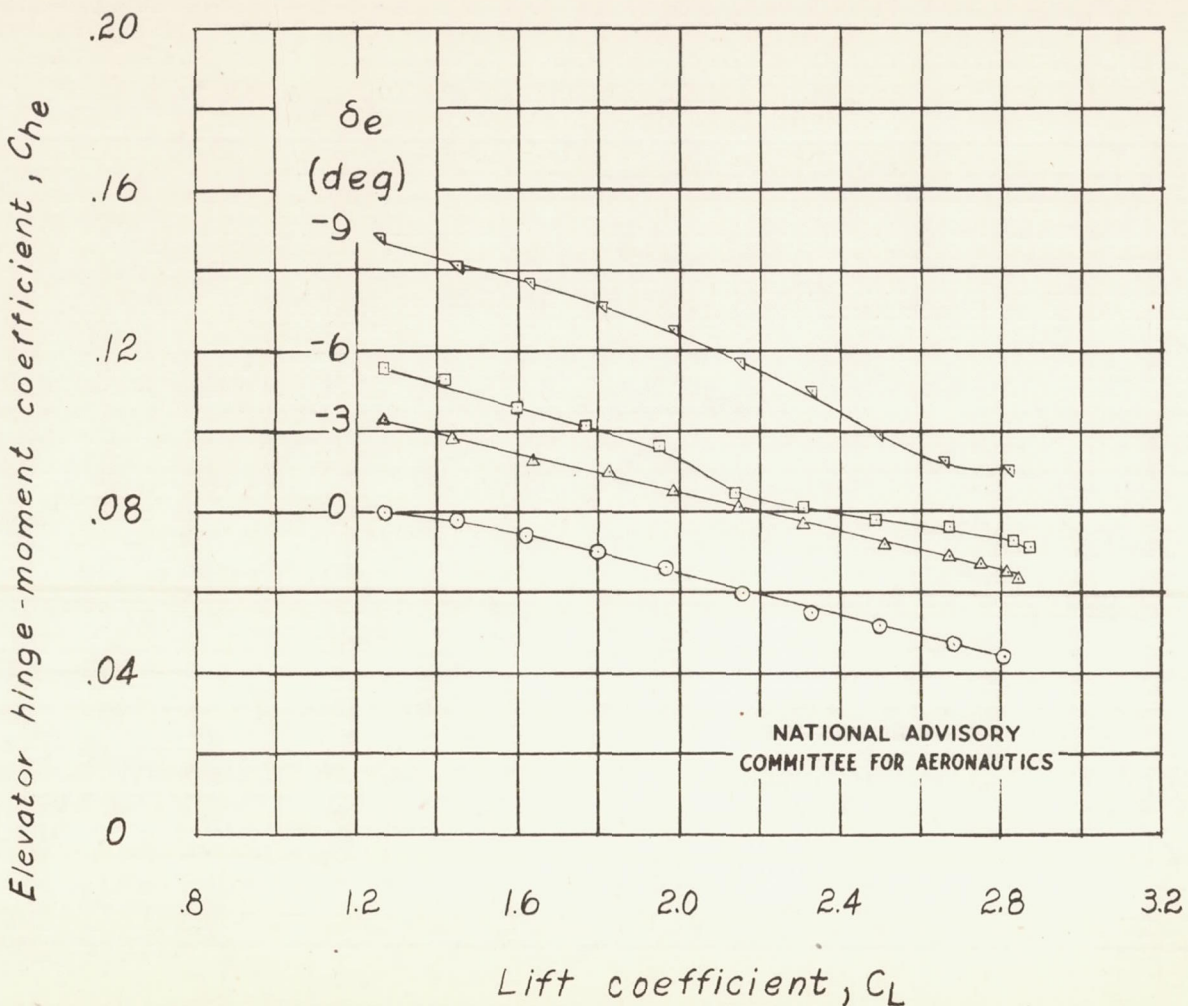


(b) Propeller windmilling.

Figure 29.- Continued.

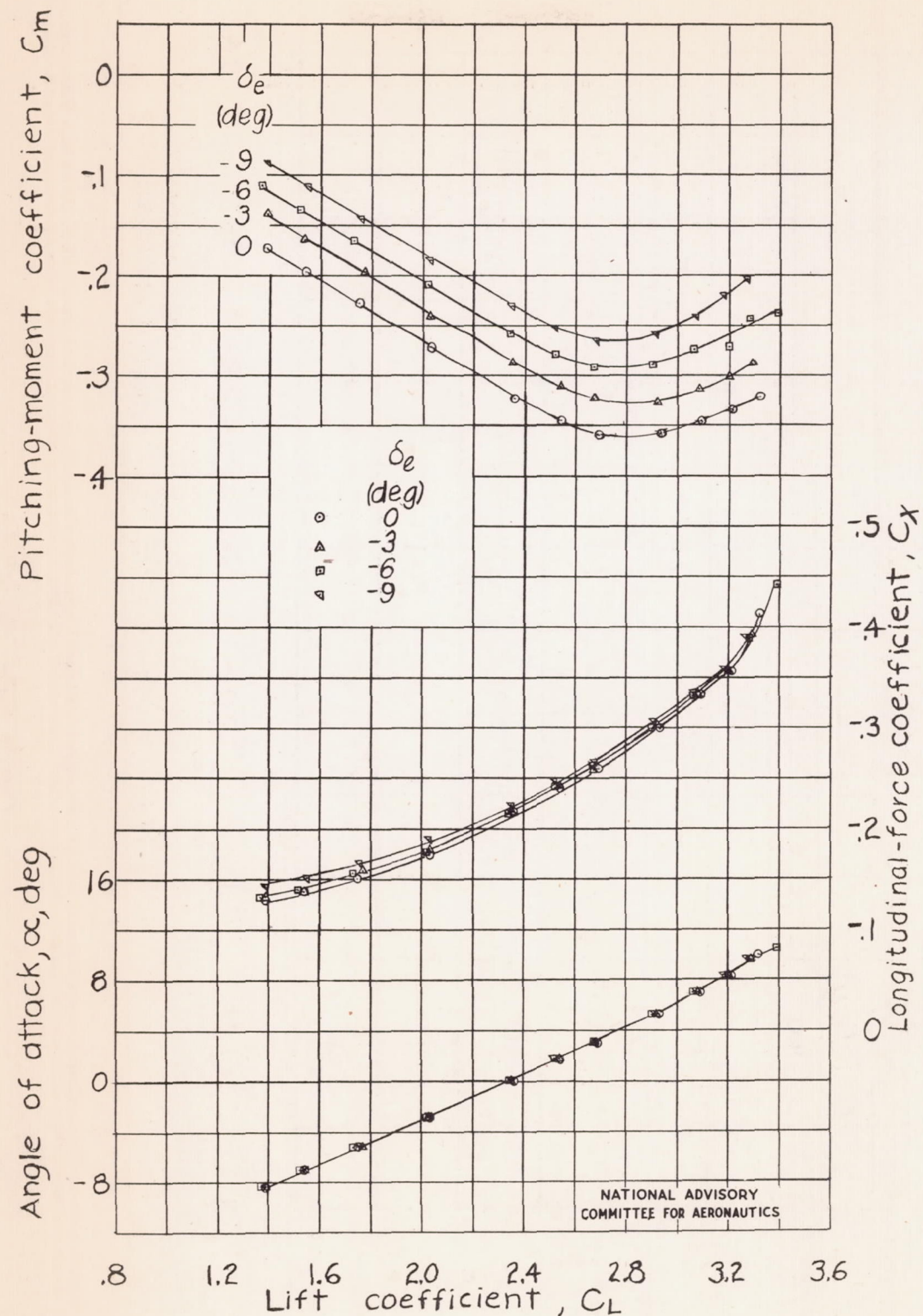
Fig. 29b conc.

NACA TN No. 1239



(b) Concluded.

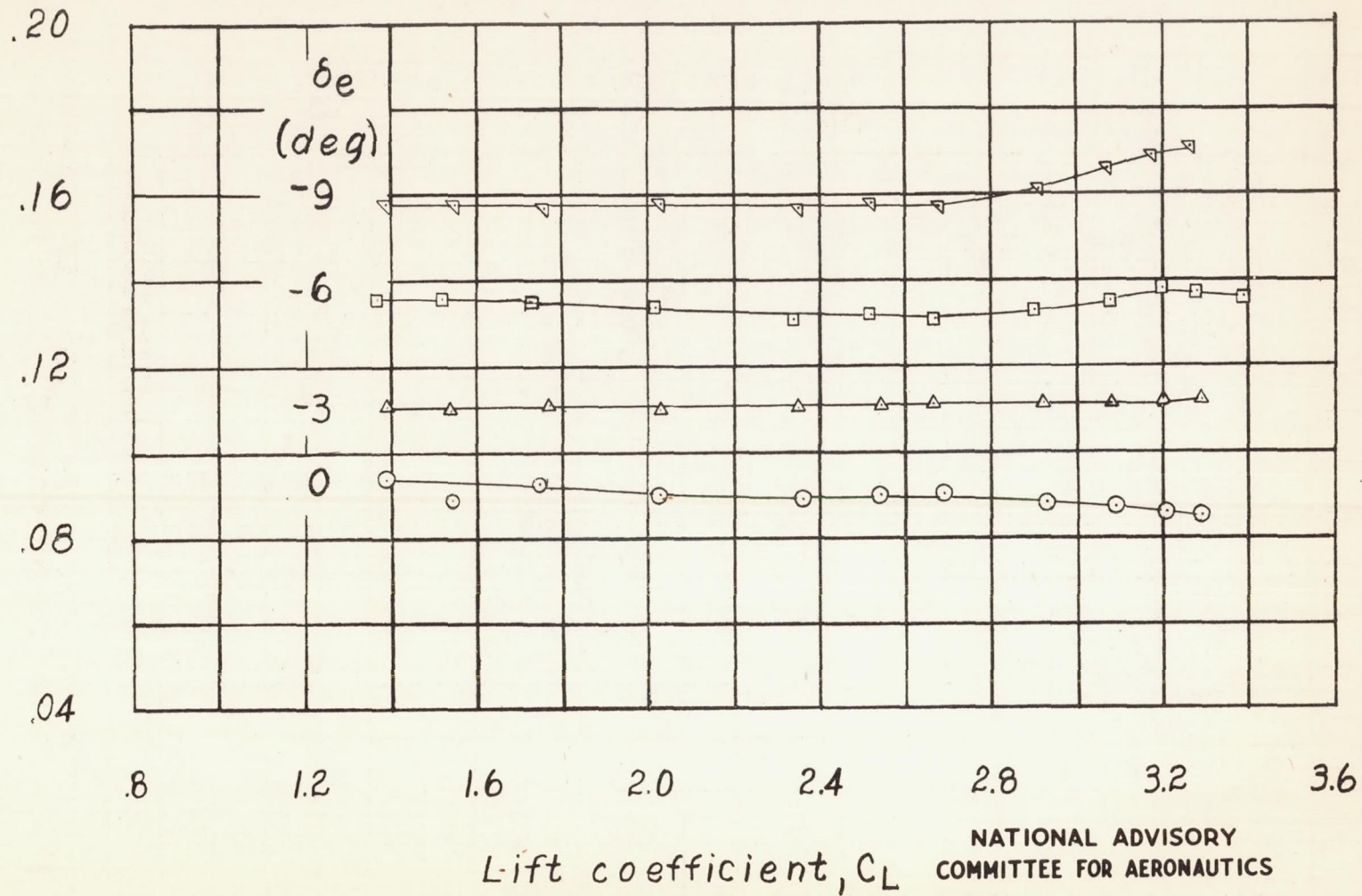
Figure 29.- Continued.



(c) Power on.

Figure 29c - Continued.

Elevator hinge-moment coefficient, C_{he}



NATIONAL ADVISORY
COMMITTEE FOR AERONAUTICS

(c) Concluded.

Figure 29.- Concluded.

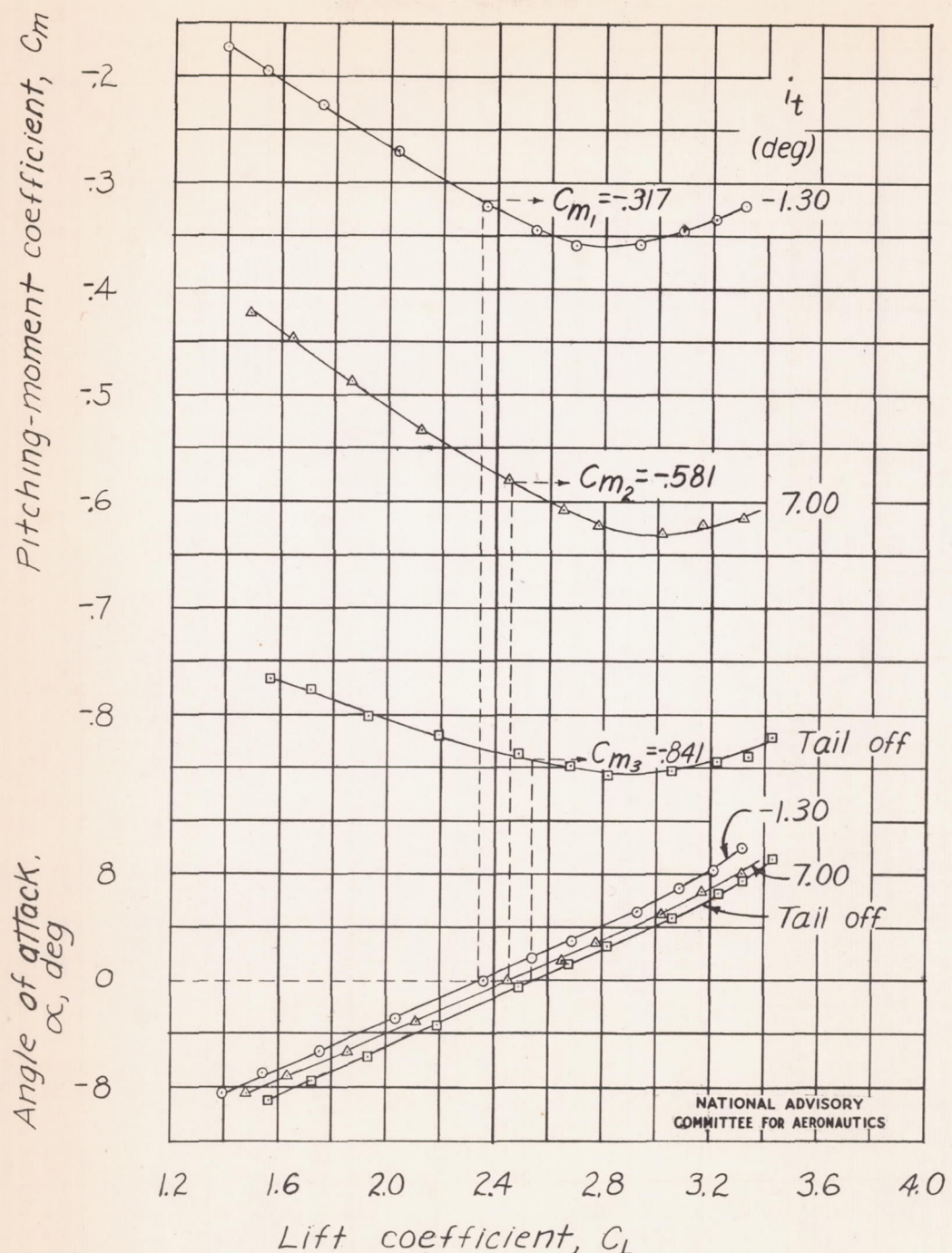


Figure 30.- Effect of stabilizer setting on the aerodynamic characteristics of the model as a low-wing airplane with full-span double slotted flap. $\delta_{f1} = 30^\circ$; $\delta_{f2} = 30^\circ$; $\delta_e = 0^\circ$; power on.

(Illustrative procedure for obtaining data for determining q_t/q and ϵ .)

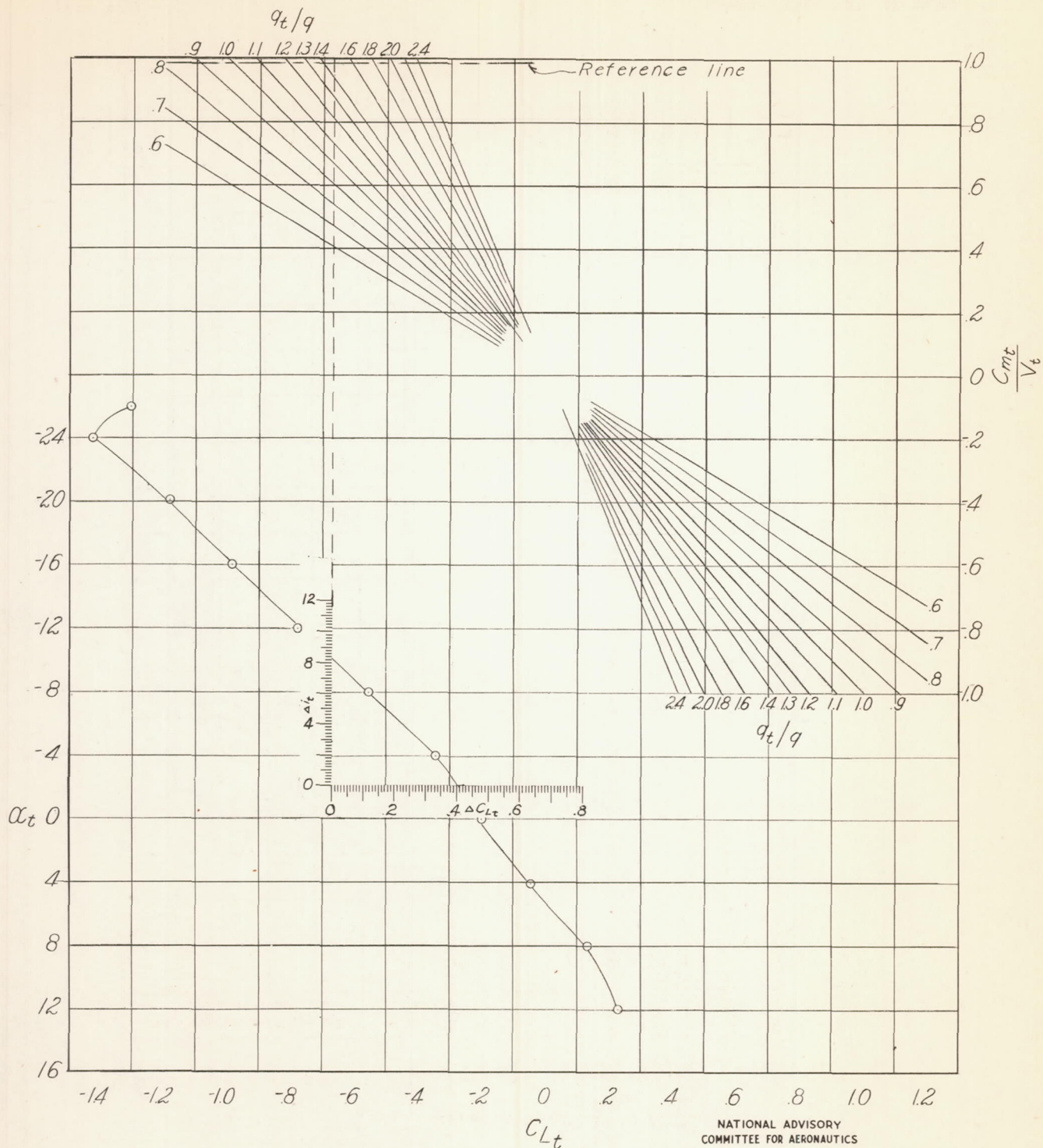
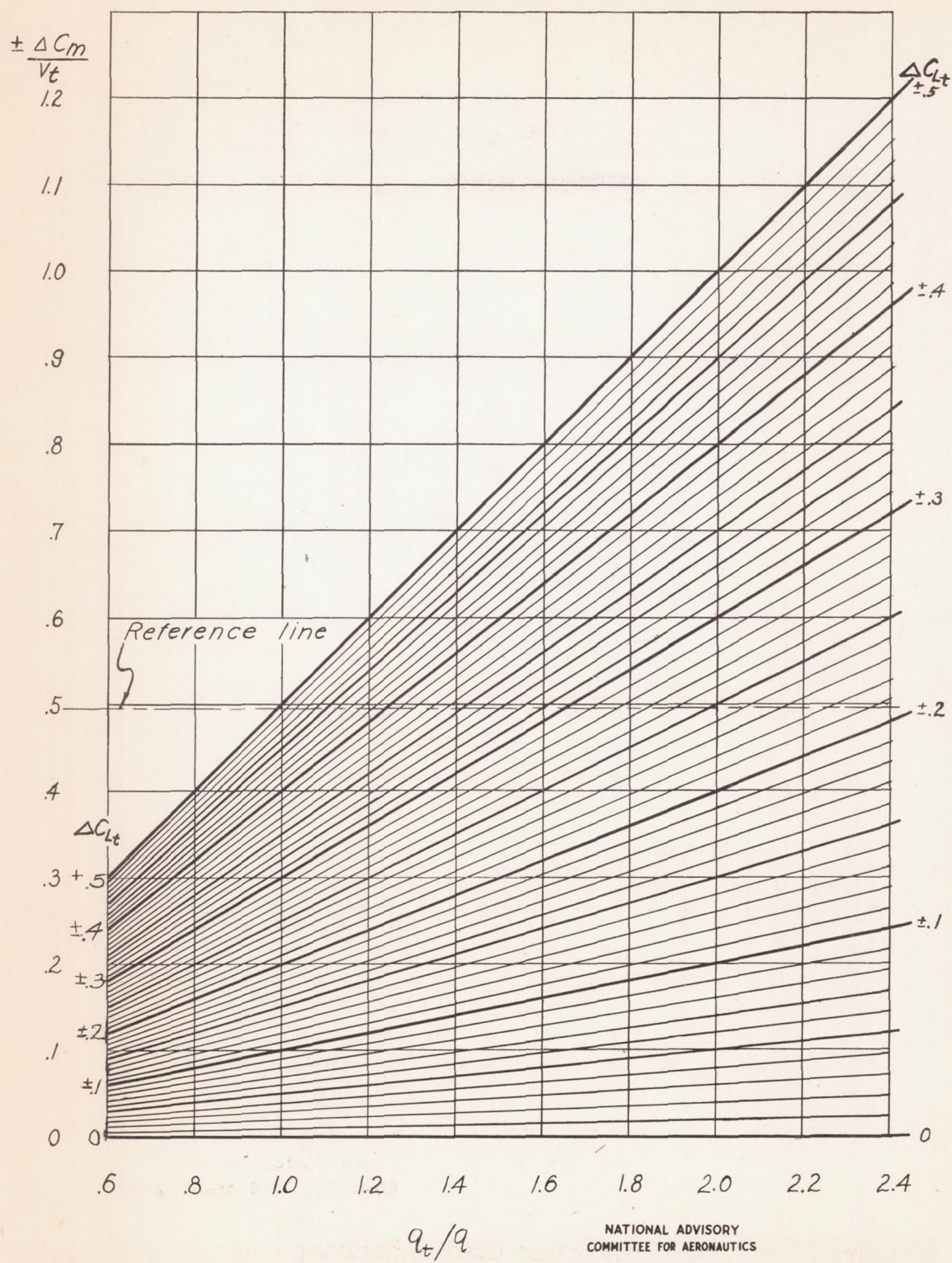
(a) ΔC_{L_t} and α_t .

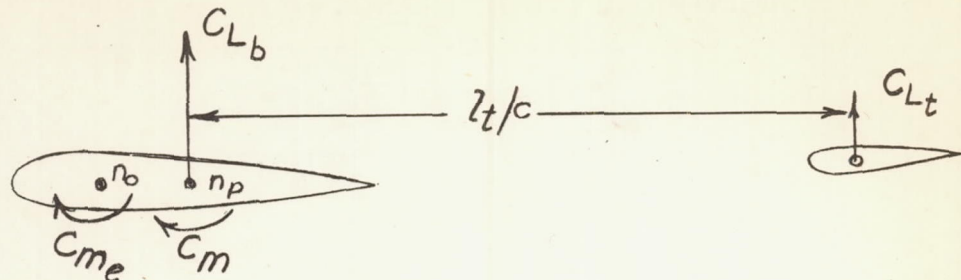
Figure 31.- Chart for graphically determining the effective dynamic-pressure ratio and effective tail angle of attack from model tail-on, tail-off, and isolated-tail data. The broken lines represent the final approximation for the sample solution of Table IV.



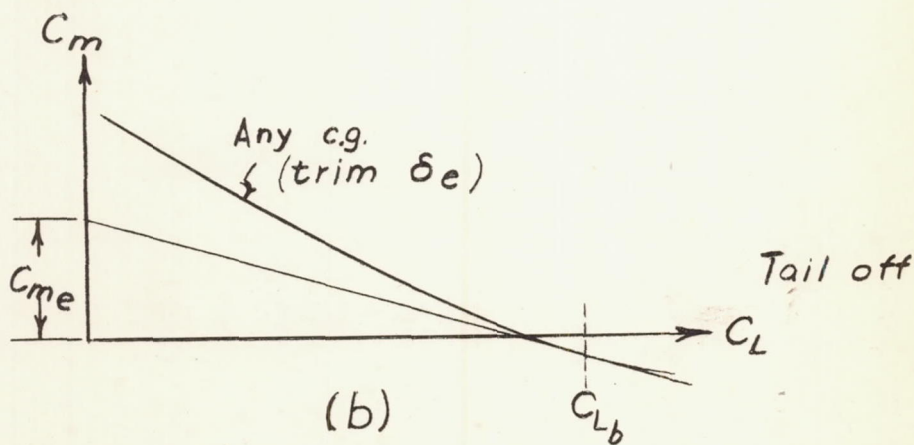
NATIONAL ADVISORY
COMMITTEE FOR AERONAUTICS

(b) q_t/q .

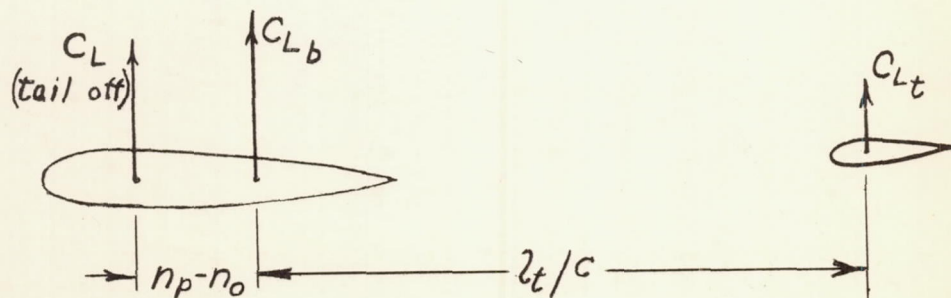
Figure 31.- Concluded.



(a)



(b)



(c)

NATIONAL ADVISORY
COMMITTEE FOR AERONAUTICS

Figure 32.- Vector diagrams used in deriving neutral-point equation.